INVESTIGATION OF THIN-FILM CADMIUM SULPHIDE SOLAR CELLS

A Thesis

submitted to the Faculty of Engineering

of the University of Glasgow

for the degree of

Doctor of Philosophy

by

Wai Ming Tsang, B.Sc.

March, 1979.

SUMMARY

This thesis gives the results of a study of the preparation, structure and electrical properties of thin films of CdS. Two methods of preparation have been investigated, firstly deposition using electron beam evaporation of compound CdS and secondly, co-evaporation of cadmium and sulphur by molecular beam epitaxy. A wide range of Si/CdS heterojunction solar cells has been fabricated. The crystal structure of the hexagonal CdS films produced by electron beam evaporation of compound CdS were polycrystalline. The structure was found to be more crystalline as the deposition temperature was increased to near the cut-off temperature of 340°C. The resistivity of such films at room temperature was typically 10 ohm cm. Thorough cleaning of the substrate in vacuum was shown to result in significant improvements in film structures and device characteristics. The efficiencies of the Si/CdS heterojunction when used as solar cells are generally less than 2%; these devices are therefore unsuitable for solar energy conversions.

Extensive investigations have beem made of the preparation of CdS films by molecular beam epitaxy, one aim of this work being to determine those factors which lead to the production of films with predictable crystal structure and electrical characteristics. It was found that epitaxial CdS film could be grown provided: (a) the constituent flux ratio was maintained at about 1:1, (b) the substrate temperature was sufficiently high and within a specific range, and (c) the substrate was sufficiently clean. A wide range of film growth rate was achieved on a (111) oriented spinel substrate, the rate ranging from 2000Å per hour to 15 microns per hour. The large lattice mismatch of about 28% between spinel and CdS did not hinder epitaxial film growth. The resultant hexagonal

CdS films at room temperature exibit a resistivity of about 10^5 ohm cm. A significant density of trap defects was found at 1.6eV below the conduction band; these traps are believed to be due to the cadmium vacancy.

It has been found possible to dope these films with indium to produce n-type CdS, using donor concentrations from 2×10^{15} to $6 \times 10^{18} cm^{-3}$. The measured value of Hall mobility, 65 $cm^2 V^{-1} s^{-1}$, of the heavily doped films indicates that the conduction in the films is dominated by ionised scattering. Substitutional doping with phosphorus has also been achieved. The films obtained are of moderately low conductivity, but the current carriers have not been identified because of the difficulty in making ohmic contacts.

A substantial part of the work described is concerned with the deposition of CdS on thin-film Au, Al and MgO substrates. It has been found that films deposited on Au are hexagonal and grew with the cadmium face on the free-growth surface. In contrast, films grown on Al and MgO were cubic and with sulphur face on the free-growth surface. Thermo-e.m.f. measurements showed that whilst CdS grown on Au was n-type, that grown on Al was p-type. The p-type conduction observed on CdS deposited on Al was attributed to the formation of an inversion layer at the interface, and a band model for the metal-insulator-semiconductor configuration of Al-Al_2O_3-CdS is proposed. Studies have also been made of Al-MgO-CdS and Au-MgO-CdS diodes, the results confirmed the MIS nature of the CdS on Al configuration. Measurements of the I-V and C-V characteristics are also consistent with the model proposed. The effects of varying the thickness of the MgO layer in Au-MgO-CdS diodes has also been investigated. Evidence of photovoltaic characteristics has been found; significant photovoltaic effects were observed for MgO thickness of less than 40Å.

ACKNOWLEDGEMENTS

I wish to express my sincere gratitude to Professor J. Lamb for the provision of research facilities and materials, and to Dr. W. Duncan and Professor A. J. Barlow who closely supervised my research work and provided much needed encouragements. I also wish to express my gratitude to Dr. J. Fryer of the Chemistry Department, University of Glasgow for help with the Transmission Electron Microscopy. I should also like to thank the technical staffs for much needed assistances. In particular, I wish to thank Mr. J. Corstorphine for much help with vacuum equipments, and Mr. J. Clark for his assistance in preparing the photographs. Thanks are also due to all my colleagues with whom I have many stimulating discussions.

I wish to express my sincere thanks to my grandmother and my parents who sacrificed much in assisting me throughout the period of my education. Finally, I thank my wife for her continual encouragement and support.

CONTENTS

INTRODUCTION

The work presented in this thesis is concerned with the evaluation of epitaxial CdS film for terrestrial solar energy conversion. The CdS films have been produced both by evaporation of compound CdS and by co-evaporation of cadmium and sulphur in vacuum. A significant part of this work is concerned with the role of the structure-sensitive properties of these component materials in affecting or influencing the behaviour of the devices fabricated.

Chapter 1 provides a general introduction to solar cell concepts and technology. The three main types of solar cell structures, namely: homojunction, heterojunction and Schottky barrier, are distinguished, and the potentials of each cell configuration are discussed. A brief summary is also given of the present state of solar cell technology. The efficiencies and characteristics of solar cells are considered, for the most commonly available silicon cells in single and polycrystalline form, and for the II-VI and III-V cells. Finally the materials availability for large scale solar energy applications is discussed.

To characterize the deposition and growth of thin films, a knowledge and an appreciation of the factors and problems involved in evaporation, condensation, and chemical interaction processes on substrate materials are needed.

The identifiable steps in film growth are discussed in Chapter 2, together with the theoretical and experimental results of other research workers, concerning the factor which affect the epitaxial growth of one material on another. In particular, the role of deposition parameters in affecting the

different properties between compound-evaporated films and co-evaporated films are considered.

Chapter 3 deals with the processes and results of p-Si/n-CdS heterojunctions. A theoretical band model is presented, together with the effects of surface and interface states, and lattice mismatch. The experimental results of other investigators for deposited CdS films are discussed in relation to the present work. The technological procedures required for the fabrication of a Si/CdS heterojunction are presented in detail. The structural properties of the CdS film grown on silicon by compound evaporation are discussed. X-ray Laue diffraction was used to obtained information on the structure of the CdS film. It was found that thermal cleaning of the silicon substrate before CdS deposition enhanced the structural quality of the film and makes it possible to produce consistent Si/CdS solar cells. Annealing of the Si/CdS cell is shown to improve the efficiency of the device by as much as 50%.

It is evident from the present work on Si/CdS solar cell that this structure is unacceptable for terrestrial solar energy conversions. Furthermore, it is necessary to obtain better structural quality of the CdS films than can be obtained by compound evaporation. Co-evaporation of cadmium and sulphur by molecular beam epitaxy is shown to be a suitable alternative mean of producing epitaxial CdS films. But before the film can be used for device fabrication, it is necessary to characterize the deposition technique so that a reliable prediction can be made of the characteristics of the CdS films.

The structural and transport properties of the CdS films grown on (111) oriented spinel substrates by molecular beam epitaxy are discussed in Chapter 4. X-ray Laue back reflection

and Bragg diffraction give information about the structure of the CdS films, and measurements of the Hall mobility, the temperature dependence of resistivity and photoconductivity are used to indicate the transport properties of the films. Substitutional doping with indium and phosphorus is discussed.

Chapter 5 deals with a different approach to the production of low cost solar cells. In order to form Schottky type solar cell structures,the deposition of CdS on epitaxial metal substrates is investigated and characterized. The deposition of epitaxial gold and aluminium thin-film substrates, and the processes involved in the deposition of CdS on the metal substrates are discussed. The characteristics of the deposited CdS film on metal substrates were measured by thermo-e.m.f. and piezoelectric methods. As a direct result of these measurements, investigation of CdS deposition on MgO substrates, to form MIS diodes, was carried out and the results are presented in the last part of the chapter.

The experimental results of studies of Au-CdS, Al-Al_2O_3-CdS and Au-MgO-CdS structures are given in Chapter 6. An energy band model of the Al-Al_2O_3-CdS is developed. It was found that Al-Al_2O_3-CdS diodes were unstable, this problem was caused by the uncontrollable Al_2O_3 insulator thickness, and was solved by controlling very carefully the thickness MgO in place of the Al_2O_3 layer.

The potentials and characteristics of minority carrier metal-insulator-semiconductor tunnel diodes for use as solar cells are discussed in Chapter 7. The experimental results of Au-MgO-CdS diodes are discussed, and are shown to be in reasonable agreement with predicted behaviours.

A summary of the important results and findings on the

growth behaviour of CdS films, and on the performance of the Si/CdS heterojunction and MIS diodes is given in Chapter 8, together with suggestions for future work in this field.

CHAPTER 1 REVIEW OF SOLAR CELLS

1.1 Introduction

The object of the work described in this thesis was to investigate thin-film CdS films for use in solar cells for terrestrial applications. Solar cells have been widely used for space vehicles and other applications in which no other viable electricity source exists. The growing interest in large-scale terrestrial solar cell systems, potentially competitive with conventional energy sources, has motivated research and development toward greatly reducing solar-cell-array costs. The program of the U.S. Energy Research & Development Administration (ERDA) is aimed at a solar-cell array cost of $0.5 per peak watt at a national cell production rate capable of generating 500MW by 1985[1]. Since the present commercial silicon-cell panels cost $12 - $20 per peak watt, major technological innovation are needed to reach the objective.

The theory of the conventional solar cell is well understood[2,3], and the efficiency limit of bulk Si devices is known to be about 22%[4]. With nearly "perfect" material and extreme process care, efficiency values close to this limit have been achieved[5]. The cost of solar cells can either be reduced by reduction in the manufacturing cost of the perfect cells or to use imperfect materials and strive to obtain the required cell efficiency value by compromises in the cell design and manufacture. The first approach is limited by the material cost, and bulk polycrystalline and thin-film materials deposited on low-cost substrates have inherent defects arising from dislocations, grain boundaries and contaminants that reduce the cell efficiency.

The basic solar cell consists of a p-n junction (although multijunction devices and Schottky barriers have also been constructed). Under illumination, a cell produces a short-circuit current density Jsc, whereas under open-circuit conditions a voltage Voc is produced. With a power density incident on the cell, the maximum power density generated is F.Jsc.Voc and the power efficiency η is

$$\eta = F.Jsc.Voc/Pi \qquad (1.1)$$

where F denotes the fill factor and Pi the incident power density. The open-circuit voltage is

$$Voc = \frac{nkT}{q} \ln\left(\frac{Jsc}{Jo} + 1\right) \qquad (1.2)$$

where n is the exponent in the diode equation (n=1-2), T is the temperature, k is the Boltzmann constant, q is the electron charge, and Jo is the saturation current density.

The material and junction quality are important in determining the cell efficiency for a given geometry, because Jo is increased by defects in the junction and Jsc is reduced by a low minority-carrier diffusion length. Therefore, grain boundaries and impurities are also detrimental to cell performance. The fill factor is reduced by a higher Jo, and also decreased with increasing cell resistance.

1.2 Solar cell devices

Although the great majority of solar cells are made with p-n homojunctions, there are other types that could exibit unique advantages of one kind or another, including heterojunctions and Schottky barriers. Heterojunction and Schottky barrier cells could be very important for terrestrial applications because of their potential low cost and because they do not necessarily entail diffusion processes, which can be detrimental

to polycrystalline devices.

1.2.1 Homojunction cells

Figure 1.1 shows the simplest form of energy band diagram for a homojunction device under (a) short-circuited and (b) load conditions, respectively. The doping is taken as uniform, and there is no built-in electric field outside the space charge region (a slight band bending at the surface due to surface states is indicated). When light falls on the active surface, photons of energy sufficient to excite electrons from the valence band to the conduction band generate electron-hole pairs on both sides of the junction. These excess minority carriers (holes on the n-side and electrons on the p-side of the junction) diffuse through the cell and those that reach the edges of the space charge before recombining are separated by the electric field; the electrons moving towards the negative contact and the holes towards the positive. The polarity of the output voltage is the same as the "forward bias" direction of the device. The generated current is directly proportional to the intensity of the light and the active area of the cell. The output voltage is less than the bandgap of the material used and is determined by the doping concentration in the n- and p-region of the device.

1.2.2 Heterojunction cells

The theoretical efficiencies of heterojunction solar cells have been calculated by numerous workers including Screeder et al. [6] and Sahai and Milnes[7]. The ideal efficiencies predicted by Screeder et al. [6] are very high and bear little relation to what might be obtained in practice. A more realistic

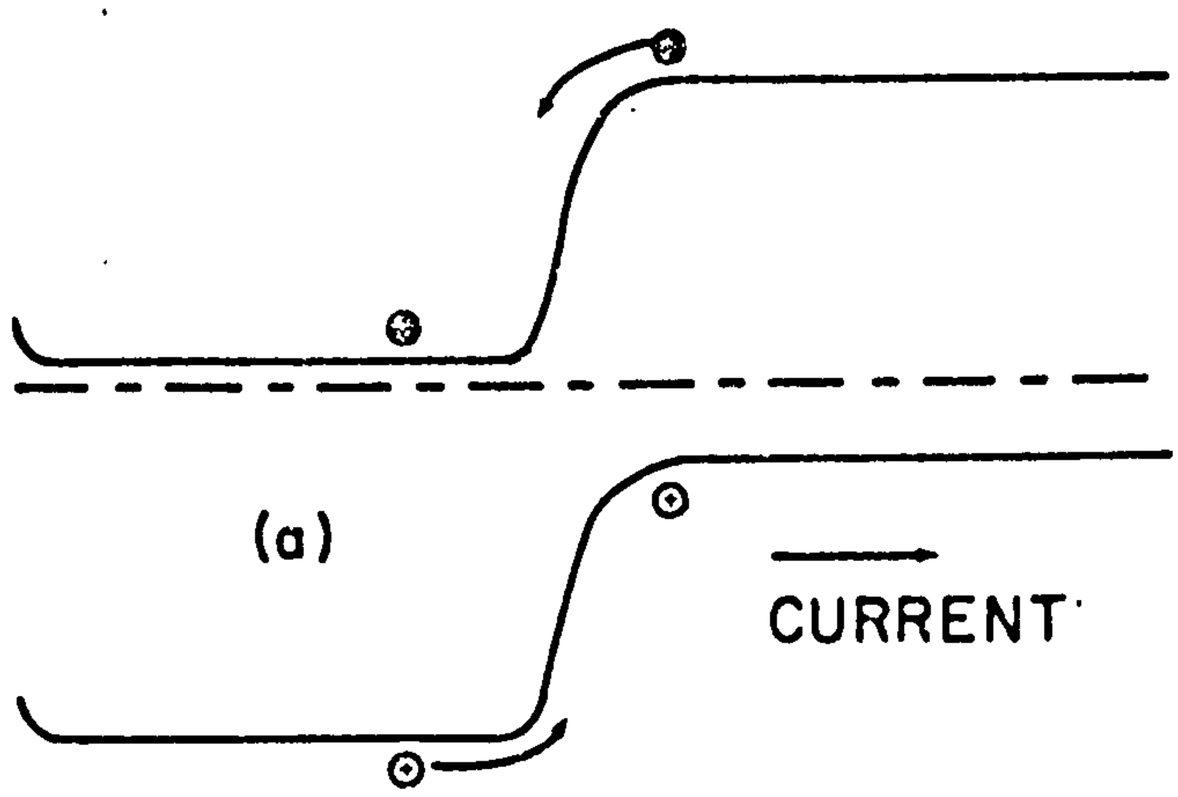

(a) short circuit conditions

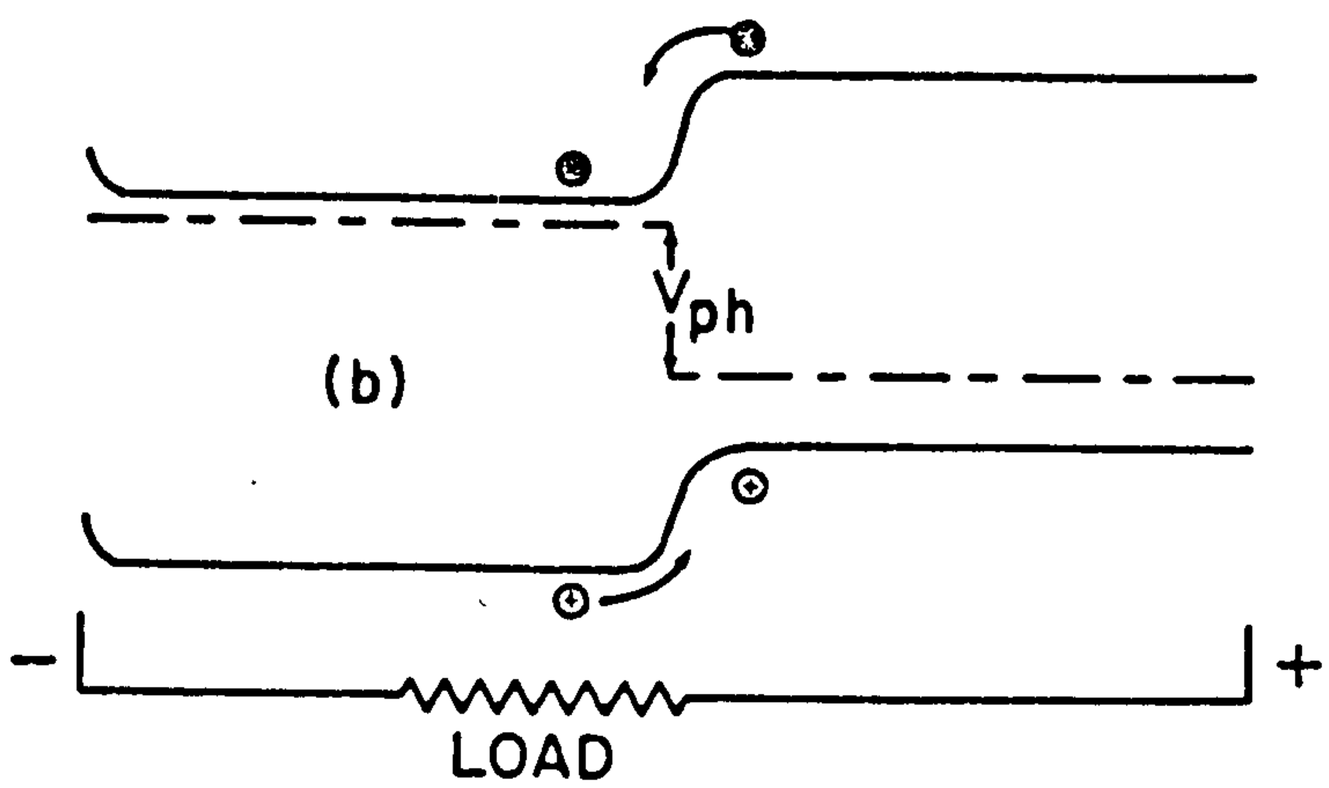

(b) a load is added

Fig. 1.1 N/P homojunction solar cell under illumination

calculation was performed by Sahai and Milnes[7], who took into account many practical considerations which might limit the performance such as space charge, recombination, reflection and series resistance.

The energy band diagram of a typical heterojunction between two single crystal materials is shown in Figure 1.2. Light of energy less than E_{G1} but greater than E_{G2} will pass through the first material (which therefore acts as a "window") and becomes absorbed by the second material. Carriers created within the depletion region and within a diffusion length of the junction will be collected exactly as in a homojunction cell. Light of energy greater than E_{G1} will be absorbed by the first material and carriers generated within a diffusion length of the junction will also be collected.

The output voltage produced by the heterojunction solar cell is determined by the barrier height Vd, and could be larger than that of the homojunction. At first glance, this seems to hold the promise of higher output from a heterojunction than can be obtained from a homojunction of the smaller gap material alone; the heterojunction photocurrent can be equal to that of the homojunction and the barrier height Vd could be larger. Unfortunately, these two thing never occur together because a large barrier height is accompanied by reduced photo-currents[8]. In general, the output power from a heterojunction solar cell is no larger than it would be from a solar cell made from either material alone, and the advantages of the heterojunction cells come from eliminating surface recombination and dead layer problems, and from potentially lower series resistance and higher radiation tolerance. The magnitude of these advantages depend on the particular design geometry and

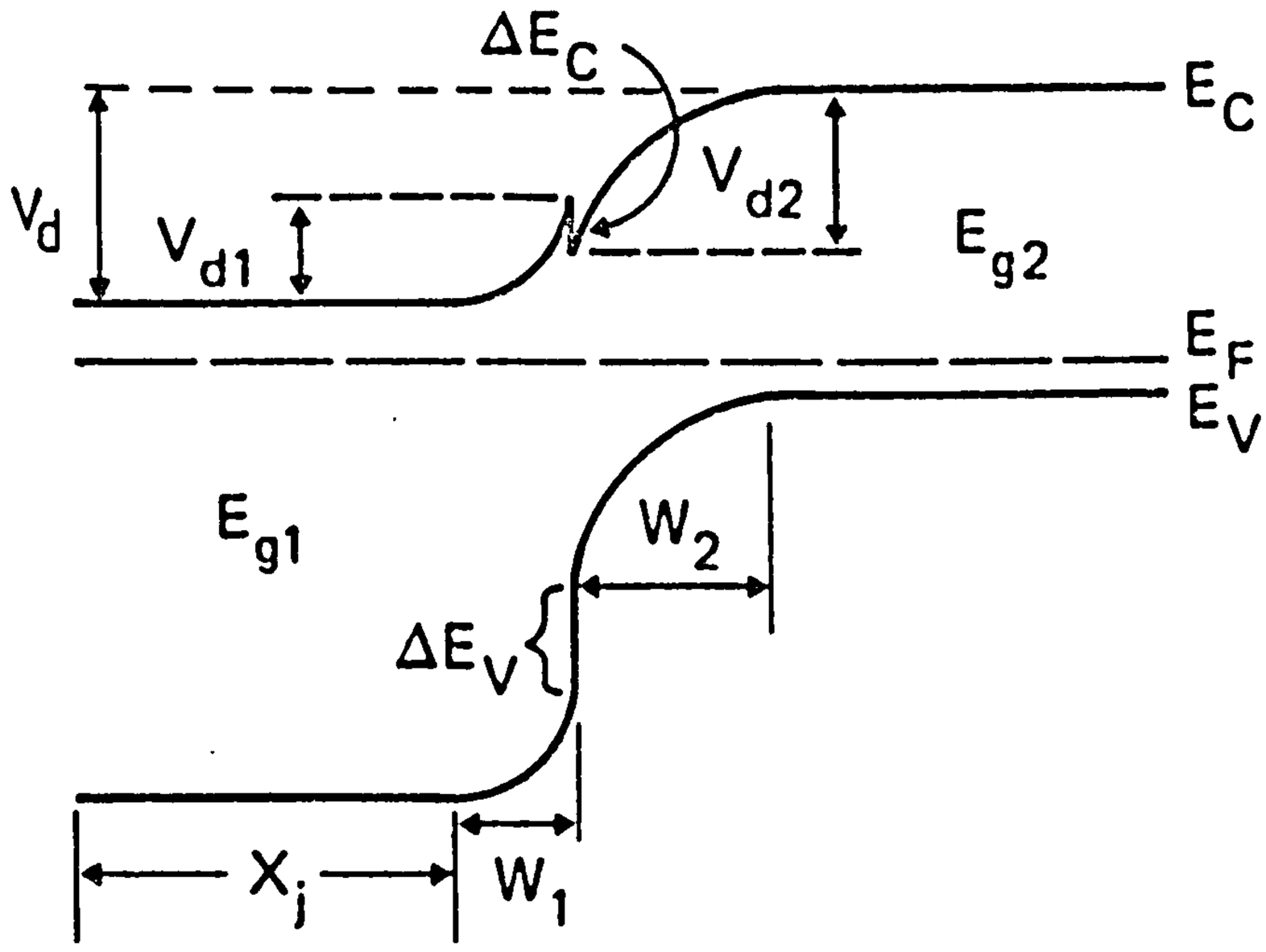

Fig. 1.2 N/P heterojunction in thermo equilibrium

other practical matter of fabrication. The performance is adversly affected, of course, if there is any tendency for the interface to have a high recombination rate.

1.2.3 Schottky barrier cells

In recent years, there is renewed interest in the Schottky barrier solar cells[9,10]. Because of their simple fabrication technology and low cost, these cells appear to be a viable alternative to the p-n homojunction solar cells for terrestrial applications.

A Schottky barrier solar cell is formed by a metal in contact with a semiconductor material. This is in contrast to the heterojunction cell where two different semiconductor materials are used. When a metal is in contact with a semiconductor material, a readjustment of charge takes place, as in other types of junctions, to establish thermal equilibrium and under certain conditions an energy band bending occurs at the interface. If the metal is thin enough to be partially transparent to light (while still retaining acceptable low sheet resistivity), then some of the incident light can penetrate to the semiconductor and a photocurrent in an external circuit is possible.

Figure 1.3 shows the simplest form of a n-type Schottky barrier solar cell where w_o is the depletion width, ϕ_{bo} the barrier height and V_{do} the diffusion voltage. There are three photoeffects that can occur. Light can be absorbed in the metal and excite electrons over the barrier into the semiconductor (1 in Figure 1.3). Long wavelength light is usually absorbed deep inside the semiconductor, creating electron-hole pairs just as a normal p-n junction; the holes then must diffuse to the junction edge to be collected (3 in Figure 1.3). Short

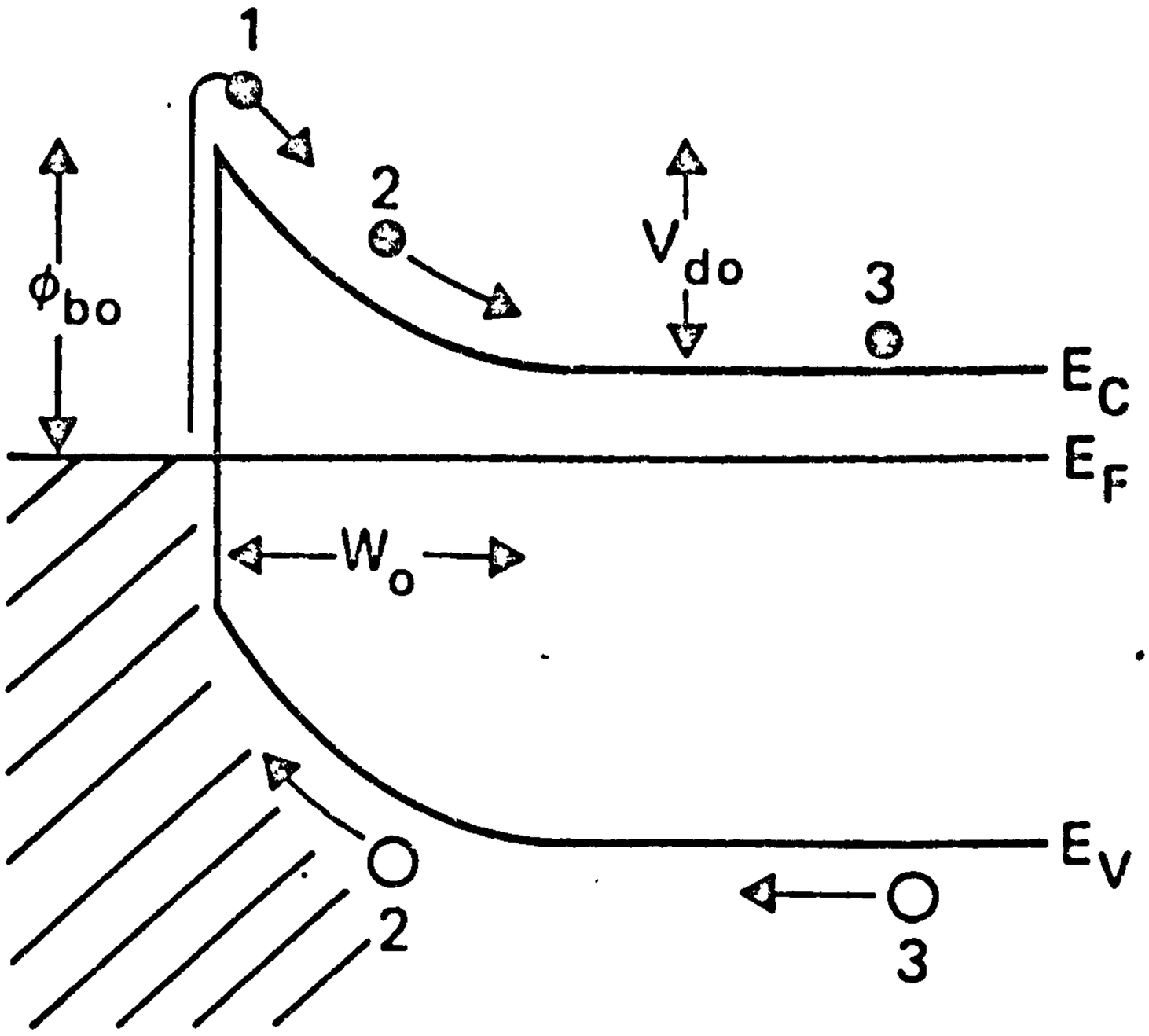

Fig.1.3 Schottky barrier on an n-type semiconductor

wavelength light entering the semiconductor is absorbed partly in the bulk and partly in the depletion region (2 in Figure 1.3), and very short wavelength light is absorbed entirely in the depletion region. The photogenerated carriers are "swept" away from the depletion region by the high electric field before recombination at the interface sites can occur, resulting in good collection of the carriers.

Schottky barrier solar cells could be highly useful for terrestrial applications where a slightly lower predicted efficiency compared to p-n junction cells would be far outweighed by their inherent simplicity and expected lower cost. They could be particularly applicable to polycrystalline Si and GaAs solar cells where normal p-n junction diffusion processes may be difficult because of the presence of grain boundaries.

1.3 Solar cell technology

The performance of a solar cell is influenced strongly by the technology that goes into making the cell, and the optimum design depends on the application for which is is intended. For space applications, high efficiency and radiation tolerance are the prime consideration. For terrestrial applications, the efficiency and efficiency per unit cost figures are important to make solar cells competitive with other means of generating large amounts of electric power.

1.3.1 Silicon cells

(i) Single crystal silicon

Virtually all solar cells now in use consist of a Si single crystal "wafer" having a very thin (0.2-0.5μm) diffused region at the surface to form a p-n junction. The highest

efficiency Si solar cells have been produced by diffusion into Czochralski-grown material. The following are known to be essential to produce cells with AM1 (sea level at noon on the equator) efficiency ≥ 15%.

(a) Shallow junctions are needed (0.2μm below the surface) with a very steep dopant profile to minimise carrier loss by surface contamination. A diffusion process is needed that eliminates the thin "dead" layer at the diffused surface of the cell.

(b) A very low surface reflectivity (~ 5%) is obtained by "texturing" the surface, and fine contact fingers are used to minimise the metallised area (≤ 10% coverage).

(c) A diffusion in the back of the cell is used to produce a potential barrier that repels minority carrier from the back contact.

(d) The device processing produces devices with carrier lifetime of tens of microseconds by minimising contaminants.

Epitaxial structures have also produces high-quality solar cells[11]. The process involved first growing a p-n on n^+ epitaxial structure, followed by a thin p^+ layer diffused into the surface. This produced a p^+-p-n-n^+ configuration with a nearly ideal p-n junction (i.e. few defects) having a low saturation current density. The highest reported V_{oc} value of 630mV has been obtained with an epitaxial structure, although the short-circuit current sensity is still not as high as in the best diffused cells[12]. This is due to carrier-lifetime limitations, possibly the result of contamination in the epitaxial layers used.

The high efficiency cells described above are relatively costly. Independent of the starting silicon crystal, the cell

fabrication process contributes a substantial cost factor. Therefore means are being explored to simplify the cell fabrication process by eliminating some of the expensive processes used. Lower-cost junction formation method, metalisation, and assembly processes are areas requiring particular attention.

Even with the maximum degree of automation in the cell and panel-assembly processes, the ultimate cost-limiting factors are the Si ingot production. This includes growth by the Czochralski process and the subsequent cutting, lapping and polishing operation, as well as the cost of the initial purified polycrystalline Si.

(ii) Ribbon-form silicon cell

The most advanced ribbon process is the "edge-defined-film-fed growth" (e.f.g) method, in which silicon flows upward from the melt by capillary action into a carbon die, from which growth proceeds by a continuous pulling action[13]. The potential of such material for solar cell fabrication is obvious, since the ribbon formats eliminates the costly cutting and polishing steps needed with conventionally grown Si. However, major metallurgical problem remain to be solve before e.f.g ribbon becomes a low-cost material for efficient cell fabrication. The silicon produced is polycrystalline with numerous grains and twin boundaries. The dislocation density is generally much greater than that found in conventionally grown silicon, and the carrier lifetime is generally much lower.

(iii) Polycrystalline silicon cell

It is well known that grain boundaries produce large saturation current densities detrimental to both the fill

factor and the open-circuit voltage,and it is therefore essential that the grain size be as large as possible. Furthmore, contaminants must be minimise to increase carrier lifetime. Large grain (~ 1mm diameter) polycrystalline silicon, produced in bulk form from relatively pure starting materials, has been used in the production of large-area solar cells with efficiencies of 8-10% by a simple diffusion process[14,15]. However, unless produced in sheet form such as thin-film cells (thus eliminating slicing and polishing costs), the cost advantage of using these materials is uncertain.

1.3.2 II-VI and III-V compound solar cells

Solar cells of II-VI and III-V materials other than Si have been produced. One of the most efficient produced is the $Al_{1-x}Ga_xAs/GaAs$ heterojunction device. Woodall and Hovel[16] have reported efficiency values of about 20% using liquid-phase epitaxial growth, and vapour-phase epitaxial growth by Johnston[17] has yield nearly comparable values (18.5%). Such cells are mainly of interest for concentrators, because they are too costly compared with Si cells for other applications.

Wagner et al.[18] have investigated CdS/InP solar cells which were made by vacuum evaporation and chemical vapour deposition of CdS on an InP bulk-grown substrate. Cells prepared using single crystal InP substrates of area ~ $0.25cm^2$ were found to have efficiency values as high as 15%, depending on the quality of the bulk InP substrate. Polycrystalline cells of InP films deposited on graphited carbon have AM2 efficiencies of 5.7%[18].

The most studied thin-film cell is the evaporated CdS/Cu_2S cell[19]. The highest efficiency reported is 7.5%, but the

reliability of these devices is still under investigation. CdS/Cu_2S cells have been produced by a chemical-spray technique on glass substrate having efficiency of about 5%.

Various other cell structures[20-22] using $CuInSe_2/CdS$ and CdTe/CdS have been reported, but efficiencies over 10% were only obtained if relatively costly single crystals of $CuInSe_2$ and CdTe are used.

1.3.3 Abundance of materials

In order that photovoltaic solar energy conversion should make a significant impact on the energy needs of any part of the world, there are at least three important conditions it must satisfy. Firstly, the cost of generating energy using solar cells must be economically competitive with other available means of producing energy. Secondly, the amount of energy obtained must be much larger than the energy needed to fabricate and operate the system. The present-day methods of fabricating solar arrays are very lossy. It has been estimated that at present, the energy consumed in the production of metallurgical grade silicon, its purification, the fabrication of solar cells, and the assembly of an array for electricity generation in the northeastern part of the United States is equivalent to its net energy output over about 40 years[23]. At today's energy prices, the cost of this energy consumption represents only a fraction of one percent of the current cost of the completed arrays. Therefore, no effort has been made towards reducing this energy consumption. Such a large energy use is clearly not permissible in future processes. Through use of energy conservative methods. Wolf[24] has shown that the energy consumption for the production of solar arrays can be reduced

by a factor of ten to twenty from the present value. This level of energy consumption for production can then be recovered by the solar arrays within ten to twenty percent of its expected lifetime of twenty years. Thirdly, there must be enough material available to fabricate solar cell arrays in sufficient quantity to generate a significant fraction (greater than several percent) of the country's energy needs.

The electrical energy demand in the United States amounted to about 2×10^{12} kW.hr/yr in 1975[25], and is likely to double by 1990. This represent about 3×10^{11} W of generating capacity on the average, and two to three times this capacity must be available to accommodate peak demands. A practical solar powered system must be able to supply a significant fraction of this, say 10^{10} W under peak conditions, and perhaps five times this amount should be a reasonable goal to take into account of the losses due to poor weather, night time, and the need for energy storage. The two chief contenders to meet this requirement are thin-film Si and thin-film CdS.

It has been estimated[8] that if the whole of the present United States' production of Cd, Ga, In and Si were converted into solar cells, assuming 10% efficiency and 100mW/cm^2 input power, the present level of Ga production could only yield 10^6 to 10^7 W under peak condition, with InP about an order-of-magnitude higher. Ribbon Si 100μm thick could yield around 5×10^8 W, while thin-film CdS or Si devices 10μm thick could yield about 10^{10} W. Therefore, if the present yearly production rate of minerals in the United States is maintained, only CdS and thin-film Si are capable of generating the minimum requirement of 10^{10} W in the relatively few years.

1.4 Conclusion

Homojunction solar cells are the most common type commercially available to date. They have the highest theoretical efficiencies, but due to inherent properties of the semiconductor material used lateral resistance loss and surface recombination prevent homojunction solar cells from achieving their predicted efficiencies.

The predicted efficiencies of heterojunction solar cells cannot be higher than that of the homojunction cells made from either of the base materials alone, but it may be easier to achieve due to the absence of "dead" layers and lower series resistance. To obtain high short-circuit currents, open-circuit voltages and efficiencies, it is imperative that materials comprising the heterojunction have close lattice match, similar thermal expansion coefficients, do not significantly cross dope each other, and do not form energy barriers that hinder photon-generated current collection.

Schottky barrier solar cells are the third major cell concept, using metal and semiconductor to form the barrier. Again, efficiencies of Schottky barrier cells cannot be higher than homojunction cells made of the semiconductor alone. Their main advantages are inherent simplicity and expected low cost which far outweighted their slightly lower predicted efficiencies.

Single crystals or large grained polycrystalline materials are needed at present to produce solar cells with AM1 efficiencies in excess of 10%, a value commonly considered to represent a lower limit for the construction of large-scale solar cell electricity generators. Substantial cost reductions are possible by automation and simplifying the fabrication process for single-crystal silicon cells, by the use of lower cost poly-

crystalline materials and by improved materials-growth processes. However, the ultimate cost limitation remains in the bulk-silicon materials and the preparative methods needed to produce the wafers. Some of the cost could be substantially reduced if suitable silicon in ribbon form could be produced. However, at present the silicon edge-defined-film-fed growth process is still in the development stage because of crystal defects that limit the yield of efficient cells.

Cells of II-VI and III-V materials other than Si have also required single (or possibly large-grained) crystals to reach efficiencies of 10%. Excess grain-boundary recombination is a general problem in the polycrystalline materials, and a dramatic improvement in thin-film cell performance on low-cost substrates will require a reduction in the impact of these boundaries, and improvements in the quality of the thin films.

CHAPTER 2 EVAPORATION AND EPITAXIAL-FILM GROWTH

2.1 Introduction

The structure and electrical and photoconductive properties of CdS are extremely sensitive to conditions of deposition and to subsequent annealing treatments[26,27]. Various preparative parameters such as evaporation rate, vapour composition, source temperature, the nature of the substrate are important variables. Of equal importance are the vapour pressure, substrate temperature and impurity content of the source.

CdS film can be grown, in vacuum, using either a compound source of the material or molecular beam epitaxy using two sources, one of each of the constituent component Cd and S . Although commonly referred as a single process, the deposition of thin films by vacuum evaporation consist of several distinguishable steps : (1) transition of a condensed phase into the gaseous state, (2) vapour traversing the space between the evaporation source and the substrate, and (3) condensation of the vapour upon arrival on the substrate.

2.2 Vapourisation of source materials

2.2.1 Compound CdS

CdS is one of many compounds which, upon vacuum evaporation, sublime before a melting point is reached. It has been found to dissociate into a vapour composed of predominantly Cd atoms and S_2 molecules[28-30], together with smaller amounts of other species of sulphur: S_3, S_4, S_5, S_6, S_7 and S_8. The relative proportions of these heavier molecules of sulphur depend on the temperature of the evaporant and the pressure during evaporation.

The net dissociation rection can be written as

$$CdS\ (solid) \rightleftharpoons Cd\ (vapour) + \sum_{n=2}^{8} (\tfrac{1}{n})\ S_n\ (vapour) \qquad (2.1)$$

The shapes and sizes of the particles of the source material may influence the vapourisation of the source material. Poly-crystalline or powdered samples have large and uncontrollable surface areas, these can result in temperature gradients across the sample which produce a time varying evaporation rate, and therefore lead to variation in the composition of the vapour evaporating from the source material. The composition of the vapour above the source material varies significantly between equilibrium and non-equilibrium conditions. Berkowitz and Marquist[28] and Goldfinger and Jeunnehomme[29] have shown that CdS under equilibrium conditions has, within the experimental accuracy of a few percent, an exact stoichiometric composition, while Ya, Pikus et al.[31] showed that under non-equilibrium conditions. The Cd to S_2 flux ratio was as high as 100:1 initially at a source temperature of 900°C, falling over a period of many hours to a stable ratio of 14:1.

2.2.2 Molecular beam epitaxy

Molecular beam epitaxy (M.B.E)[32] is a term used to denote the epitaxial growth of compound semiconductor films by a process involving the reaction of one or more thermal molecular beams with a crystalline surface under ultra-high vacuum conditions. The main advantage of M.B.E lies with its improved control over individual incident atomic or molecular fluxes so that differences in sticking coefficient may be taken into account. The successes of M.B.E have been shown in the case of III-V compound semi-conductors such as GaAs and $Al_xGa_{1-x}As$ layers which have been

grown with electical and optical properties comparable to high quality material grown by conventional techniques. Devices such as IMPATT diodes[33], double heterojunction lasers[34] and optical waveguides[35] have been fabricated.

Ideally, the beam source should be in Knudsen cell[36-39] containing vapour and condensed phase at equilibrium; in this case the flux F at the substrate is then

$$F = \frac{P_{(T)}{}^{a}}{\pi L^{2}(2\pi mkT)^{1/2}} \quad \text{molecules/cm}^{2}.\text{s} \qquad (2.2)$$

where $P_{(T)}$ is the equilibrium pressure at the cell temperature T, a is the area of the cell aperture, L is the distance to the substrate and m is the mass of the effusion species. Equation 2.2 assumes an impinging angle of $\phi = 0^{o}$. The flux intensity distribution at various impinging angles ϕ is shown in Figure 2.1. In practice, a true Knudsen source, where the diameter of the orifice of the effusion cells must be about one-tenth or less of the mean free path of the gas molecules at equilibrium pressure $P_{(T)}$, is inconvenient because a wide aperture is needed to produce sufficient rate of mass transfer. In practice, the requirements of the source ovens should have (a) very low production of impurities in the molecular beam, either from outgassing or from reaction of the crucible wall with the content, (b) fairly small size so that several may be placed in close proximity to the substrate, (c) rapid thermal response in order that cell temperature may be accurately controlled, and (d) low radiant power loss and uniform temperature within the crucible. Cho and Arthur[32] in their evaporation of GaAs have used turbular crucibles (~1.5" x 3/4") open at one end made from pyrolytic BN or high purity graphite. Their crucibles

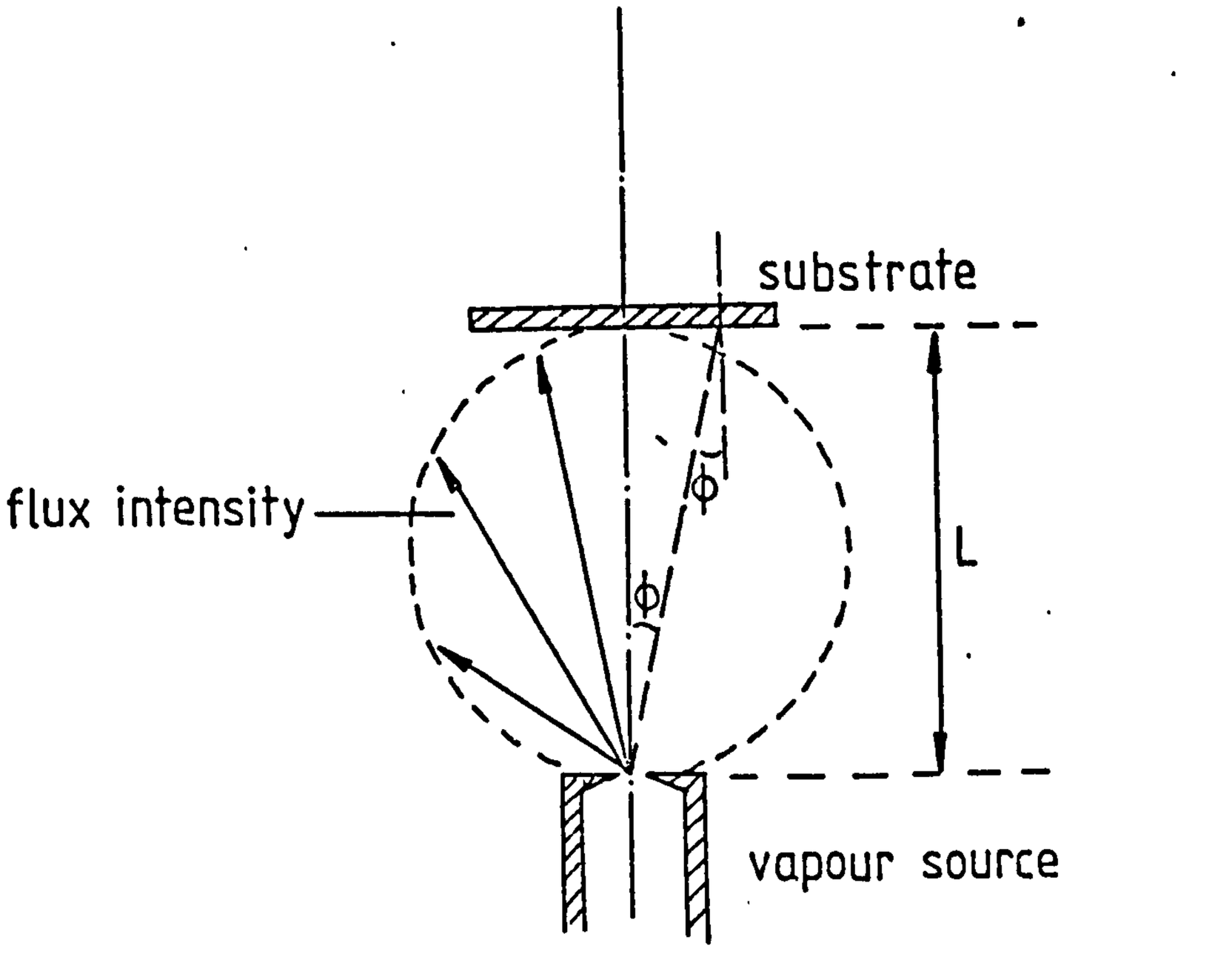

Fig. 2.1 Flux intensity distribution of vapour beam

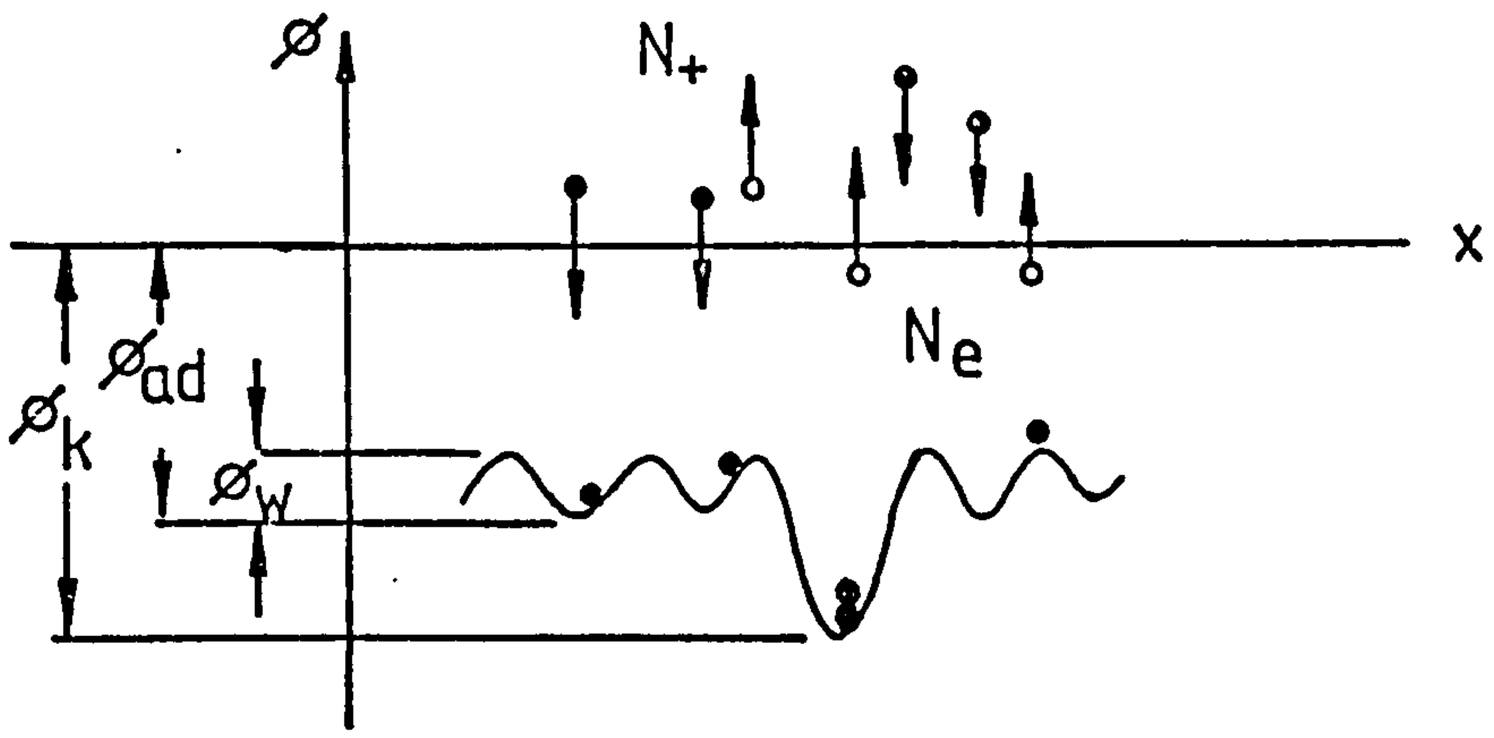

Fig. 2.2 Molecular process during condensation

N_+ = number of incident particles

N_e = number of reflected particles

ϕ_{ad} = energy of adsorption

ϕ_w = average energy of position-change

ϕ_k = energy of condensation

are mounted within spiral Ta heater winding which are themselves enclosed within Ta foil radiation shields. Outgassing was further reduced by providing cryogenic pumping in the form of a liquid-nitrogen-filled chamber surrouding the source ovens.

For source material to generate the molecular beam, pure elements of sulphur and cadmium would be more suitable than compound CdS. The reason is that a much lower source temperature is required to produce sufficient fluxes for film growth (Figure 2.8).

2.3 Condensation

The condensation of clemental vapour onto a solid surface is determined by its interaction with the surface on which it impinges. It is a function of complex adsorption, surface diffusion and nucleation phenomena[40-42]. When the vapour consist of two or more components, the process is further complicated by the interaction between the different vapour components.

During condensation, the following steps are considered to occur[42-45]. A vapour beam impinging on a condensation surface will be partially reflected. The main part, however, will be absorbed and at least temporarily retained on the surface. The adsorbed particles gain a definite surface mobility which is determined by the temperature and energy of the position change. If no re-emission to the vapour phase occurs during their surface diffusion, they will reach favoured, so-called growth centres of high bonding energy. Final condensation takes place at such sites. Growth centres exist at irregularities of the surface, such as at steps and edges of the already condensed film, or they are built by interaction with other adsorbed

particles.

The probability that an impinging particle will be adsorped, thermally equilibrated and incorporated into the substrate surface is called condensation coefficient, A, which is given by:

$$A = \frac{N_+ - N_e}{N_+} = 1 - \text{Const.} \times \exp(-\phi_{ad}/kT) \qquad (2.3)$$

where N_+ and N_c are the number of incident and reflected particles respectively per unit time and unit surface area. The condensation coefficient A depends strongly on the impinging density N_+, the condensation temperature T and the energy ϕ_{ad} of the adsorption (Figure 2.2).

The first comprehensive theoretical approach to the formation of thin-film was made by Frenkel[46]. He visualised the atoms condensing on the substrate as forming a two-dimensional gas and considered the kinetics of clustering of the atoms to form stable nuclei. This consideration led to the concept of a critical substrate temperature above which no deposition would take place. At a given substrate temperature there is also a critical deposition rate below which no deposition is possible.

Gunther[45,47] has analysed the problem of condensation of compounds consisted of more than one constituent. He developed an emperical model which gives a good description of the observed behaviour.

2.3.1 Gunther's model of evaporated film growth

The condition for progressive condensation at a given temperature involves exceeding a critical incident flux, i.e. the incident fluxes will condense on the substrate if and only

if the incident flux N_+ exceeds the critical flux N_{+c}. The condensation flux then rises rapidly and approaches its maximum value given by:

$$N_{k\ max} = \alpha(N_+ - N_e) \qquad (2.4)$$

where N_k is the condensed flux, α the sticking coefficient and N_e the emitted flux from the substrate. A schematic diagram showing this behaviour is given in Figure 2.3. The actual slope of the function $N_k = f(N_+)$ depends on the mechanism of nucleation, and can vary from one case to another.

If a constant flux N_+ of vapour particles on a substrate is assumed, the condition for progressive condensation can be expressed alternatively in terms of a critical substrate temperature T_c. The incident flux will condense on a substrate if and only if the substrate temperature T is below a critical temperature T_c. Thus by analogy with Figure 2.3, the condensation can be expressed schematically as a function of substrate temperature as shown in Figure 2.4, T_e is the equilibrium temperature corresponding to N_+ . During the deposition and condensation of the first monlayer of the incident vapour on an unlike substrate, the interfacial forces and consequently the critical value T_c may change, reaching a constant equilibrium value when the deposited layer itself acts as a substrate. All further condensation will be related to the equilibrium value because the first monolayer plays a relatively insignificant part in the process of film deposition as a whole.

If two different vapour beams of molecules consist of component A and B, both being incident on the substrate under consideration, it is necessary to look at the mutual reaction

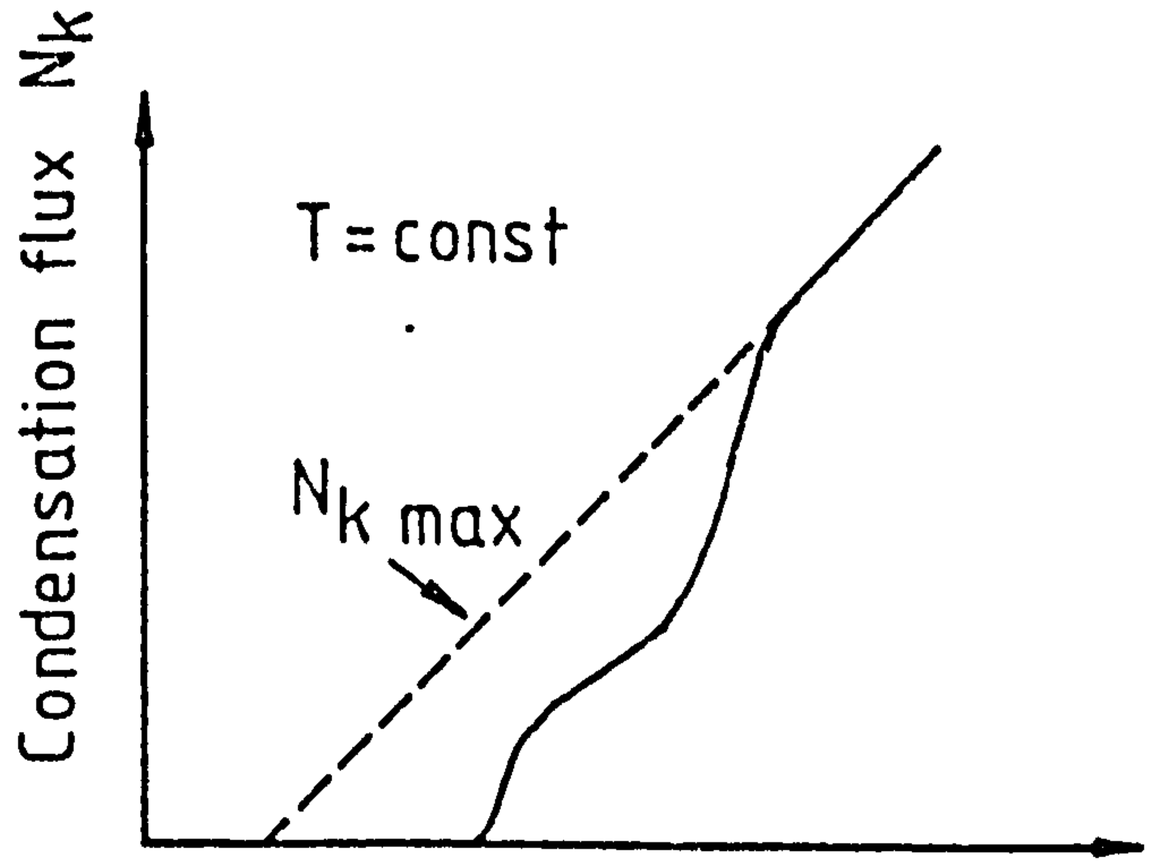

Fig. 2.3 Variation of condensation flux N_k with incident flux N_+

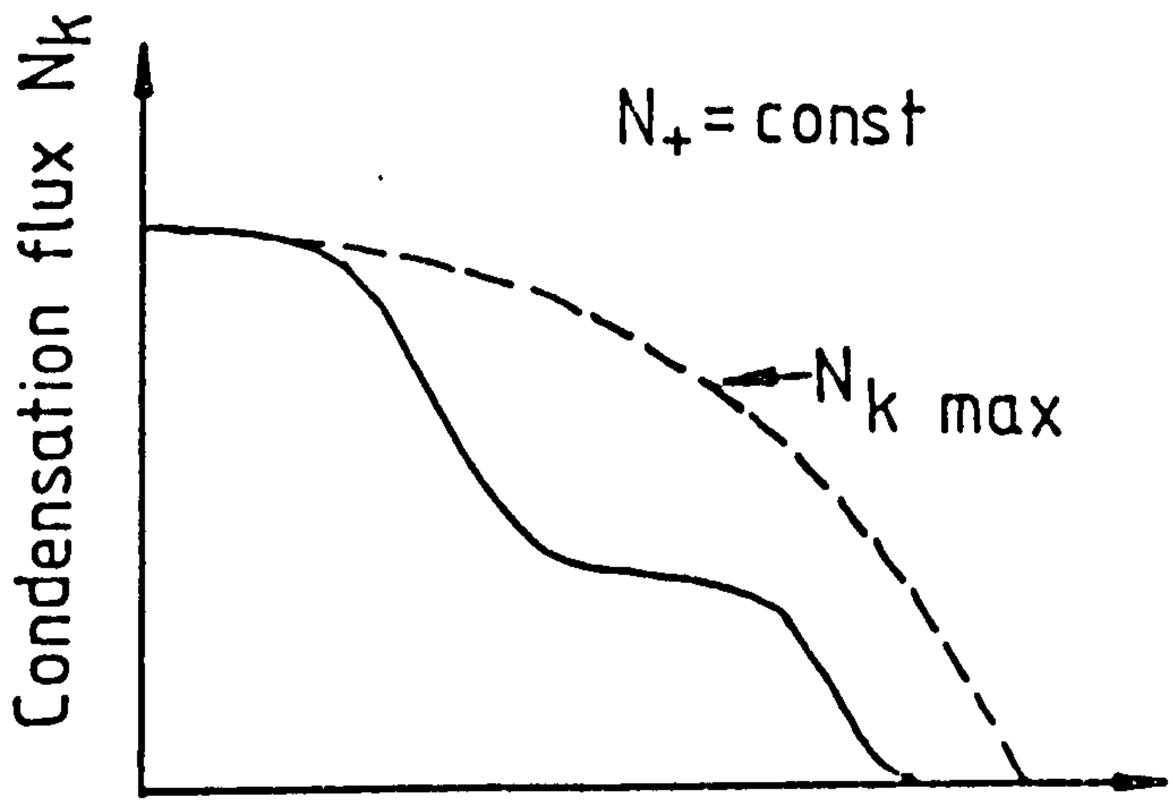

Fig. 2.4 Variation of condensation flux N_k with substrate temperature T

between both kind of molecules in addition to the phenomenon mentioned above. With evaporation process the usual density of N_+ varies from 10^{14} to 10^{18} particles per second per cm^2. No significant number of reactions between molecules A and B can take place in the vapour phase. They must react on the condensation surface while travelling in the adsorbed phase. These interaction may lead to the formation of molecules of a stable compound A_xB_y, where x and y may not equal.

An estimate of the interaction probability on the surface gives a density

$$n_{AB} \propto n_A . n_B . \bar{D} \qquad (2.5)$$

of adsorbed molecules AB. The density of either particle, n_A or n_B, is proportional to the actual vapour pressure P or the incident flux N_+ of that particular vapour. The density n_{AB} of the adsorbed molecules AB is therefore proportional to the product of the incident flux ($N_{+A} . N_{+B}$) or vapour pressure ($P_A . P_B$). $\bar{D}$ being the mean diffusion coefficient.

To determine the critical conditions for the condensation of a two-component vapour, the equilibrium pressure of the components P_{eA} and P_{eB}, and of the compound P_{eAB} must be considered. P_{eAB} usually corresponds to the dissociation pressure of the compound and is equivalent to the partial pressure $P_e(B/AB)$ of the more volatile compound, say B, in equilibrium with the compound. In most cases, this value is much lower than the equivalent vapour pressure P_{eB} of the component B. Thus, the critical values of one component B in the presence of the other component A, $N_{+cB}(A)$, can be expressed as

$$N_{+cB}(A) \ll N_{+cB} \; ; \quad \text{if} \quad P_e(B/AB) \ll P_{eB}$$

$$T_{cB}(A) > T_{cB} \tag{2.6}$$

That is, the critical rate at which B will condense when A is present is very much less than the critical rate at which it will condense when A is not present, assuming the pressure of B in the presence of A is much less than the pressure of B by itself.

Figure 2.5 demonstrate that at a given substrate temperature and for incident flux $N_{+A} < N_{+cA}$, no condensation of any kind is possible while the incident rate N_{+B} and the related adsorption density n_B are low. However, at a critical value $N_{+cB}(A)$, sufficient molecules AB are formed on the substrate to start nucleation and progressive condensation of the compound AB which then rapidly approaches the maximum flux $N_k = 2N_{+A} - N_{eA}$. The critical value $N_{+cB}(A)$ itself depends on the incident flux of component B; it is considerably lower than the analogous value N_{+cB} without the presence of A. When the maximum flux condition is reached, each incident A particle reacts with one of the simultaneously impinging B particle. With further increase of flux N_{+B}, no increase of condensation flux N_k is possible until $N_{+B} > N_{+cB}$ when the condensation of the non-interacting particles of B takes place, thereby increasing the total condensation flux to a final value of $N_{+B} + N_{+A} - N_e$. In terms of substrate temperature this is shown in Figure 2.6. With decreasing substrate temperature, the condensation of the compound AB starts at a certain critical value T_{cAB} and continues with decreasing temperature to $T_{sub} < T_{cA}$, where additional condensation of pure component A occurs. This results in a further increase

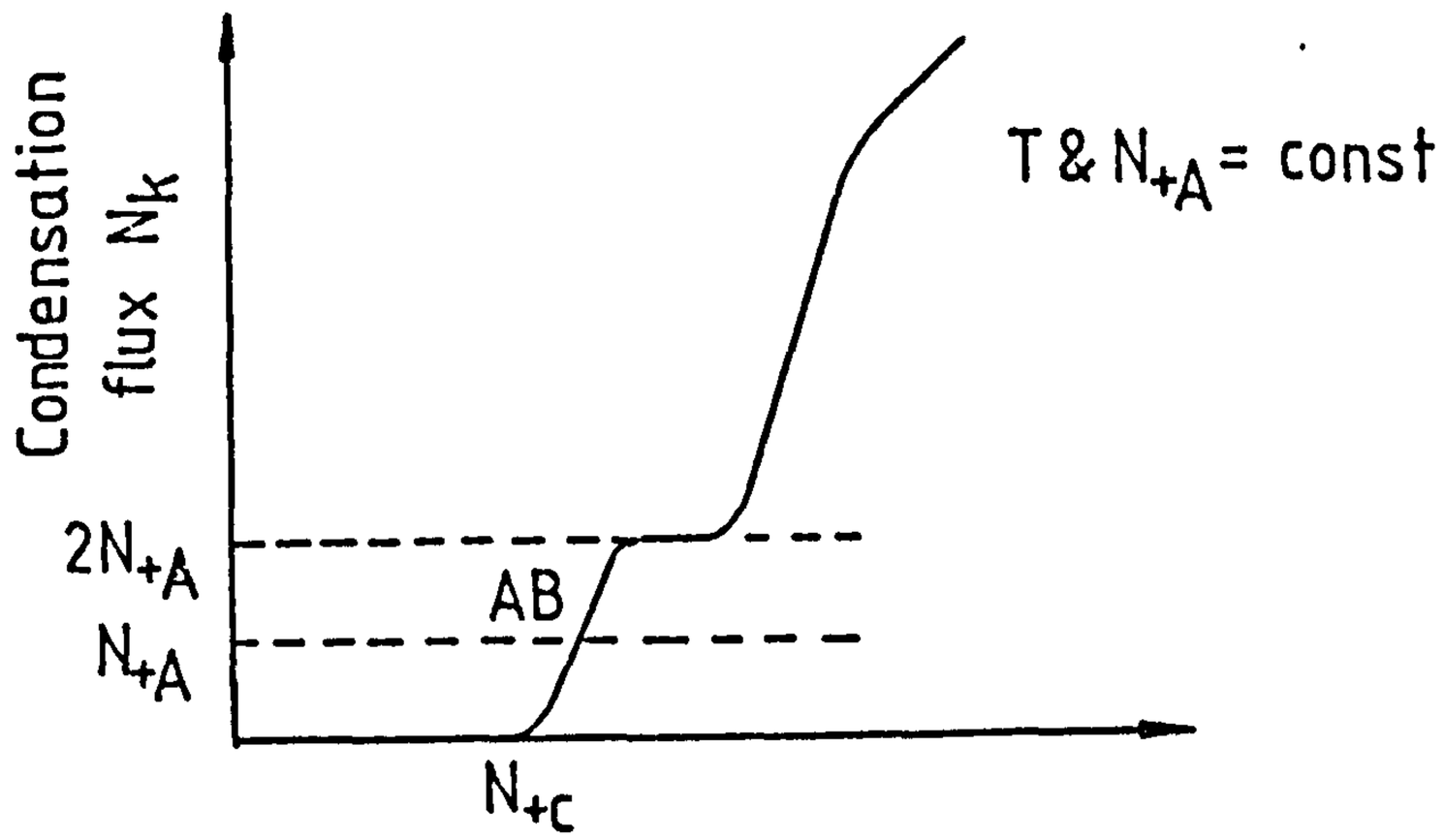

Fig. 2.5 Condensation flux N_k vs. Incident flux N_{+B}

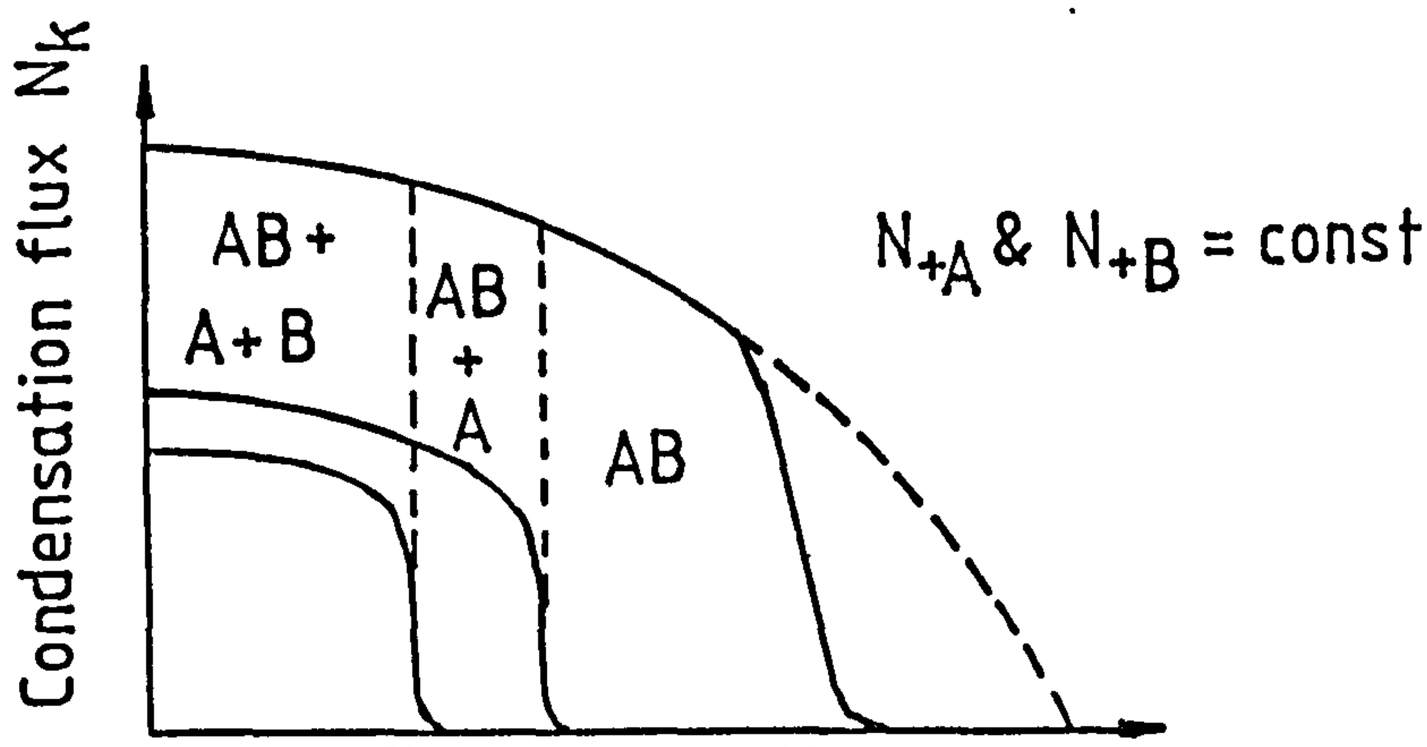

Fig. 2.6 Condensation flux as a function of temperature

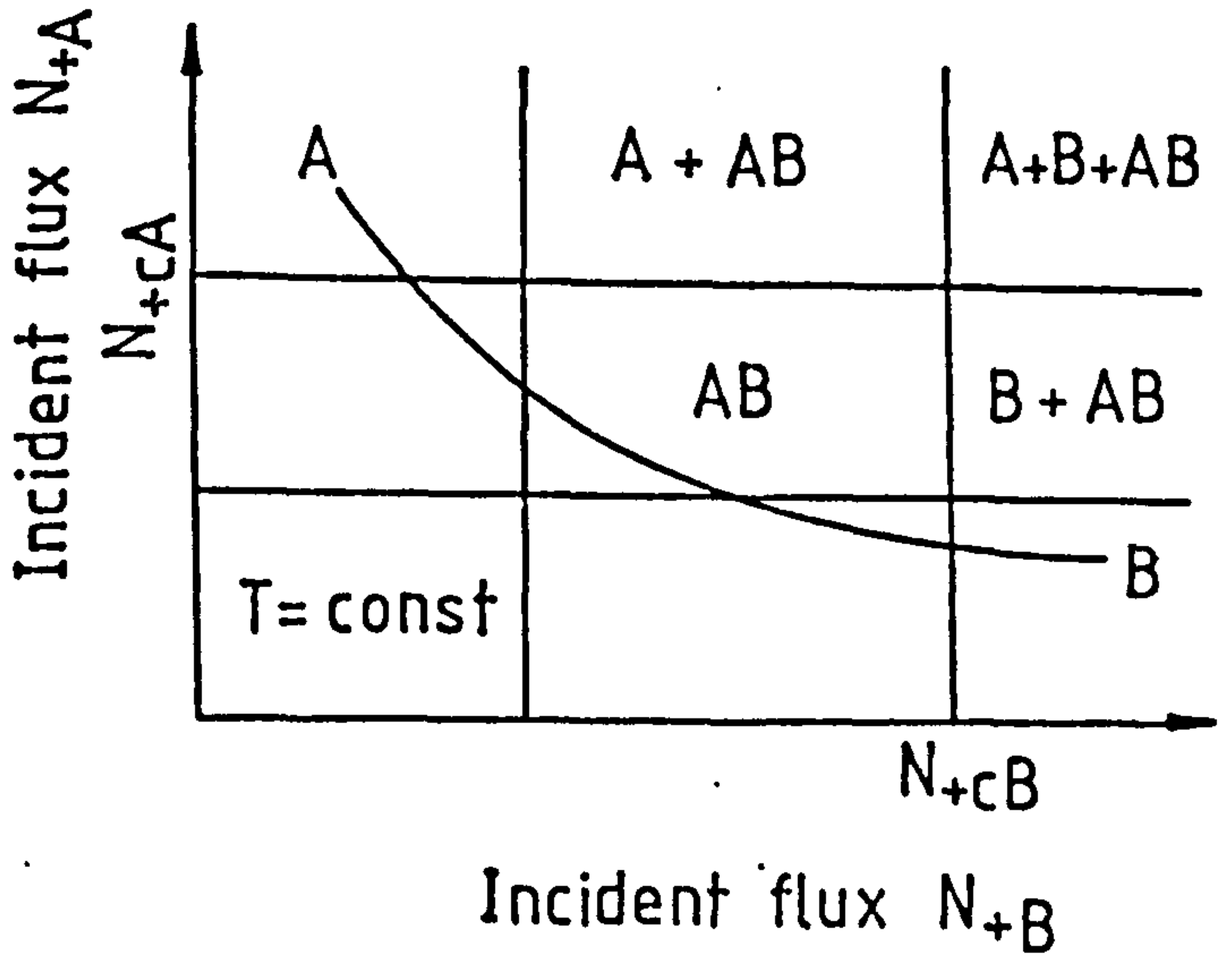

Fig. 2.7 Composition of resultant film

in N_k which rapidly approaches a final value.

In contrast to the conditions for single components, the critical values T_{cAB}, N_{cAB} of the compound can be very different from the equilibrium values since the adatom densities of the two components, and not the existing compound, determine the condensation flux. Hence not only the condensation flux, but also the composition of the condensed film, are affected by the incident fluxes and substrate temperature. This is shown in Figure 2.7. It can be seen that there exist one region that only stoichiometric compound layers of composition AB are obtained, while the unsaturated components are reemitted into the vapour phase. This region is defined by the straight lines $N_{+A}=N_{+cA}$, $N_{+B}=N_{+cB}$, and by the curve $(N_{+A}.N_{+B})=\text{const.}$, as indicated by equation 2.5 above. This stoichiometric region should occur in all cases where

$$P_e(i/AB) < P_{ei} \; ; \quad i=A,B \qquad (2.7)$$

is satisfied. The area of the region is dependent on the substrate temperature T and increases with T, within a limited temperature range. Provided the above assumptions are correct, the deposition of exact stoichiometric compound layers should be possible by simultaneous evaporation of the constituent components. For this purpose, it is merely necessary to have a suitable substrate temperature and adequate incident rates for both components, none of which are critical.

2.3.2 Cadmium - Sulphur system

The composition of saturated sulphur vapour has been the subject of much investigation for more than half a century. It

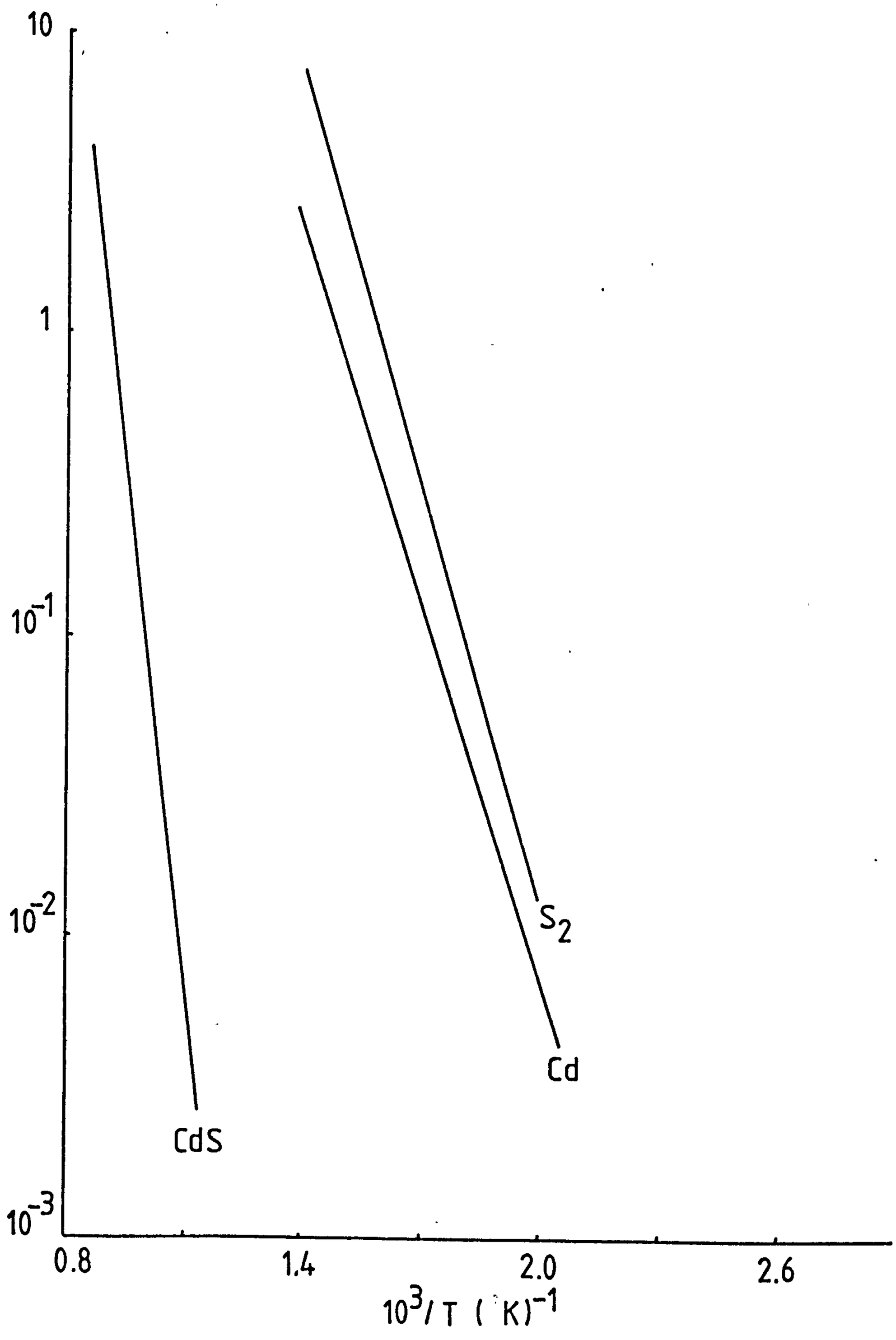

Fig. 2.8 Vapour pressure of CdS, Cd and S_2

is well known that if a complex vapour such as sulphur is superheated, the equilibrium constituent in the vapour is of simpler (lower molecular weight) species. From all available evidence, sulphur vapour at 2500°C and 10^{-5} torr is probably monoatomic. The vapour-density measurements of Braune et al.[48] showed that the degree of association should increase monotonically with decreasing temperature (at constant pressure) and should approach pure S_8 at saturation point. Cadmium[49], on the other hand, in common with most metals is monoatomic in the vapour phase. The curves of equilibrium pressure for the elements cadmium and sulphur, in the interval of interest, are shown in Figure 2.8. They are relatively close together. Sulphur being more volatile than cadmium. The elements can react with each other to form the stable compound

$$Cd + \frac{1}{2}S_2 \longrightarrow CdS. \qquad (2.8)$$

CdS usually has the wurzite (hexagonal) structure but the existence of the zinc-blende (cubic) structure is also possible. The stacking arrangement in the related structures is illustrated in Figure 2.9. The basic difference between the two structure is the stacking sequence of the atomic layers. In the wurzite structure the atomic stacking pattern can be represented as A-B-A-B etc. whereas in the zinc-blende structure the repetition of stacking occurs according to A-B-C-A-B-C etc. The vapour pressure of CdS at a given temperature is far below the values of the components (Figure 2.8). The assumption according to equation 2.6, and the conditions for the existence of a "stoichiometric range" are therefore satisfied.

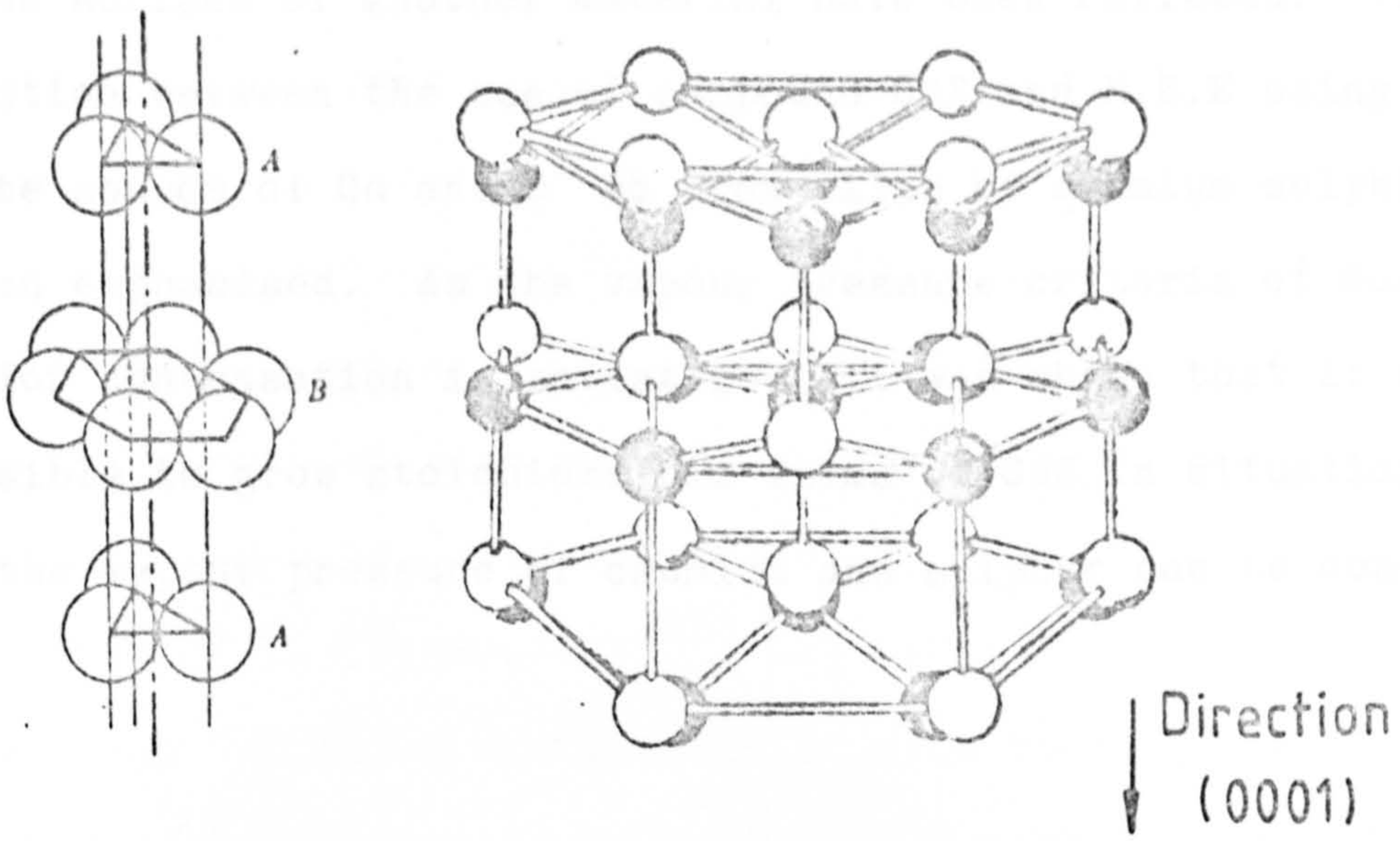

(a) Hexagonal

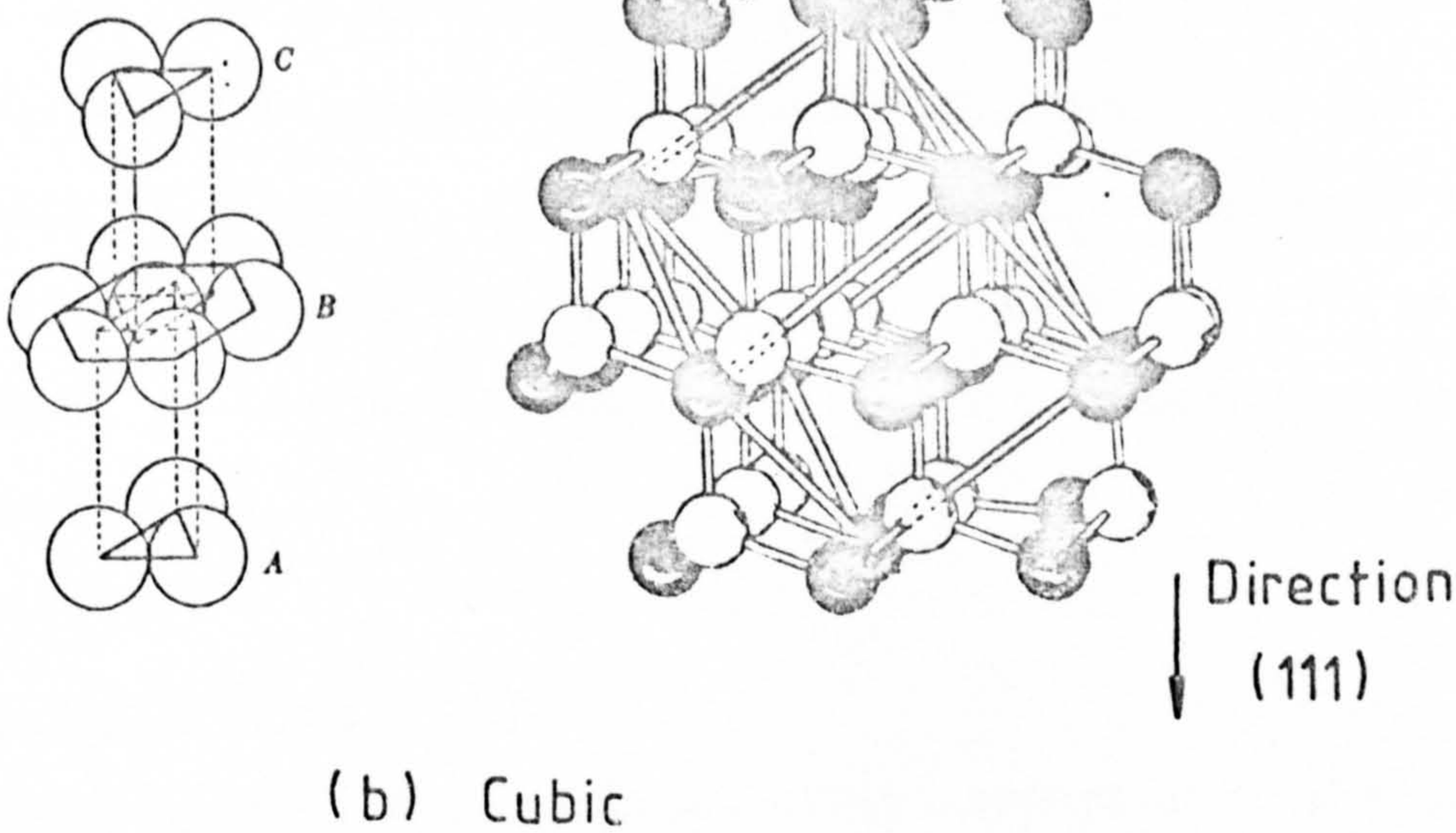

(b) Cubic

Fig. 2.9 Structure symmetry in (a) wurtzite (ABAB) and (b) zinc-blende (ABCABC) layers

2.4 Summary

In this chapter the vapourisation and condensation of CdS onto the surface of another material have been reviewed. The distinction between the use of compound CdS and M.B.E using a separate source of Cd and S to grow films of cadmium sulphide has been emphasised. As the vapour pressure criteria of Gunther's model for condensation is satistfied, it was shown that it should be possible to grow stoichiometric films of CdS in situation where the vapour pressure of cadmium and sulphur can be controlled.

CHAPTER 3 p-Si/n-CdS HETEROJUNCTION SOLAR CELLS

3.1 Introduction

Numerous investigators have studied the photovoltaic characteristics of a range of heterojunction solar cells fabricated by growing a semiconductor film on a single crystal substrate. Within the past few years, four alterative CdS-based heterojunction solar cells now exist with more than 5% energy conversion efficiency. These are the traditional Cu_2/CdS cell[19] and the novel InP/CdS[18], $CuInSe_2$/CdS[22] and CdTe/CdS[20] solar cells. The fact that CdS films are present in each case affirms the importance of CdS thin-film technology. A feasibility investigation on Si/CdS structure has been carried out here by the deposition of CdS films on Si substrates. The advantage of the Si/CdS cell is the high availability of single crystal Si substrates. The photovoltaic characteristics of heterojunction solar cells are expected to be strongly influenced by the processing techniques. Therefore, the effect of the device fabrication processes e.g. substrate doping and CdS film growth conditions, on the photovoltaic properties of the heterojunction were studied.

3.2 Heterojunction effects

The idealised band diagrams of two examples of the p-Si/n-CdS heterojunction given in Figure 3.1 are based on the Anderson model[50] and show the effects of changes in Si doping. The diagrams do not include the effect of charged interface states or traps within the bandgap. The diffusion potential can be varied by changing the doping of either or both of the semiconductor materials. It is clear that the above model does not

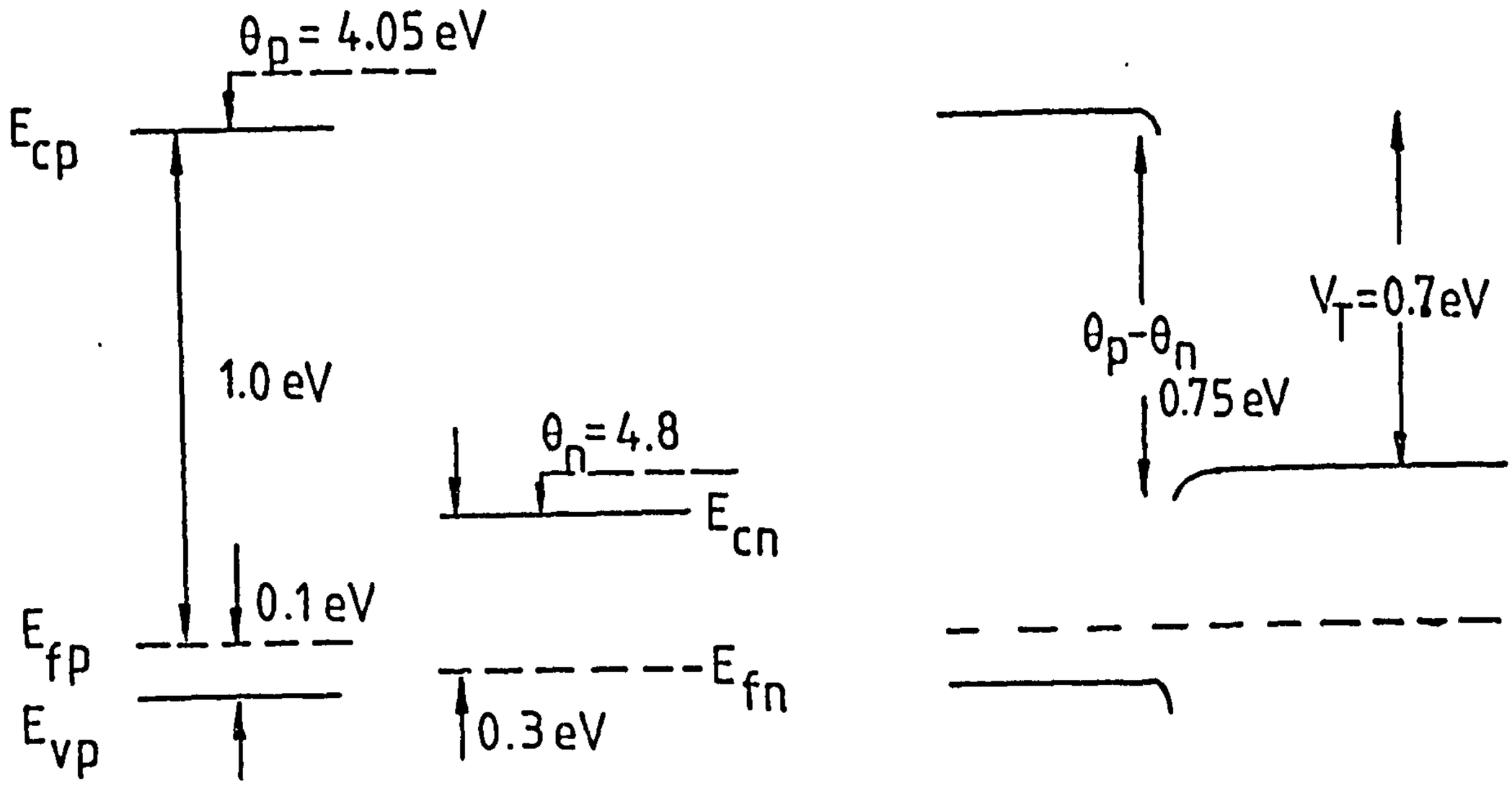

Fig. 3.1(a) $N_A = 3 \times 10^{17}$ cm^{-3}

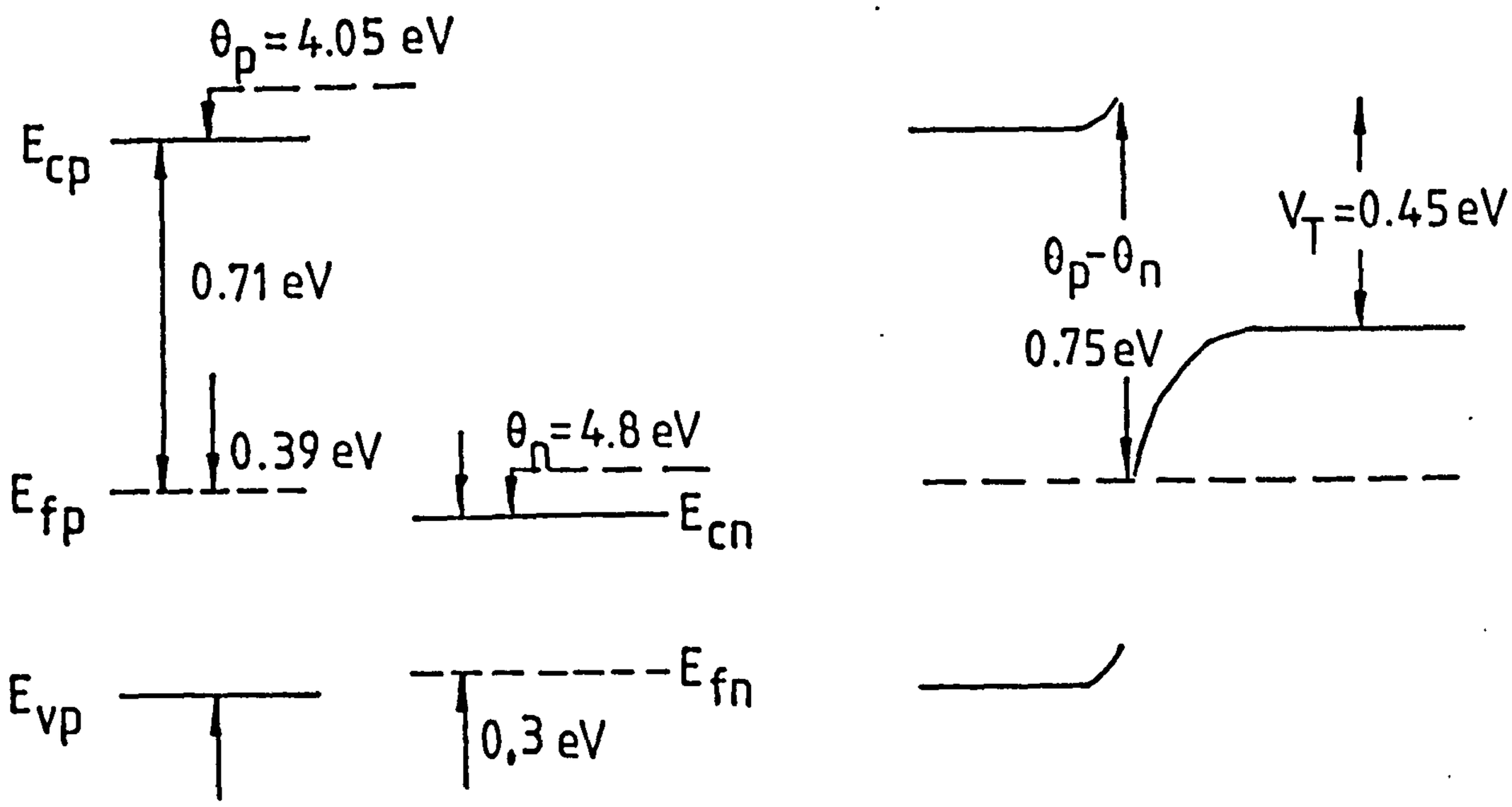

Fig. 3.1(b) $N_A = 6 \times 10^{12}$ cm^{-3}

adequately represent the p-Si/n-CdS heterojunction experimentally, mainly due to the effect of surface states present on the surface of both semiconductors[51,52] and interface states produced by strains caused by the different lattice properties of the materials[53,54]. Thus even before contact is made between the semiconductors the energy bands may be bent and therefore have considerable effects on the junction formed. As the effects of surface and interface states cannot be quantified, the idealised model therefore can only be expected to predict approximate values.

3.3 Growth of CdS on Si substrates

Holt[55] has shown that there exist a cut-off temperature of the deposition of compound/substrate combinations, above which no film is deposited. The cut-off temperature is well defined, unlike the gradual fall in sticking coefficent with increasing substrate temperature. The cut-off temperature is insensitive to contamination.

In the case of Si substrates the cut-off temperature is far below that of the substrate sublimation temperature and varies with the compound being evaporated. Holt found that, in general, for Si substrate held above the cut-off temperature, when a II-VI compound was evaporated onto the surface, a pitted, roughened or tarnished appearance was obtained. This suggested that some form of chemical attack reaction had taken place.

The case of CdS on Si has been studied in detail by Holt and Steyn[55]. The deposition cut-off temperature at 10^{-5} torr was only 300°C and only polycrystalline films were obtained below this temperature. Cleaner techniques and a better vacuum (a oil-free pressure of 10^{-9} torr) brought the cut-off

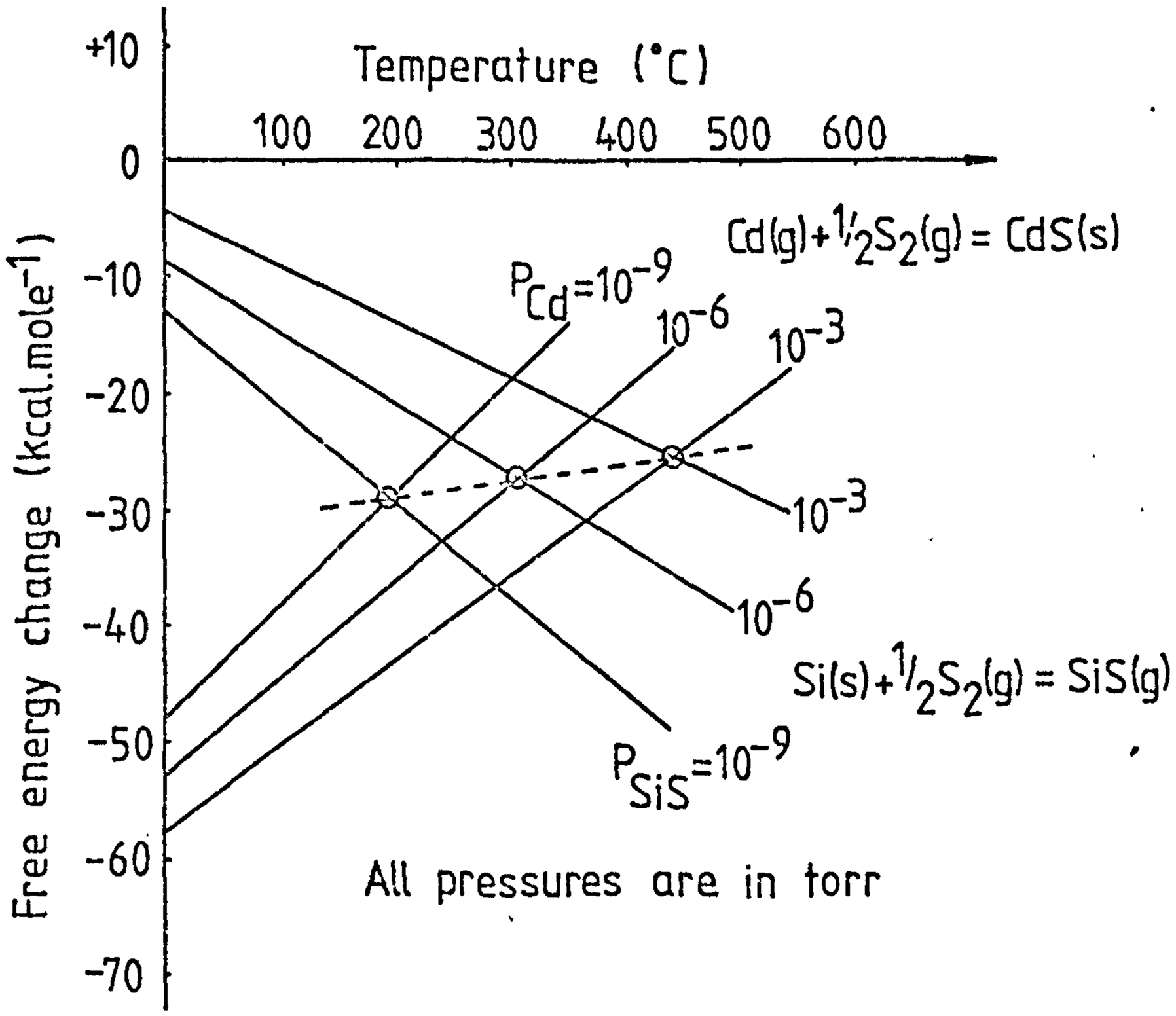

Fig.3.2 Free energy changes between Cd and S vapour and Si

temperature down to 250°C. Thermodynamic calculations were made of the free energy changes involved in the reaction:

$$\begin{aligned} Cd\ (g) + 1/2\ S_2\ (g) &\longrightarrow CdS\ (s) \\ Si\ (s) + 1/2\ S_2\ (g) &\longrightarrow SiS\ (g) \\ Si\ (s) + S_2\ (g) &\longrightarrow SiS_2(s) \end{aligned} \qquad (3.1)$$

where (s) and (g) indicated that the material is solid or gaseous, respectively. The essential features of the results are shown in Figure 3.2. At a given temperature and pressure, the lowest energy signifies the most favourable reaction. If the silicon substrate is at 200°C with a pressure of 10^{-6} torr, CdS will nucleate and grow. However, at 300°C both reactions are equally favourable and above this temperature the mono-sulphide formation dominates. The cut-off temperature is thus determined by the pressure of the constituent gases, and in particular by the more volatile component which in this case was sulphur. Holt and Steyn[55] confirmed experimentally that the cut-off temperature was in fact pushed up to 400°C by increasing the sulphur pressure in the vacuum system to this extent. Increased in sulphur pressure is thought to promote the formation of an SiS_2 compound rather than the SiS, as the former is less volatile it will deposit on the silicon surface and form nucleation sites, allowing the CdS to grow.

3.4 Vacuum equipment

The vacuum system used here for CdS evaporation onto Si substrates was a U.H.V system consisting of an all stainless chamber evacuated by a 50 litres per second diode ion pump backed by a two stage 200litres per second rotary pump with a zeolite

trap to evacuate the chamber to 10^{-3} torr prior to the starting of the ion pump. A schematic diagram of the vacuum system is shown in Figure 3.3. A titanium sublimation pump (T.S.P) cooled by liquid nitrogen was attached to the chamber. The liquid nitrogen also acts as a cryopump. Cryopumping gave a much faster pumping speed which was advantageous because of the amount of thermal outgassing during thermal cleaning of the Si substrate. The entire system was baked out at $100^{o}C$ for 12 hours in order to achieve a residual pressure below 10^{-9} torr.

An Edward E12 oil-pumped coating unit giving a vacuum of 3×10^{-5} torr was used for metal evaporation. Metal coatings were either evaporated from a filament heater or an electron beam gun. Metal thicknesses were typically of about 0.5 micron.

3.5 Fabrication technique of p-Si/n-CdS heterojunction solar cells

The process involved in the fabrication of the Si/CdS heterojunction solar cell can be divided into the following operations:- Polishing, oxidation, diffusion, cleaning of Si, CdS evaporation, photolithography, and bonding.

3.5.1 Polishing

The silicon used for fabrication was supplied unpolished by R.S.R.E. The silicon wafer was mechanically polished to an optical finish, using a carborundum powder for initial polishing and one micron diamond compound for the final operation. After polishing, the silicon was thoroughly washed successively in electronic grade trichloroethylene, acetone and deionised water before oxidation in the next process.

All mechanically lapping or polishing of silicon tends to leave the surface layers structually damaged. This damaged

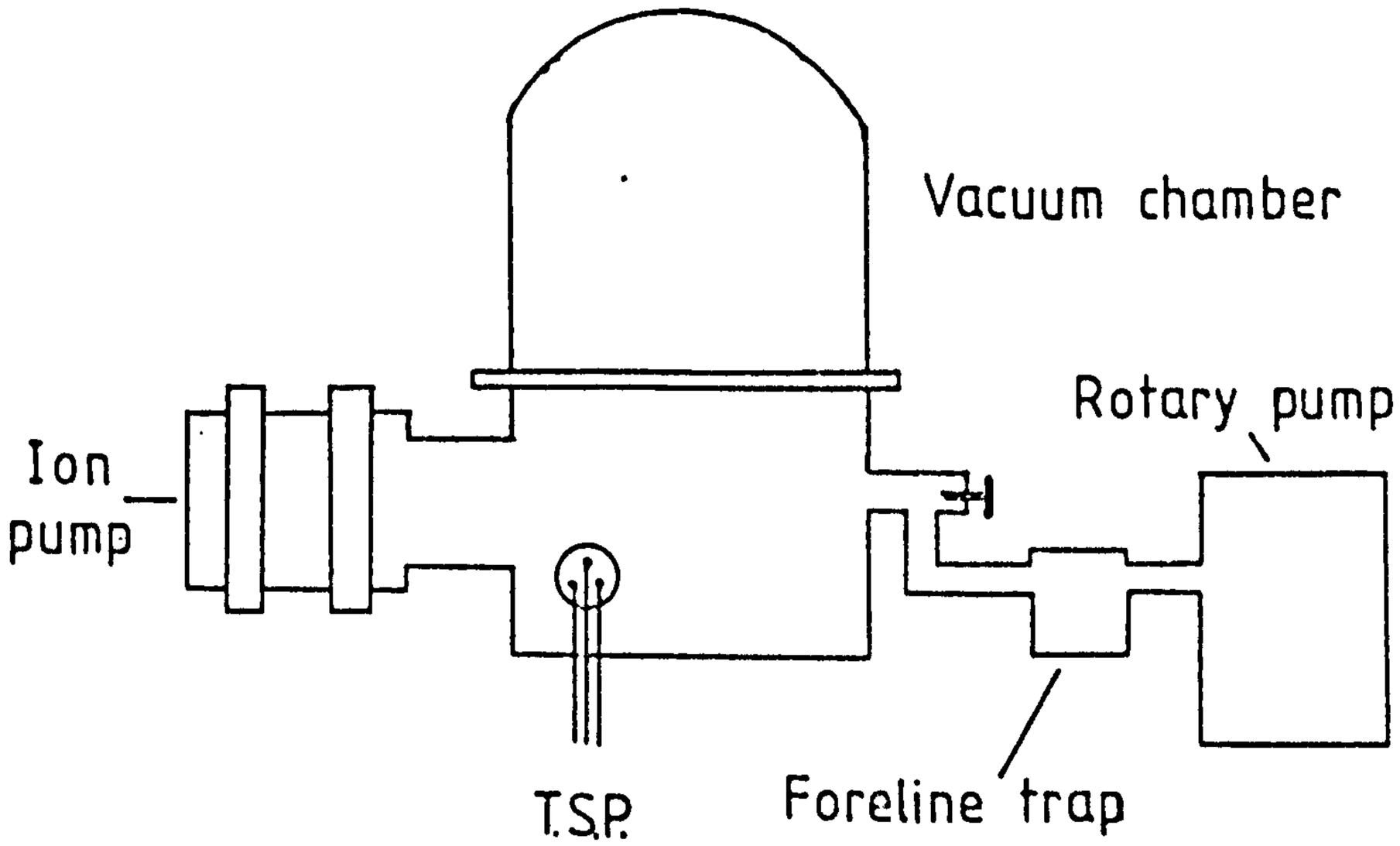

Fig. 3.3 Vacuum system

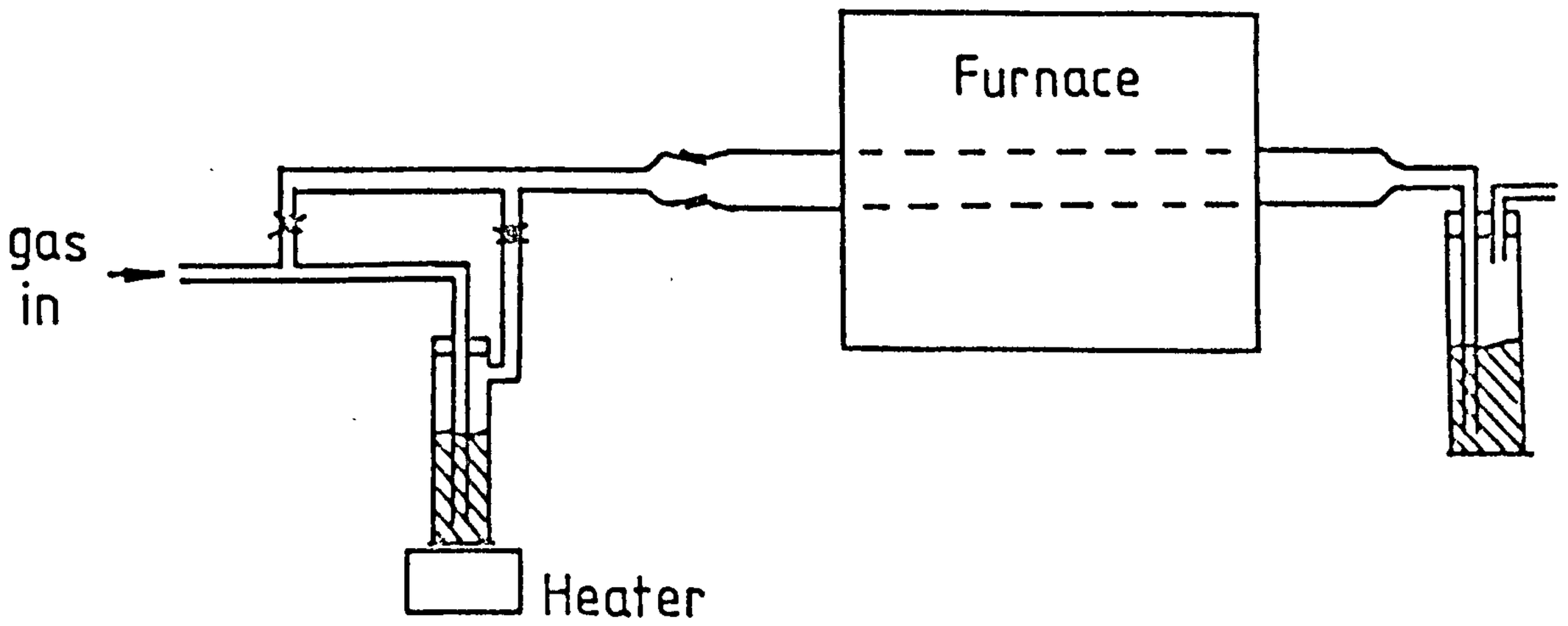

Fig. 3.4 Oxidation and diffusion furnace

layer was removed by oxidation of the surface and followed by etching of the oxide with buffered hydrofluoric acid.

3.5.2 Oxidation

This process shields the cleaned silicon surface from any unwanted contaminants, Thermal oxidation[56] was the method used for the production of SiO_2 on the silicon wafer surfaces. The silicon wafers were placed in a furnace at 1200°C. Wet oxygen was then passed through one inch diameter quartz furnace tube coupled to the remaining parts of the system by 'Q' type glass to glass fittings on the input of the furnace. Wet oxygen was obtained by passing dry oxygen at 0.6 litre per minute through a heated water bath at 90°C. Since oxidation proceeds much more rapidly in water vapour than in dry oxygen, the water content of the carrier gas is the most important variable in determing the oxide thickness for a given time and temperature. To prevent condensation, a heating tape was wound round the entrance of the quartz furnace tube which was exposed to the ambient. The oxide thickness obtained, for the condition described, was 0.6 micron after two hours of oxidation at 1200°C. This thickness was shown to be adequate to prevent boron diffusion into SiO_2 protected surfaces[57]. Figure 3.4 shows the layout of the furnace.

The next process was to protect one side of the SiO_2 covered silicon surface with Dettel paint. This enables the SiO_2 on the unprotected side be removed by hydrofluoric acid, which then allows boron diffusion for ohmic contact.

3.5.3 Diffusion

The diffusion process in the Si/CdS heterojunction fabrication

produces a heavily doped p surface for ohmic contact to the back surface. Diffused layers of either conductivity type are normally formed in two steps. In the first step, called the predeposition step, impurities are introduced into the surface of the silicon. The maximum amount of impurity that can dissolve in the silicon, the solubility limit[58,59], can be used to determine the doping level. Once the impurities are introduced onto the silicon surface, they are then diffused to the required depth. This is the drive-in step. The impurity profile is dependent on the time and temperature at which the diffusion is carried out. From the initial impurity concentration, the depth of the diffusion can be calculated if the diffusion constant of the impurity in the silicon is known[59].

Boron nitride[60] was used throughout as a source of boron for diffusion in silicon. The Union Carbide "Ucar" grade H.B.G. boron nitride was in the form of a white wafer. This was placed about 0.5 cm from the silicon during the predeposition step. Before the boron nitride could be used, it was activated in oxygen at 0.5 litre per minute for 30 minutes at 950°C. Once oxidised and stabilised, the boric oxide produced on the surface of the boron nitride was used as the boron source. The silicon wafer was placed behind the boron nitride wafer, both being perpendicular to the direction of flow of the nitrogen gas, which was passed over the wafer at 0.2 litre per minute at 950°C for 30 minutes. The furnace used for the diffusion process was similar to that used for the oxidation process (Figure 3.4). The nitrogen gas was introduced directly into the furnace and the output of the furnace was connected to the ambient via a water "bubbler".

A short drive-in period of 30 minutes was performed at

1100°C with wet oxygen gas flowing at 0.2 litre per minute after predeposition. This stage was not essential as far as making ohmic contact to the silicon surface was concerned, but the film so formed acted as a boron sealer so that boron on the doped surface may not out-diffuse during electron-beam cleaning of the silicon substrate in a later process. A four-point probe was used to verify that the resistivity of the silicon was sufficiently low for ohmic contact. It was found that staining effects on the surface of the silicon caused by the formation of silicon nitride were non existent if the furnace temperature was maintained below 1100°C.

3.5.4 Silicon cleaning in vacuum

Silicon is known to react with atmospheric oxygen to form a SiO_x layer, $(1 \leq x \leq 2)$, which may be as thick as 30Å[61]. It is desirable to remove this layer prior to the growth of the CdS film. The reason is that (a) adhesion of CdS film on SiO_x layer is poor and inconsistent, (b) the structure of the oxide layer, being armorphous, will influence the growth conditions for epitaxy[62], and (c) the resultant interfacial insulating oxide layer will affect the barrier potential at the junction interface. Removal of the oxide layer on the silicon wafer so that CdS film may evaporate onto a clean surface of silicon is therefore necessary. This was achieved by cleaning the silicon surface with hydrofluoric acid followed by deionised water before the substrate was placed into the vacuum system. Thermal cleaning[63] was then used in vacuum prior to CdS evaporation. Haneman[64] has shown that this procedure allows several minutes of working time after cleaning if the vacuum is below 10^{-8} torr.

The temperature required to clean silicon thermally in

vacuum depends on the partial pressure of oxygen at the surface. Lander and Morrison[65] found that there was a critical temperature above which a clean surface could be obtained, and the greater the excess of the temperature over the critical value, the greater was the rate of cleaning. This process, however, is not often used with semiconductor materials as they often decompose before a temperature which is sufficient for the cleaning effect to occur is attained.[66]

Several techniques are available to raise the silicon temperature to about 900°C to produce the cleaning effect, such as resistive heating[67,70], argon ion bombardment[68] and electron-beam bombardment[69,71]. The simplest techniques to produce the requied temperature of about 900°C appear to be resistive heating and electron-beam bombardment. The resistively heated tungsten radiator of Jones et al.[70] and Unvela et al.[67], while able to produce uniform heating at the required temperature, would require an electrical power of 1/2 kW and thereby would involve an internal heat shield with water cooling to minimise excess degassing from adjacent equipment within the vacuum chamber. The electron-beam bombardment technique, however, requires only about 180W for a uniform temperature of 1000°C across a silicon wafer diameter of 19mm. The main advantage of electron-beam heating is that the heated region can be increased or decreased to suit the sample, and thereby outgassing can be kept to a minimum.

The electron-beam gun was designed by W. Duncan and A.R. Smellie and used electrostatic focussing[71]. The electrons were focussed onto the reverse of the silicon wafer as shown in Figure 3.5. The area of heating can be varied by varying V_1 and V_2. A temperature of the silicon in excess of 1400°C

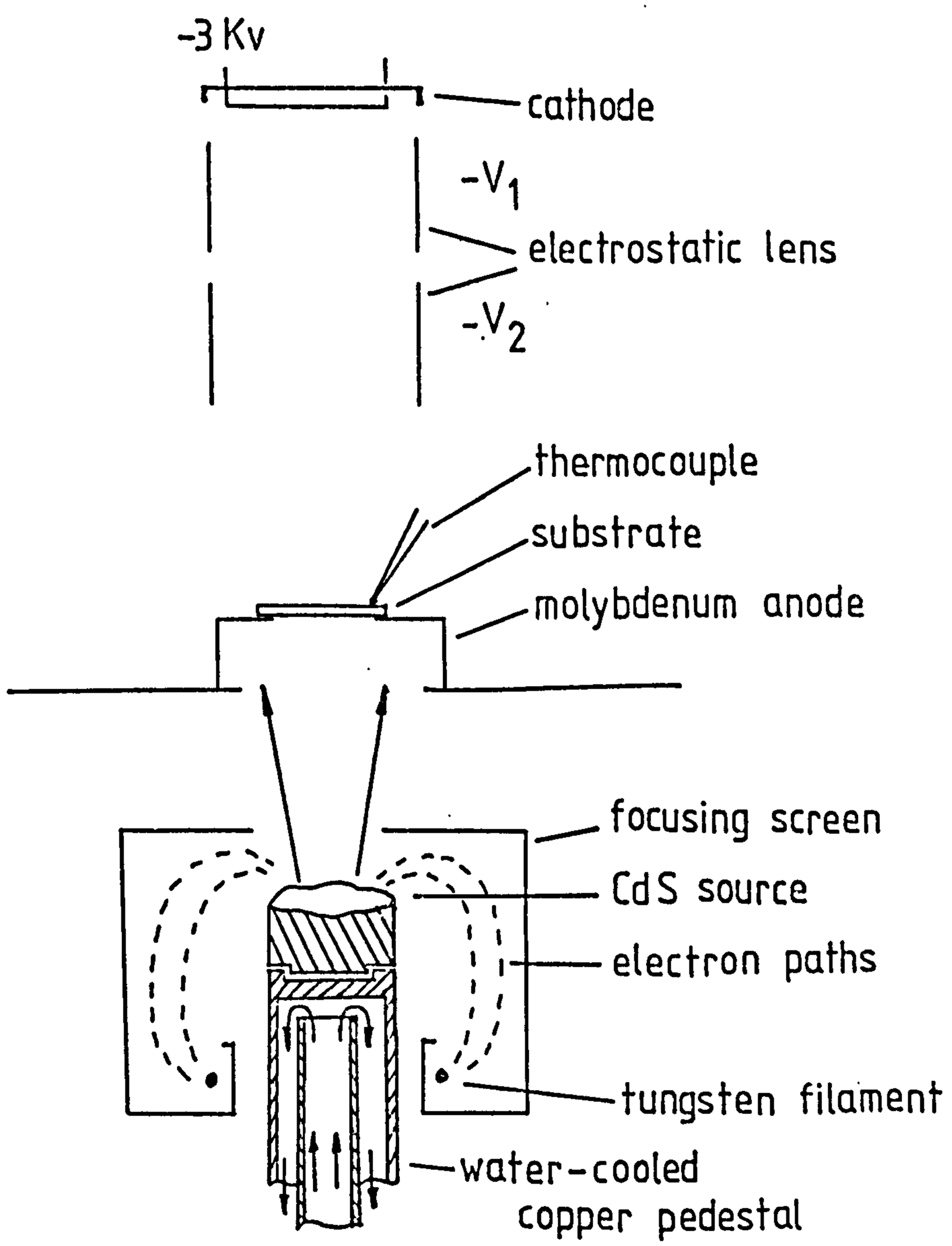

Fig. 3.5 Electron beam gun assembly

could be achieved, this was uniform across the wafer.

At a high enough temperature, silicon as well as SiO_x can be evaporated[70]. This may be beneficial for it removes surface damages created during polishing. In this particular case, however, the complete evaporation of the SiO_2 on the back surface would allow the out-diffusion of boron and thereby the doping of the Si/CdS interface. Smellie[61] found that a substrate temperature of 900°C held for 5 minutes was sufficient to remove from a chemically cleaned silicon wafer surface the thin SiO_x layer which had formed at room temperature, and together with any remaining solvent or chemical contaminants, without the occurance of excess thermal etching or SiO_2 removal. As there was no surface-study equipment, such as LEED or Auger, available, the main criterion for sufficient cleaning was the good adhesion of CdS film on silicon. X-ray back-reflection Laue photographs showed that polycrystalline CdS were obtained on (111) oriented silicon at a growth temperature of 200°C, whereas CdS film grown at 320°C on the same type of substrate showed preferred orientations. The cut-off temperature, above which no film growth occurred, was found to decrease with thermal cleaning. This is thought to be caused by the absence of impurities on the cleaned substrate acting as nucleation centres. Heterojunction devices fabricated using cleaned silicon showed significantly more reproducible characteristics compared with those made from "uncleaned" silicon.

The temperature of the substrate during electron-beam cleaning and CdS film growth was measured by a platinum-platinum 13% rhodium thermocouple which made a pressure contact on top of the silicon. As the platinum forms a eutectic with silicon at about 1000°C, a small piece of thin molybdenum sheet was

placed between the thermocouple and the silicon substrate.

3.5.5 CdS evaporation

CdS films were grown at a pressure below 10^{-7} torr, using an electron gun (Vacuum Generator type EG2) on (111) oriented silicon substrate which had been previouly cleaned at 900°C for 5 minutes. The EG2 electron gun, shown in Figure 3.5, utilised a water-cooled hearth. The hearth held approximately 0.5g of source material, which limited the film thickness obtainable. The substrate temperature was maintained by another electron gun mounted vertically above the substrate. A schematic diagram of the electron-beam gun assemblies is shown in Figure 3.5. Typical substrate temperature during CdS film growth ranged from room temperature to 320°C. The cut-off temperature above which no film growth took place on thermally cleaned silicon was 340°C. At room temperature, the films were dark and cadmium-rich; while at higher temperatures yellow sulphur-rich films were obtained. Typically, film thicknesses of two microns at 240°C, decreasing to approximately one micron at 320°C, were obtained.

The source material used was either single crystal Eagle Picher grade A or polycrystalline BDH Optran electronic grade cadmium sulphide. Mass spectrometer readings during evaporation showed no significant changes in the relative amplitudes of the Cd and S_2 peaks with changes in source temperature. The evaporation rate of the CdS was not controlled, other than by holding the emission current of the electron-beam gun constant during the evaporation.

3.5.6 Photolithography and bonding

Electrical contact to the Si/CdS heterojunction solar cell was made by evaporation of aluminium onto CdS to form a contact area defined by a photolithographic process. Contact to the boron doped Si surface was made by evaporated aluminium. Electrical connections to the metal electrdes deposited on CdS films were made using a Hughes Model HPB-360 pulsed thermal compression bonding machine to attach gold wires.

A positive-working Shipley AZ-1350H photoresist was used in the photolithographic process. The area of the resist exposed to light through a photographic mask became polymerised, and was removed by washing in a developer, leaving only the resist which was not exposed to the light. The exposed area of the CdS in the shape of the photographic mask was then coated by aluminium. The surplus metal film on the resist coated CdS was then removed by a lift-off process, leaving untouched the metal grid contact to the CdS film. It was found that 0.5 micron was the optimum metal thickness for lift-off and thermal bonding.

No attempts was made to optimise the design of the contact grid. The metal contact on the CdS face was of the "fingered" congiguration shown in Figure 3.6.

3.6 Results

3.6.1 Characteristics of CdS films

The transport properties of CdS films are known to be highly sensitive to small changes in their chemical composition and to crystallographic imperfections. The use of thin CdS film in device structures requiresnot only the specification of a wide range of common electrical characteristics such as

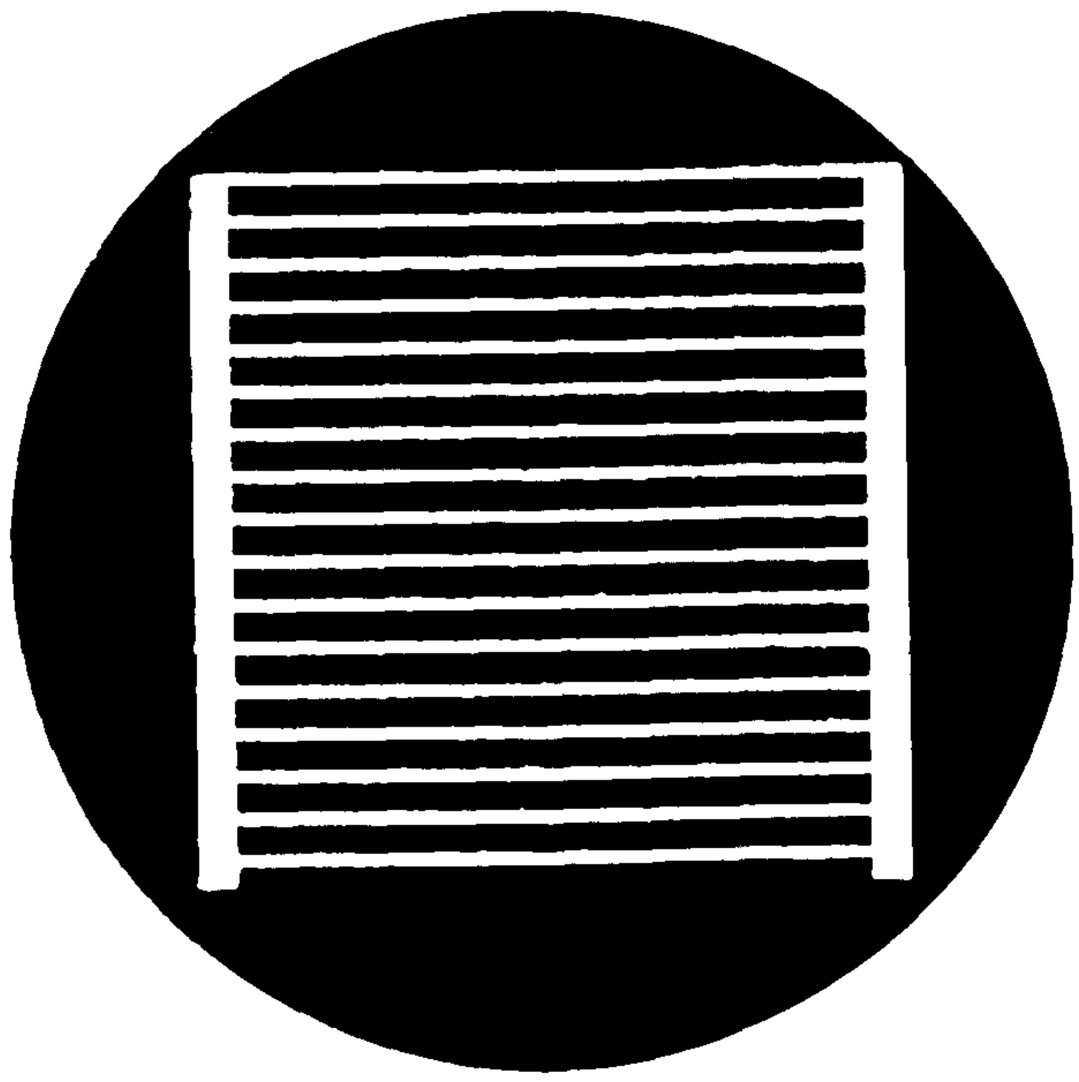

Fig. 3.6 Contact grid on CdS face

resistivity, mobility and lifetime, but also high levels of chemical and structural perfection. It is therefore desireable to produce a CdS film whose quality, if not the same as the bulk, can be predicted from it. It has been shown that CdS films grown on several different substrates[55] have the crystal structure of good quality bulk material. Films of such quality, however, have not been achieved using silicon as a substrate, and it was for this reason that some effort was put into the characterisation of the CdS film grown on (111) oriented silicon for the Si/CdS solar cells.

Investigations into the structure of the CdS films were carried out using two of the main X-ray diffraction techniques viz., the Laue and powder method[72]. A Phillips diffractometer with nickel-filtered Cu Kα radiations and a pulse height discriminator was used for the powder method. The back-reflection Laue was performed using unfiltered cobolt radiations.

3.6.2 Crystallographic structure of evaporated CdS

The powder method using a Phillips diffractometer was also employed to find the orientation of polycrystalline CdS films grown on (111) oriented Si. The presence of only (002) and (004) reflections indicated that the films consisted of hexagonal CdS structure. The C-axis of the CdS was close to the normal to the silicon substrate.

Back-reflection Laue was used to examine CdS films on (111) oriented silicon substrates at growth temperature ranging from 200°C to the cut-off temperature of 340°C. On a thermally cleaned substrate it was found that polycrystalline films grew at 200°C indicated by the ring diffraction patterns, whereas streaky spots appeared at 320°C. Photographs of the diffraction

patterns at substrate temperature of 200°C and 320°C are shown in Figure 3.7. Analysis of the symmetry of the diffraction pattern indicated that the films were of the hexagonal structure with preferred orientations. The cut-off temperature above which no film grew on thermally cleaned Si substrates was found to be 340°C.

The importance of thermal cleaning of the Si substrate prior to CdS deposition was investigated. Films were grown on chemically cleaned Si substrates up to the cut-off temperature. X-ray Laue diffraction of the CdS films showed that all the films were polycrystalline. A Laue diffraction pattern of a CdS film grown at 340°C on (111) oriented silicon which has not not cleaned is shown in Figure 3.8.

The resistivity of the CdS films deposited on high resitivity (10^5 ohm cm) (111) oriented silicon substrates at deposition temperatures from 200°C to the cut-off temperature did not varied significantly, and were of the order of 10 ohm cm.

The CdS film thickness was found to decrease with an increase in the deposition temperature. At 200°C CdS films of two microns were produced, and the thickness decreased to less than one micron at 320°C.

3.6.3 J-V characteristics

The current density-voltage characteristics of the cells were measured using an x-y chart recorder. A tungsten lamp was used to approximate AM1 conditions and the intensity of 100 mW/cm^2 was calibrated by means of a pyrometer.

When the J-V measurements are plotted as $\log_e(J)$ versus bias voltage, it is possible to calculate the diode "perfection factor" n, the parameter described by the normal p-n junction

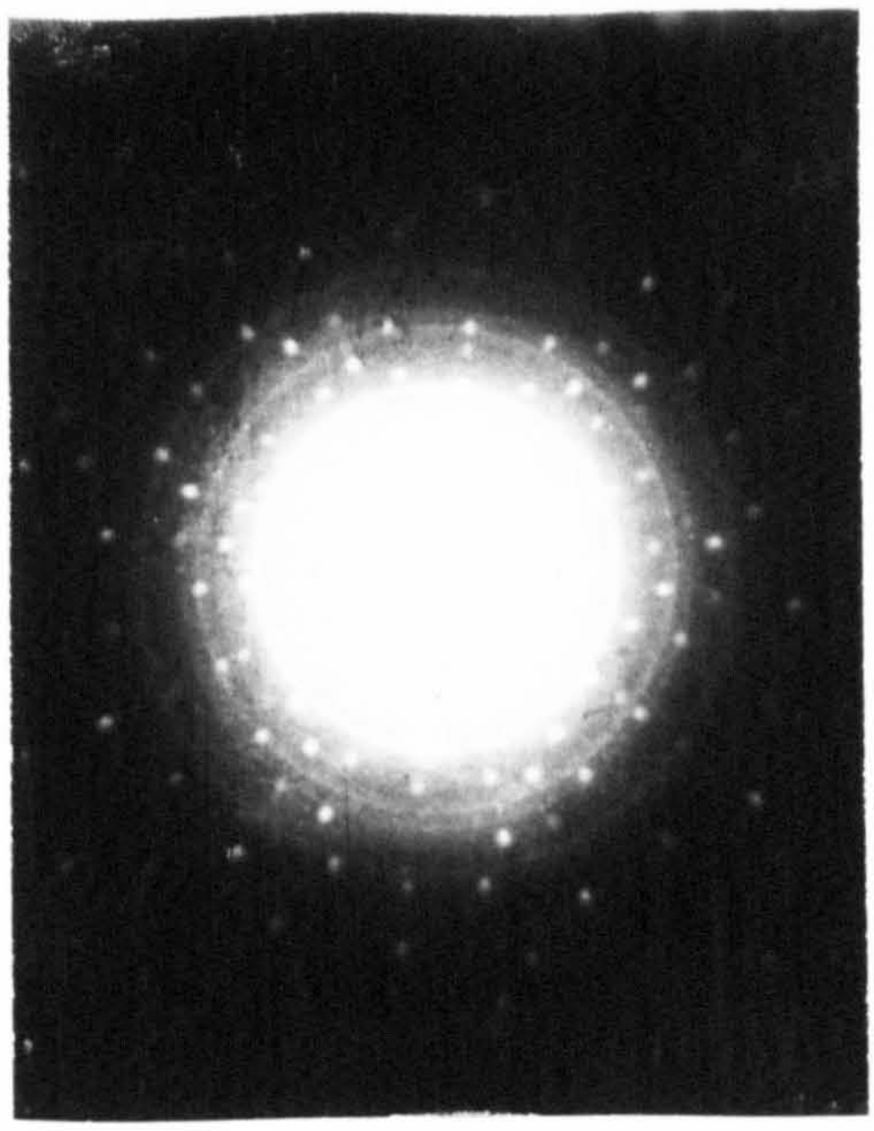

Substrate temperature = 200 °C

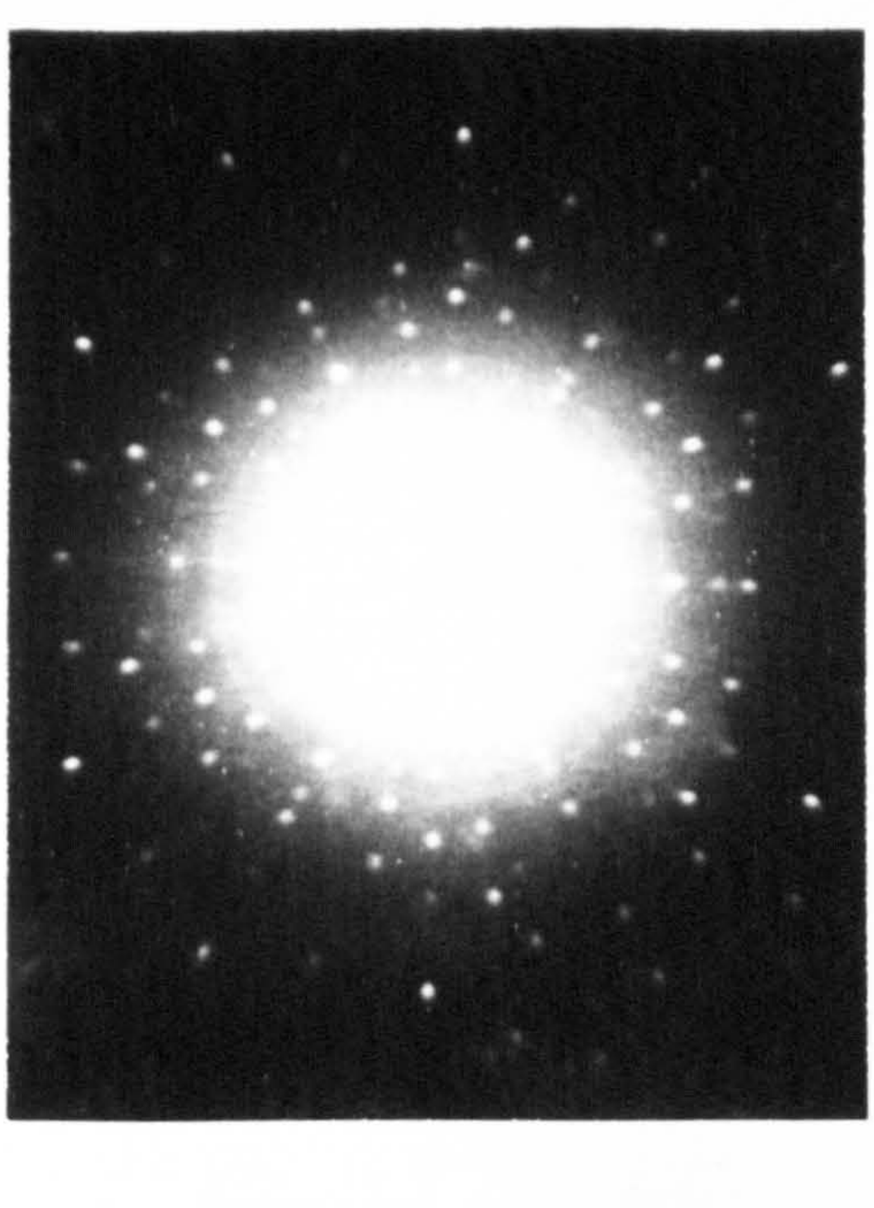

Substrate temperature = 320 °C

Fig. 3.7 X-ray Laue photographs of CdS on (111) Si

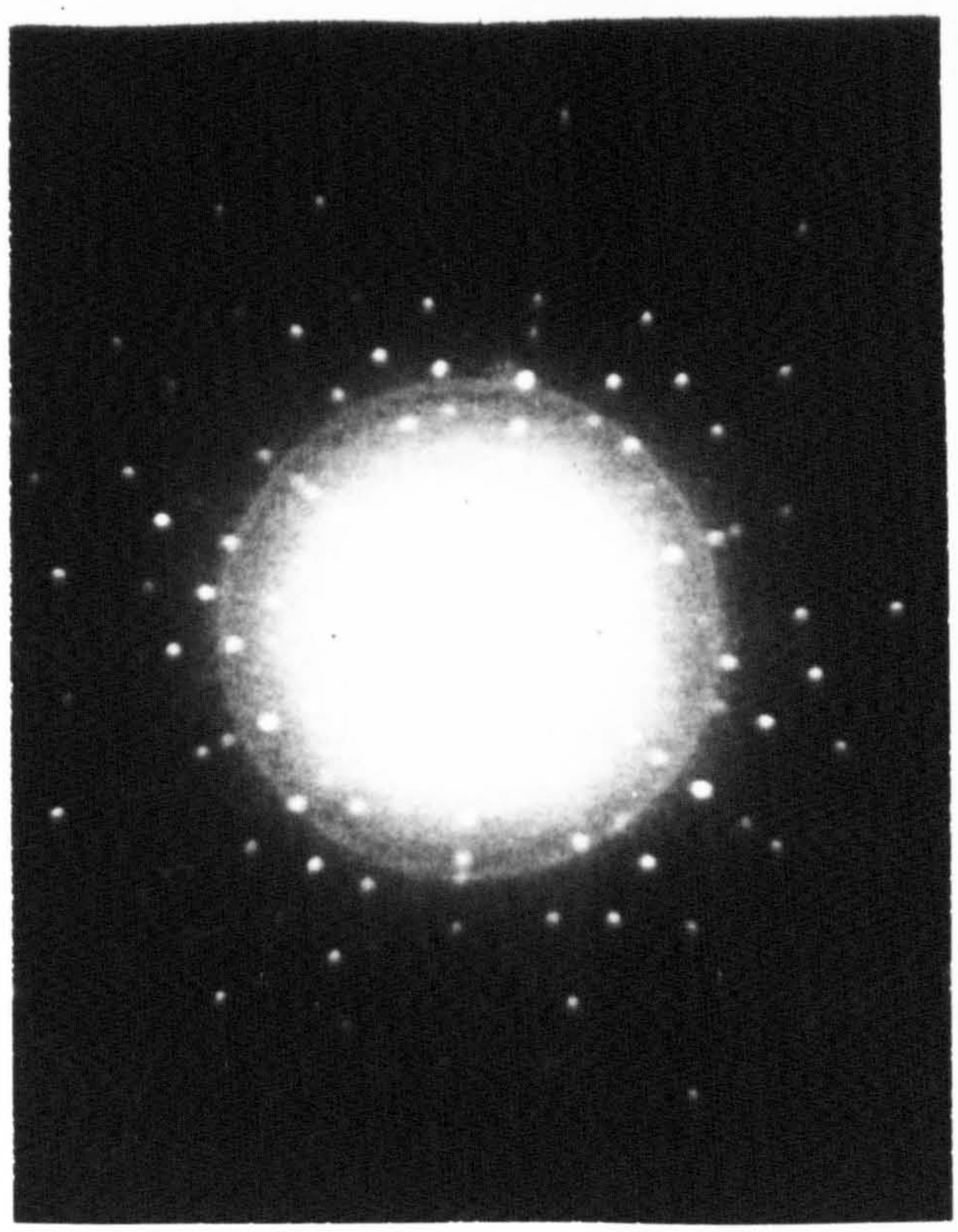

Fig. 3.8 X-ray Laue photograph of CdS film grown at 340 °C on (111) oriented Si

The substrate was not electron beam cleaned

equation

$$J = J_s \exp(qV/nkT) \qquad (3.2)$$

The value of the n can be calculated from the slope of the straight line portion of the characteristic which is equal to q/nkT.

3.6.4 Experimental results

The electrical properties of Si/CdS heterojunction solar cells, illustrating the effect of thermal cleaning of the Si substrate prior to CdS deposition are shown in Table 3.1. The thermally cleaned cells are significantly better than "uncleaned" ones. The current density-voltage characteristics of cells fabricated with 150 ohm cm (111)oriented silicon substrates that have been thermally cleaned and "uncleaned" are shown in Figure 3.9a and Figure 3.9b respectively. Corresponding plots of $\log_e(J)$ versus bias voltage are shown in Figure 3.10a and Figure 3.10b respectively. The diode factors n are 3.3 for the cleaned cell and 5.6 for the "uncleaned" sample. The high values of n, much higher than 2, indicated that effects other than recombination are involved, for example, trapping effects in the CdS film and interfacial defects at the heterojunction. The J-V characteristics with illumination intersect the dark characteristics, this behaviour is typical of the devices fabricated. Shirdland[73] suggested that it is due to photo-resistive effect in the CdS film. It could also be due to the photogeneration of electrons from traps present in the CdS film, the free electrons then being injected over the barrier. The injected current reduces the open circuit voltage as the forward bias voltage required to balance the photo-electron current

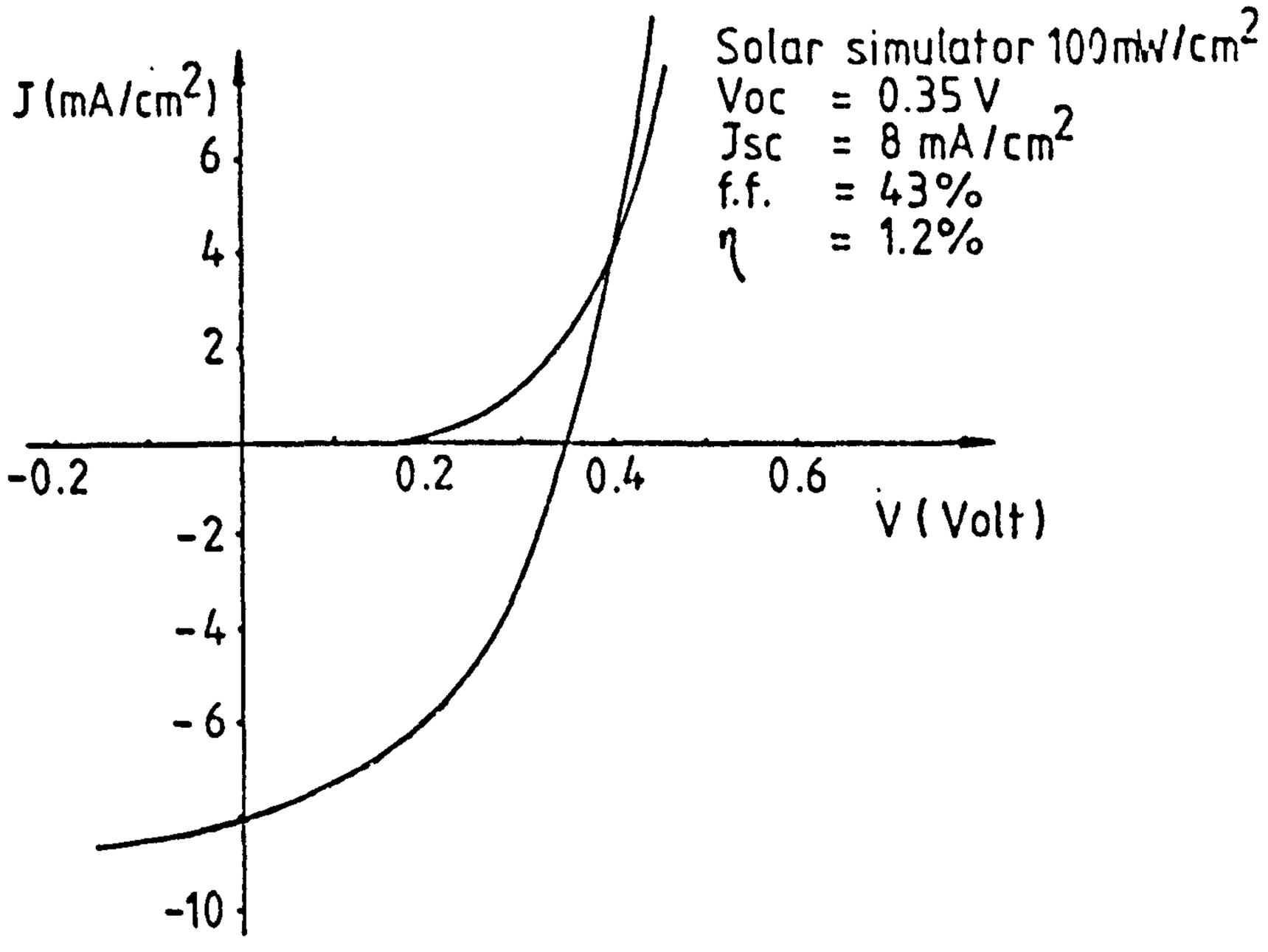

Fig. 3.9a Photovoltaic response of thermally cleaned n-CdS/p-Si cell

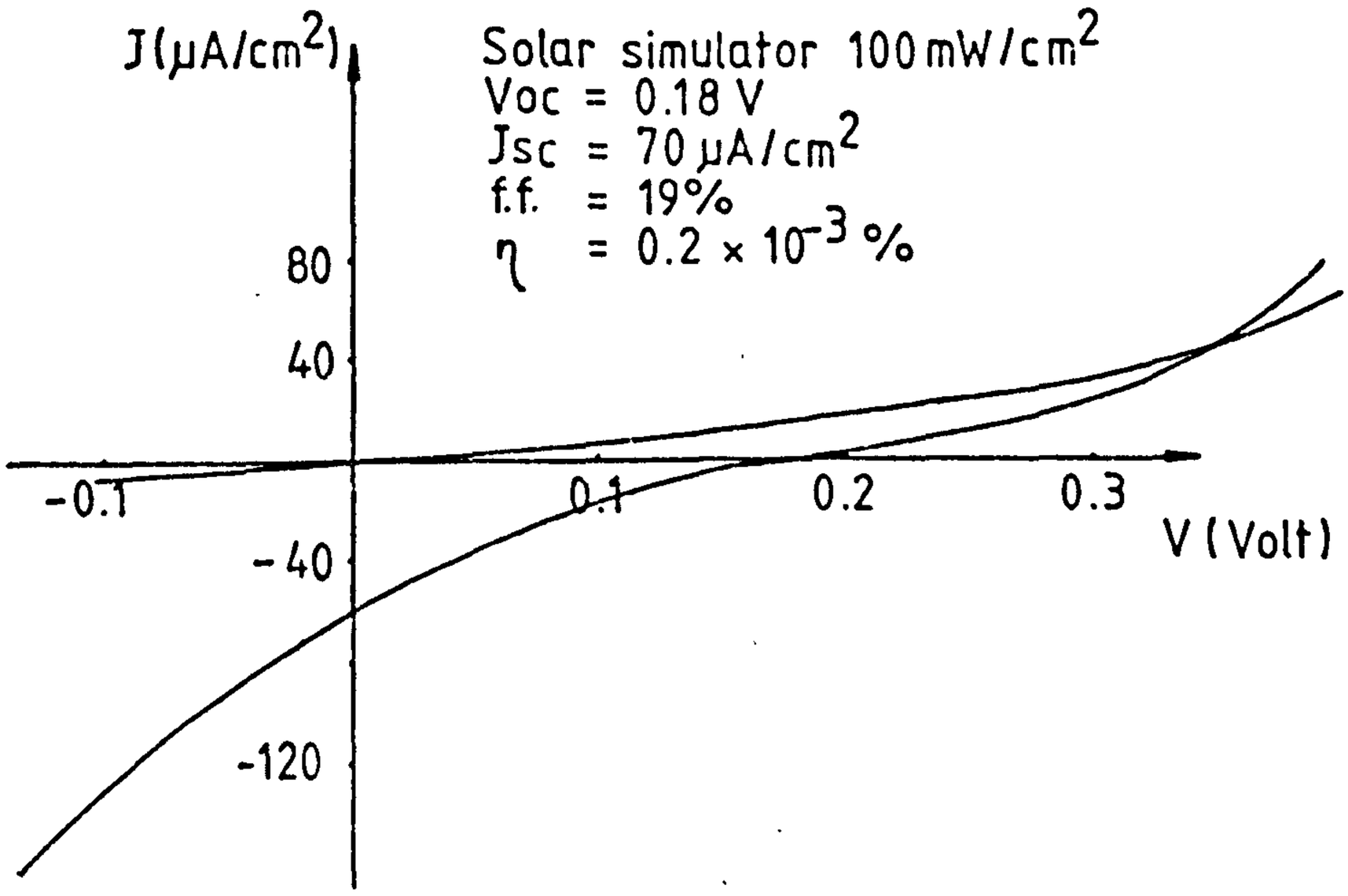

Fig. 3.9b Photovoltaic response of uncleaned n-CdS/p-Si cell

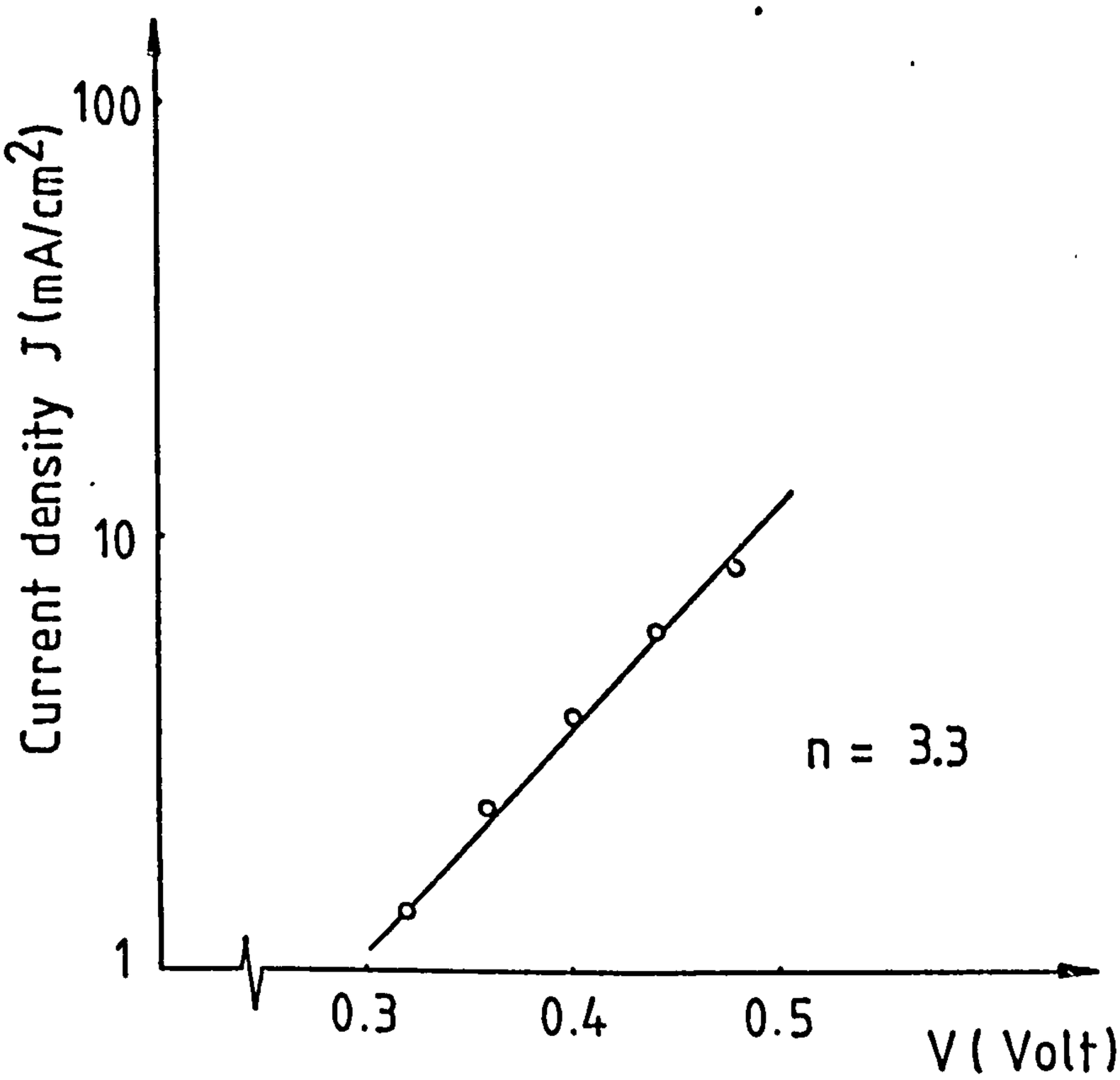

Fig. 3.10 a $Log_e J$ vs V of thermally cleaned CdS/Si cell

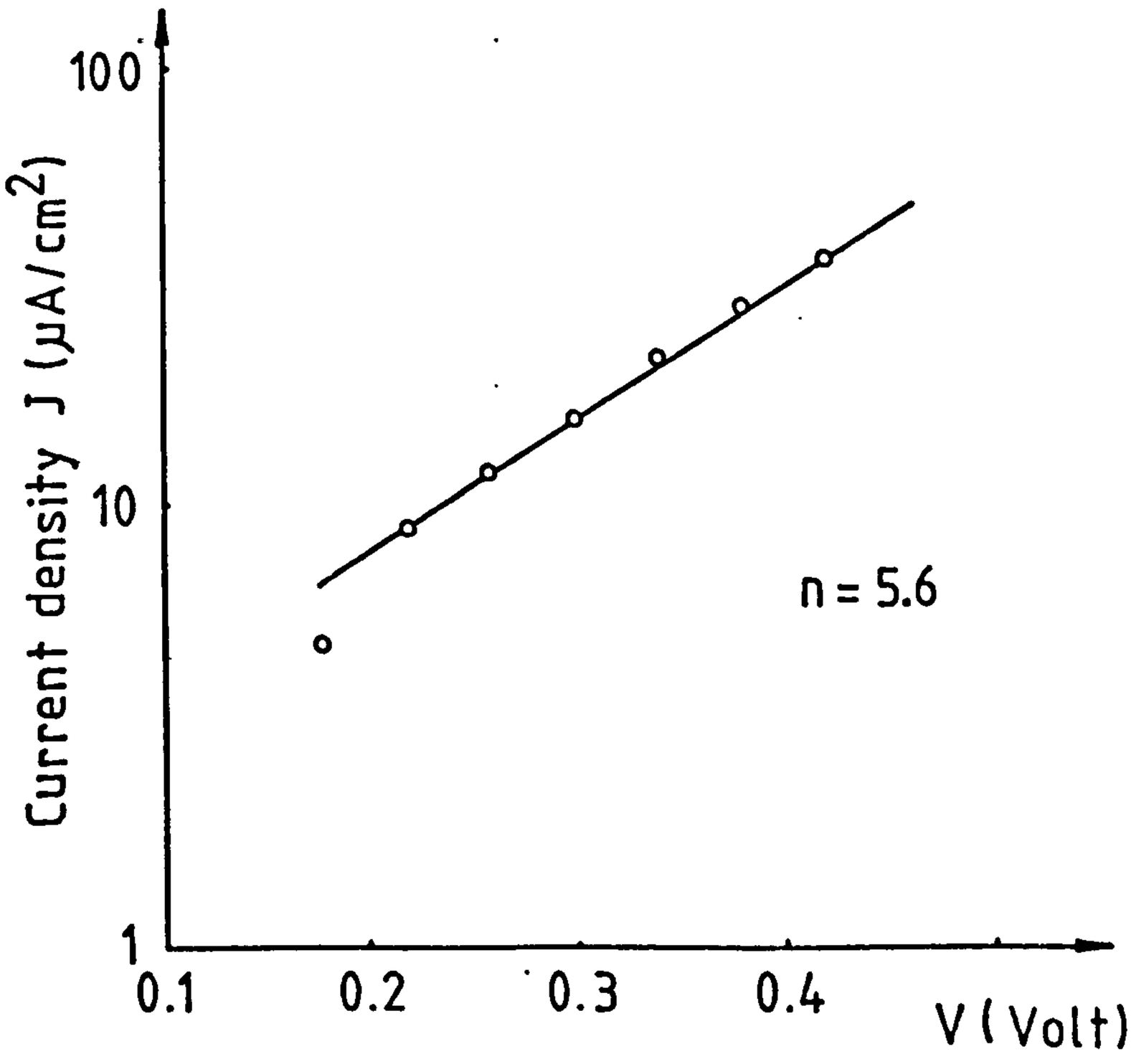

Fig. 3.10 b $Log_e J$ vs V of uncleaned CdS/Si cell

Properties	Uncleaned	Cleaned
Voc (V)	0.18	0.35
Jsc (mA/cm^2)	0.07	8.0
Fill factor (%)	19	43
Diode factor n	5.6	3.3
Solar eff. (%)	0.2×10^{-3}	1.2

Table 3.1 Photovoltaic characteristics of CdS/Si cells with thermally cleaned and uncleaned Si substrate

Resistivity ohm cm. / Properties	0.05	2.0	50	150
Voc (V)	0.40	0.34	0.32	0.37
Jsc (mA/cm^2)	9.0	8.0	6.8	8.5
Fill factor (%)	36	42	33	30
Diode factor n	3.3	3.3	2.2	3.0
Solar eff. (%)	1.3	1.1	0.7	1.0

Table 3.2 Photovoltaic characteristics of CdS/Si cells at different Si resistivity

flowing from the Si into the CdS is thereby reduced.

The properties of Si/CdS heterojunction cells fabricated with different silicon substrate resistivities are shown in Table 3.2. All the silicon substrates of these cells were thermally cleaned before CdS deposition. The open-circuit voltage, short-circuit current and the fill factor of the cells did not differ significantly with different substrate resistivities. It was thought that surface state effects caused by the large lattice mismatch at the heterojunction and high lateral resistance of the thin CdS films are responsible.

Heat treatment in a forming gas ($25\%H_2/75\%N_2$) has been shown to give a large improvement in the photovoltaic properties of the Si/CdS heterojunction cells both by lowering the resistivity of the CdS layer and by the improvement of the junction properties[74,75]. The effects of heat treatment in a forming gas on the characteristics of a CdS/Si(150 ohm cm) cell are summarised in Table 3.3. It is evident that all cell parameters are improved by the heat treatment. The illuminated current density-voltage characteristics of a cell fabricated on a 150 ohm cm (111) oriented silicon substrate before and after annealing are shown in Figure 3.11. Ma et al.[75] showed by Auger analysis that heat treatment of CdS (by spray pyrolysis) produced a higher Cd:S ratio near the surface.

3.7 Summary of p-Si/n-CdS heterojunction solar cell work

A wide range of Si/CdS heterojunction devices has been studied to determine the optimum fabrication condition for using the devices as solar cells. It has been shown that the resistivity of the substrate is not as critical as indicated by the idealised model (Figure 3.1). This insensitivity is

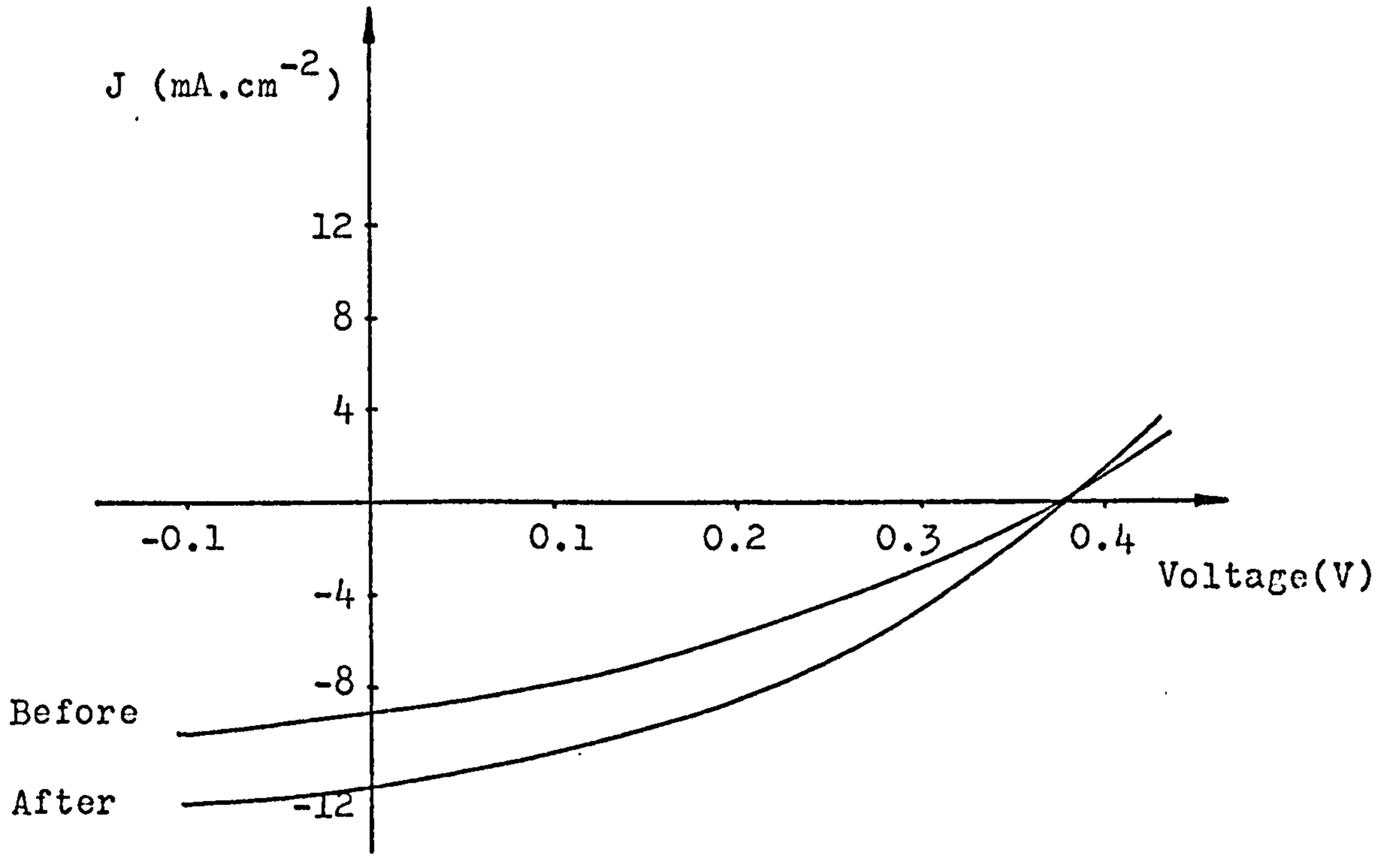

Fig. 3.11 Illuminated characteristics of Si/CdS cell before and after annealing

Properties	Before	After
V_{oc} (V)	0.37	0.37
J_{sc} (mA.cm^{-2})	9.0	12.0
Fill factor (%)	30	35
Diode factor n	6.3	4.6
Solar efficiency	0.95%	1.54%

Table 3.3 Photovoltaic characteristics of Si/CdS cell before and after annealing for 10 minutes in forming gas at 400^{o}C

chiefly caused by unknown interfacial states at the heterojunction and the density of traps in the evaporated CdS film.

Substrate cleaning was found to have a dominant influence on both the cell characteristics and the crystallographic structure of the evaporated film. Devices fabricated with substrate cleaning were found to produce much more consistent characteristics, and X-ray Laue photographs clearly indicated improved crystal structure of the evaporated CdS film at higher growth temperatures. CdS films deposited at lower temperatures were polycrystalline, such Si/CdS devices showed poor photo-voltaic characteristics similar those of devices made from CdS films deposited on "uncleaned" silicon substrates.

Annealing of the completed cell significantly improved the performance of the Si/CdS solar cells. This was attributed to the improved crystal structure of the CdS, and reduction of the interfacial states at the heterojunction. The improved characteristic could also be due to some improvement in the metal-CdS contact.

It is thought that no further improvements in the CdS film structure quality may be obtained on the silicon by the method of electron-beam gun evaporation from compound crystals. The most serious disadvantage of this method is that it is not possible to control the constituent fluxes independently. The resultant CdS films grown under such non-equilibrium conditions show significant non-stoichiometry. These films have high defect densities which acts as trapping and recombination centres. Another disadvantage is that the thickness of such evaporated films is severely limited by the amount of material the hearth can hold. A technique called molecular beam epitaxy (M.B.E) is a possible method of obtaining high quality films.

As separate sources of cadmium and sulphur are used it should be possible to control independently the vapour pressure of Cd and S_2 to maintain stoichiometric ratio at different deposition temperatures.

Interface states at the Si/CdS heterojunction are thought to be an important influence in the cell performance. It is inevitable that some disorder at the interface occurs as a result of a lattice mismatch of 7.7% between the silicon and CdS lattice. In addition, there is experimental evidence to show that Si is chemically attacked by the sulphur and/or cadmium vapour. Again, this will have significant effect on the cell performance. The efficiencies of the cells in this work, without antireflection coatings, of 1 to 2% clearly demonstrated the above inherent defects of the Si/CdS heterojunction. In fact, even it is possible to grow epitaxial CdS on Si, it is probable that the interfacial layers, perhaps extending to several hundred angstroms, may be polycrystalline due to the mentioned above lattice mismatch. The Si/CdS heterojunction solar cell is therefore unsuitable to terrestrial applications because of low efficiency and high cost. The cost of single crystal silicon remains the dominant factor. The use of thin-film silicon substrates would reduce the cost and weight of the device considerably, but the inevitable further decrease in the already low efficiency would be unacceptable. This apply even with the expected improvements in CdS films deposited by M.B.E. techniques. A more suitable alternative approach for terrestrial applications is the wholly thin-film structure based on low cost substrates. The simplest would be the Schottky barrier type configuration where cheap epitaxially grown metals may be used as substrates. Al-CdS and Au-CdS Schottky barrier diodes[76] are such examples.

CHAPTER 4 MOLECULAR BEAM EPITAXIAL GROWTH OF CdS FILMS ON SPINEL

4.1 Introduction

This chapter describes an investigation into the epitaxial growth of monocrystalline films of CdS by molecular beam epitaxy (M.B.E.) on (111) spinel ($MgAl_2O$ a_o=8.09Å)[77] substrates. The aim of this investigation was to study the basic electron transport properties and the structural properties of the deposited films. A knowledge of such properties is necessary for the fabrication e.g. Schottky structures so that films with predictable characteristics may be produced. The following section (4.2) describes the M.B.E. system, and the methods of evaporation. The investigation of the CdS films used several techniques: (a) X-ray Laue back reflection was used to determine the degree of orientation of the CdS crystallites in the basal plane, (b) Bragg diffraction using a double diffraction method was used to determine the orientation of the C-axis of the crystallites with respect to the substrate, and (c) measurements of Hall mobility, the temperature dependence of resistivity, and photoconductivity gave an indication of the transport properties of the films. Each of the above techniques produced information on the deposited CdS films which enable better predictions of the characteristics. Also included here is a description of the process of substitutional doping of the CdS films in situ by indium and phosphorus, and their related characteristics.

4.2 Vacuum system

The UHV system used is shown in Figure 4.1. It consisted of a 140 l/s diode ion pump with a titanium sublimation pump. To realise a pressure of approximately 10^{-9} torr it was neces-

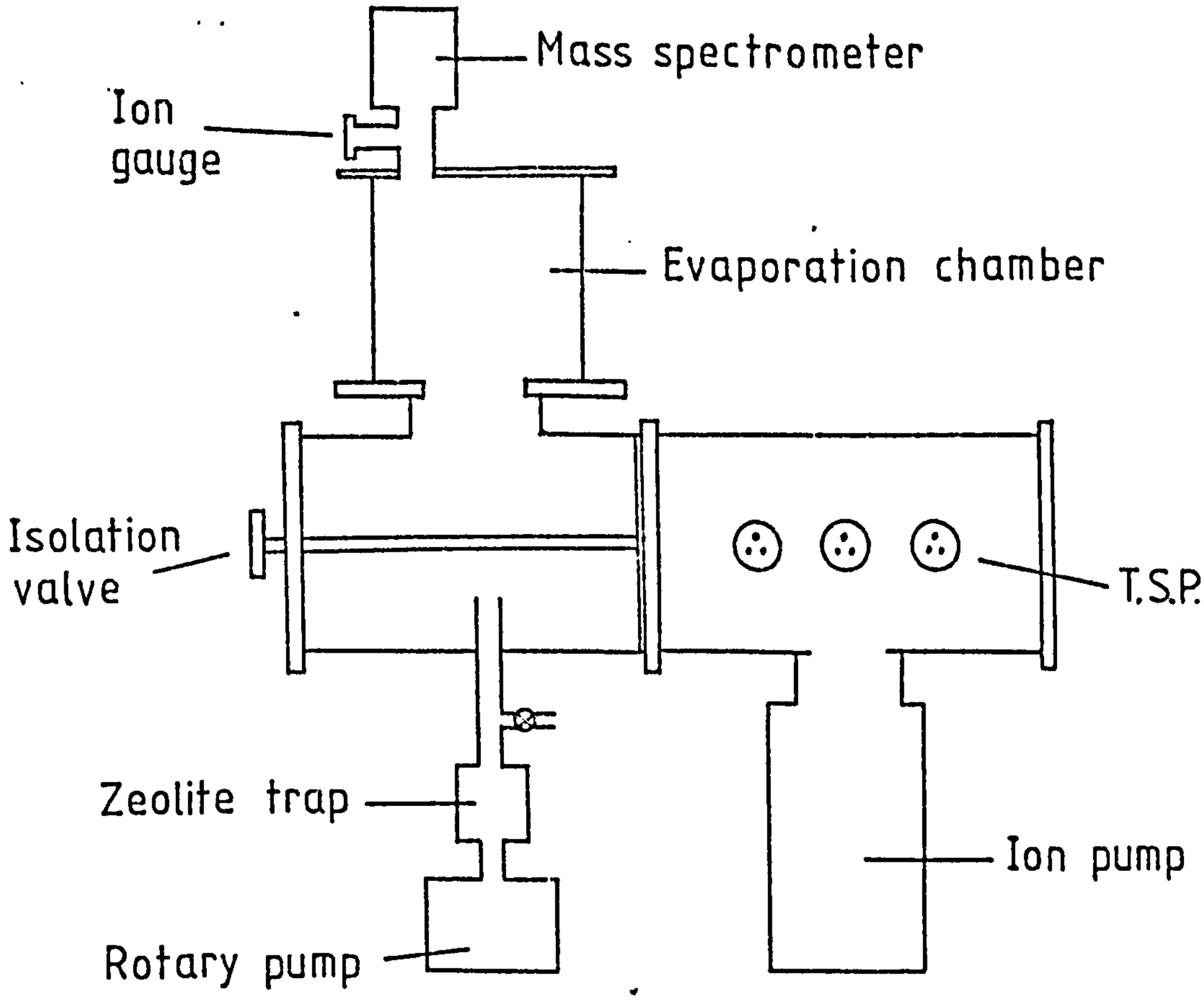

Fig. 4.1 Experimental U.H.V. system

sary to bake the chamber out to at least 100°C for approximately 12 hours. However, because of the high vapour pressure of sulphur at this temperature, ($\sim 10^{-2}$ torr), it was necessary to maintain the sulphur at a much lower temperature during bake out. This was done by maintaining the sulphur oven at 0°C by a recirculating refrigerant during bake out, at this temperature the vapour of sulphur is about 10^{-7} torr. The residual sulphur vapour was further reduced by enclosing both Knudsen cells in a copper box with a 5cm diameter aperture at the top to allow the molecular beam to impinge on the substrate. The copper enclosure getters the sulphur by forming a copper sulphide and by this means the sulphur pressure could be maintained below 10^{-8} torr during bake out. The cadmium and sulphur vapour beams were collimated by a liquid nitrogen cooled copper panel which had a 3.5cm diameter aperture, the low temperature ensuring a high sticking coefficient for the diverging vapour beams. The panel also serves as a cryo-pump for residual water vapour and carbon dioxide but not for nitrogen and carbon monoxide which are the main constituents of the residual gas. The chamber pressure was measured by an ion gauge positioned at the top of the bell jar and the residual gas analysed by an AEI MS10 mass spectrometer which has a limiting sensitivity of 5×10^{-11} torr. A schematic diagram of the evaporation chamber is shown in Figure 4.2.

4.2.1 Evaporation chamber

The Knudsen cells are shown schematically in Figure 4.3. These were fabricated from spectroscopic grade graphite rods machined to a length of 5cm and 3cm diameter. A series of 2mm diameter holes were drilled through the rod parallel to its axis. Ceramic insulator tubes were inserted in the holes, and

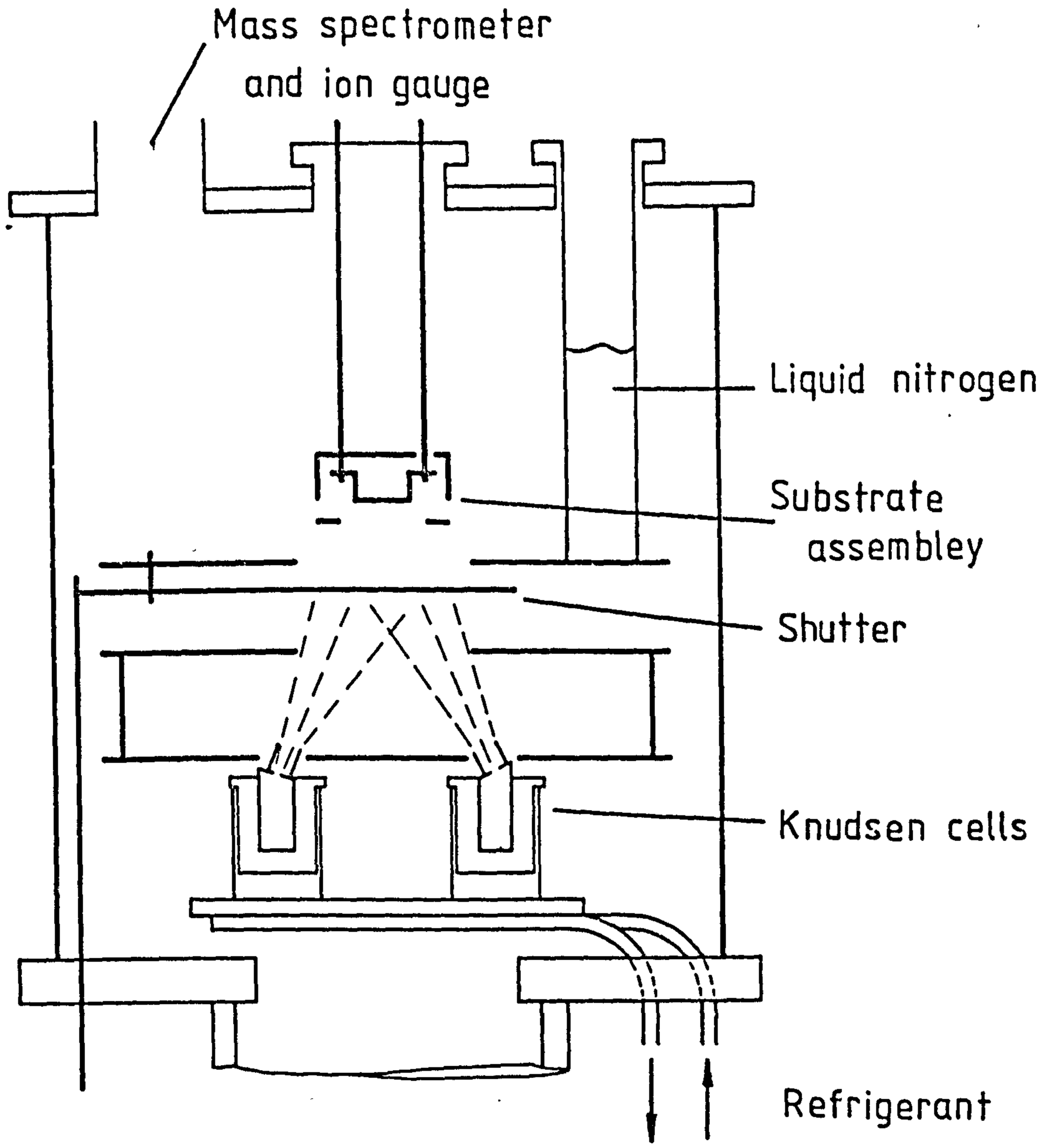

Fig. 4.2 Evaporation chamber

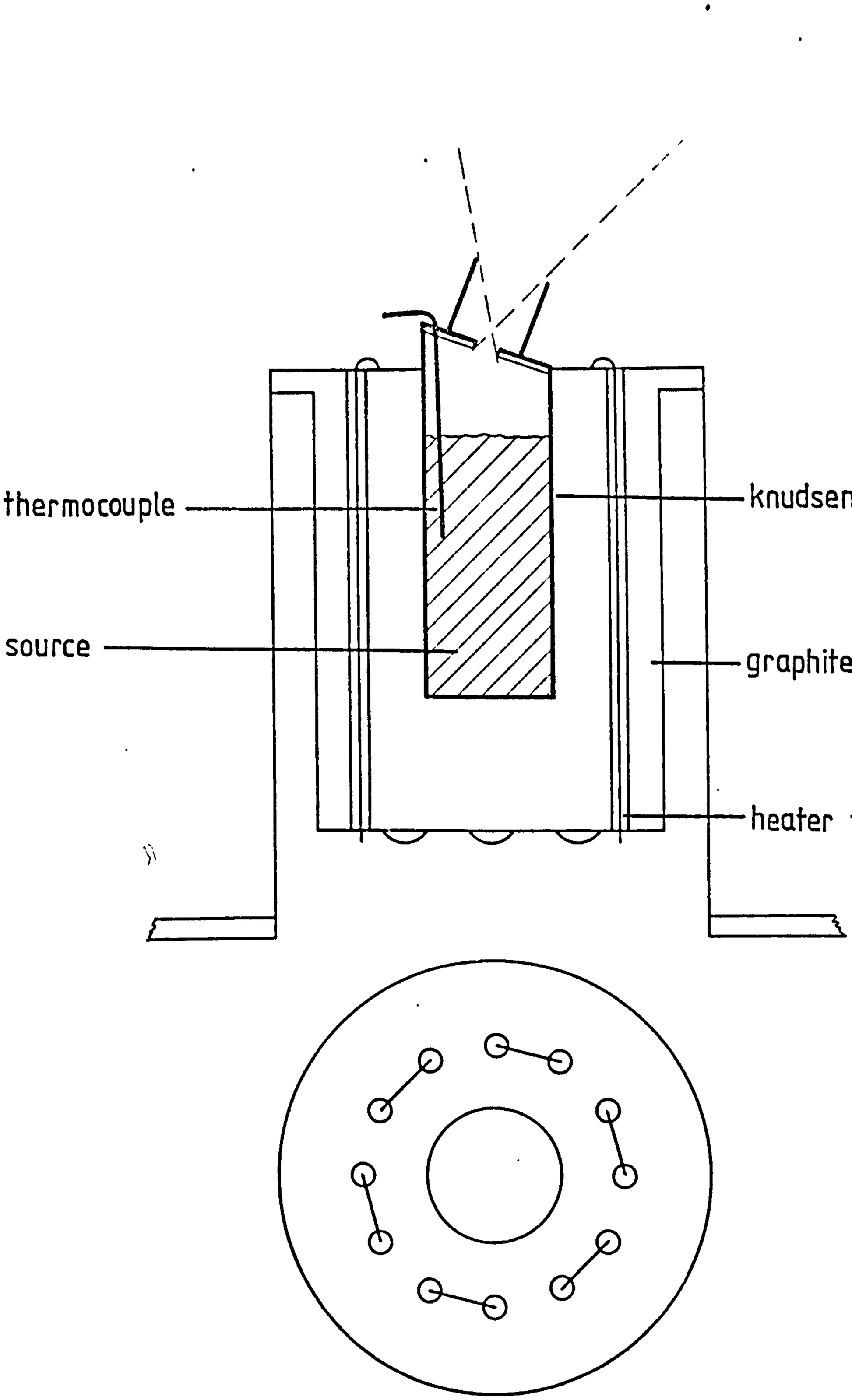

Fig. 4.3 Knudsen cell

tungsten heater wires were then threaded through the insulator tubes. The source material was contained in aluminium tubes 2cm long and 1cm in diameter, and each tube was inserted in a central hole drilled in each graphite rod. The open end of the tube was sealed by a tight fitting aluminium plug with a 2mm diameter orifice. The cells were inclined at approximately 10^{o} to the vertical and positioned to give a source to substrate distance of 10cm, thus ensuring that both vapour beams overlapped. The source temperature was measured by an iron-constantan thermocouple which was inserted into the aluminium tube via a small hole in the plug, the thermocouple making contact with the source material. Each cell was enclosed by a thin walled gold plated stainless steel radiation shield mounted on a stainless steel plate which was maintain at $0^{o}C$ by a circulating refrigerant. The temperature stability of the source material during a one hour evaporation was $\pm$ $1^{o}C$ for the sulphur and $\pm$ $2^{o}C$ for the cadmium. The source material used was of spectroscopic grade, the sulphur being of 99.9995% purity and the cadmium 99.9998%.

The substrate was mounted on a molybdenum foil ring supported by tungsten wires and was heated by radiation from a tungsten filament. Its temperature was measured by a platinum-platinum/13% rhodium thermocouple held in contact with the surface of the substrate. A shutter was mounted immediately below the substrate.

4.3 Source flux calibration

An important parameter associated with the film growth process is the molecular beam flux, i.e. the number of atoms incident on unit area per unit time. The beam flux for each

cell as a function of the source temperature was measured with a quartz crystal oscillator maintained at 77K and positioned immediately below the substrate. The crystal was isolated from the vapour beam by a shutter until the source was stabilised at the required temperature, the crystal was then exposed and the rate of change of frequency measured. The vapour was then allowed to fall on a cooled glass substrate for 10 minutes and the mass of the material deposited was measured and hence the flux. This procedure was repeated over a range of temperature for each cell to determine the flux as a function of source temperature. The results for each cell are shown in Figure 4.4.

There is a problem regarding the calibration of the sulphur flux by this method because the sulphur vapour consists of a number of molecular species as discussed in Section (2.2). Only above 900^{o}C does the vapour consists of solely of S_2 and at any lower temperature consisting of a mixture of heavier molecules, i.e. $\sum_{n=1}^{8} S_n$. The mass spectrometer indicated that the vapour was predominantly S_2 over the range S_1 to S_6. The difficulty with this method of identifying the molecular species of the vapour beam is that the instrument can reduce a higher order molecule to S_2 by a "cracking process". The fragmentation pattern of S_8 has been determined by Berkowitz and Chupka[78] and the data is listed in Table 4.1. The measured peak intensities are also shown, and it can be seen that the ratio of any mass peak at this range to that of S_2 is much smaller than that could be ascribed to fragmentation of the S_8 molecules. Consequently is has been assumed that the sulphur vapour beam is predominantly composed of S_2 molecules.

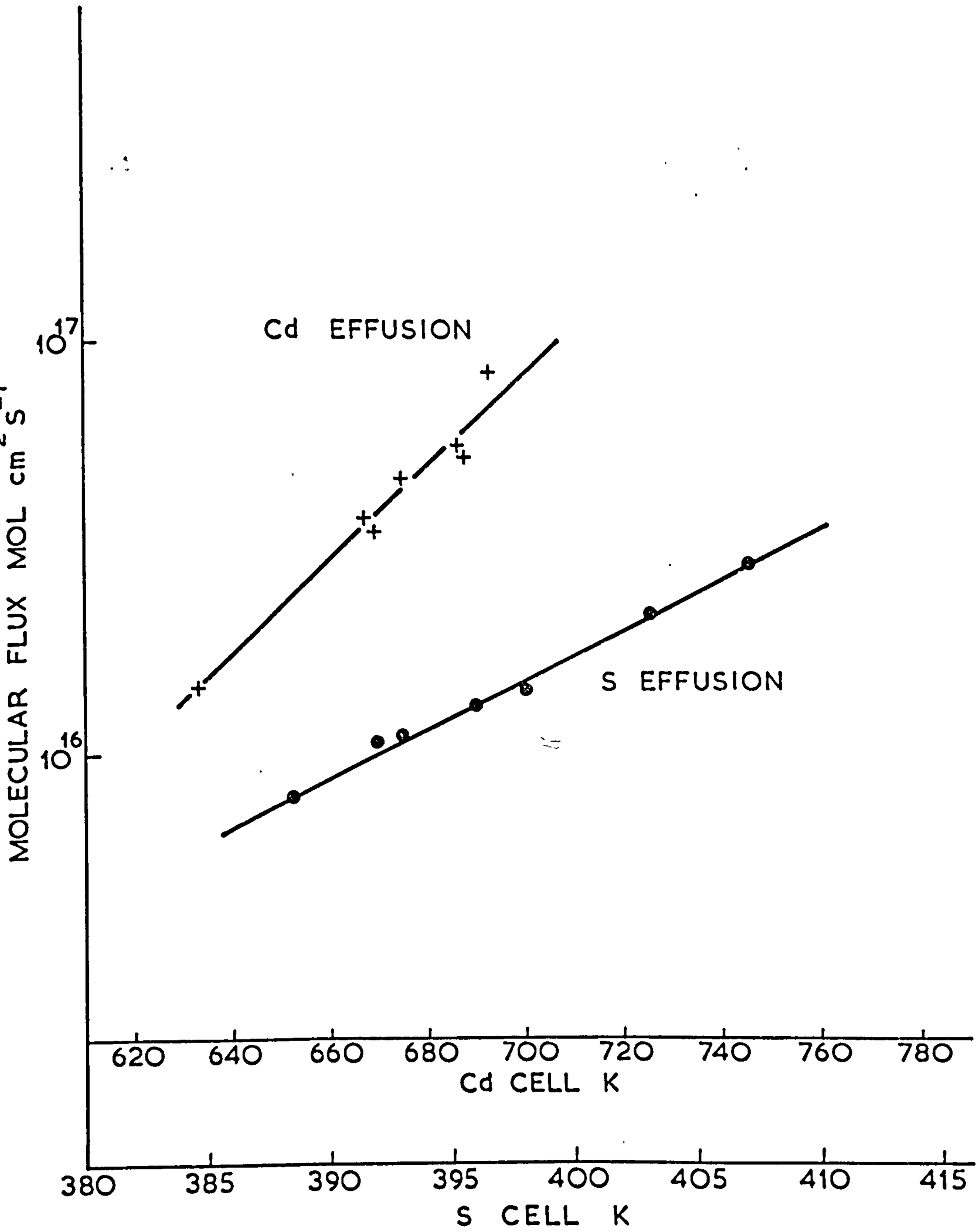

Fig. 4.4 Molecular flux vs Cell temperature

Molecular species	Relative peak height	
	Due to S_8 fragmentation	Measured*
S_2	100	100
S_3	26	17
S_4	63	5.8
S_5	44	5.7
S_6	22	7.4
S_8	131	-

Vapour temperature = 400 K

Acceleration potential = 75eV

* corrected for ionization efficiency differences

Table 4.1 Relative Sulphur Intensity

4.4 Film growth procedure

A reliable and controllable technique for depositing CdS films on spinel was developed after much trial and error experimentation. The procedure finally adopted was as follows. The (111) oriented spinel substrate was polished flat with one micron diamond compound followed by 0.3 micron alumina and finally with 0.05 micron alumina. The specimen was then cleaned successively in electronic grade trichloroethylene, acetone and distilled water. With the substrate in position and the required vacuum attained, the source ovens were brought to the operating temperatures. The substrate was then heated to over 700°C and maintained at this temperature for approximately 10 minutes. The substrate temperature was then reduced to the required value and when it had stabilised the shutter was opened. During the evaporation, which normally lasted for an hour, the respective vapour pressures were monitored on the mass spectrometer. Throughout the evaporation, from the moment the source oven temperatures were raised, liquid nitrogen was maintain in the stainless steel tube which served as a cryo-pump (Figure 4.2). This procedure was found to give reliable and reproducible results.

4.5 Structural properties of CdS films

The structural properties of CdS films which were a few microns thick were analysed by X-ray Laue[72] and Bragg diffraction[79] techniques, using in the latter case, a double diffractometer. With the former method polycrystalline films show up as a series of concentric rings whereas with single crystal type films discrete spots with the appropriate symmetry are observed. In general CdS films can occur either as the

cubic sphalerite phase or the hexagonal wurzite phase. With Bragg diffraction the structural phase can be readily determined from the Bragg angle, which for the former is 13.25° and 13.2° for the latter[80]. It was pointed out by Holloway [79] that the double diffraction method is both a convienent and sensitive method of assessing the quality of single crystal films of a few microns thick. The width of the diffraction line can range from a few a few tens of seconds for high quality single crystals to one degree for poor quality crystals. The double diffractometer used here was the nonparallel or (1,1) type[79] although of slightly inferior resolution to that of the parallel arrangement is somewhat more convienent. The minimum dispersion angle detectable with the instrument used here is 45 seconds which compares with the values of 40 seconds quoted by Holloway[79].

The CdS films were grown over a wide range of substrate deposition temperatures, 50°C to 420°C with source temperatures of 120°C and 380°C for the sulphur and cadmium cells respectively. With deposition temperatures below approximately 260°C polycrystalline cubic films were observed. With increasing substrate temperatures the Bragg angle decreased progressively from 13.25° to 13.2° at approximately 320°C. With further increase of temperature hexagonal single crystal type films were observed at approximately 360°C with a spread in the Laue spots of $\pm$10°. The angular spread in the Laue spots decreased with further increase in temperature until at approximately 400°C well defined Laue spot patterns exibiting six fold symmetry were observed, as shown in Figure 4.5a.

The other parameter which can affect the film growth process is the magnitudes of the respective beam fluxes as they determine the film growth rate. The influence of the beam fluxes

on both the growth rate and the structural properties of the films studied. Firstly, the sulphur flux was maintained at a value of 1.7×10^{16}molecules/cm^2.s and films grown with a cadmium flux ranging from 0.6×10^{16} to 8×10^{16}molecules/cm^2.s. Shown in Figure 4.7 is the film growth rate as a function of cadmium flux and it can be seen that a linear relationship is obtained below a flux of 1.5×10^{16}molecules/cm^2.s, but that above this the growth rate becomes constant or saturates. The X-ray Laue patterns for these two regions are shown in Figure 4.5. The result shown in Figure 4.5a was obtained with a cadmium flux of 0.5×10^{16}molecules/cm^2.s and this structure was observed throughout the linear region. Near the on-set of saturation the Laue pattern of Figure 4.5b was obtained which shows a faint continuous ring on which is superimposed the six intense hexagonal spots. Thus films which posses such a pattern are composed of both a polycrystalline and an epitaxial region. It is most likely that the initial growth process results in a polycrystalline structure which converts to an epitaxial film as the growth proceeds. Shown in Figure 4.5c is the film structure obtained with a cadmium flux of 8×10^{16}molecules/cm^2.s and it is evident that the film is highly disordered. Thus it can be concluded from Figures 4.5 and 4.7 that although the cadmium flux determines the film growth rate, it is only effective over a limited range in obtaining single crystal crystal films.

The above procedure was repeated with a higher sulphur flux of 2.7×10^{16}molecules/cm^2.s but with similar levels of cadmium flux as those used in the case of Figures 4.5a, 4.5b and 4.5c. Shown in Figures 4.6a, 4.6b and 4.6c are the Laue photographs of films grown under these conditions. There is no noticeable difference between results 4.5a and 4.6a, the

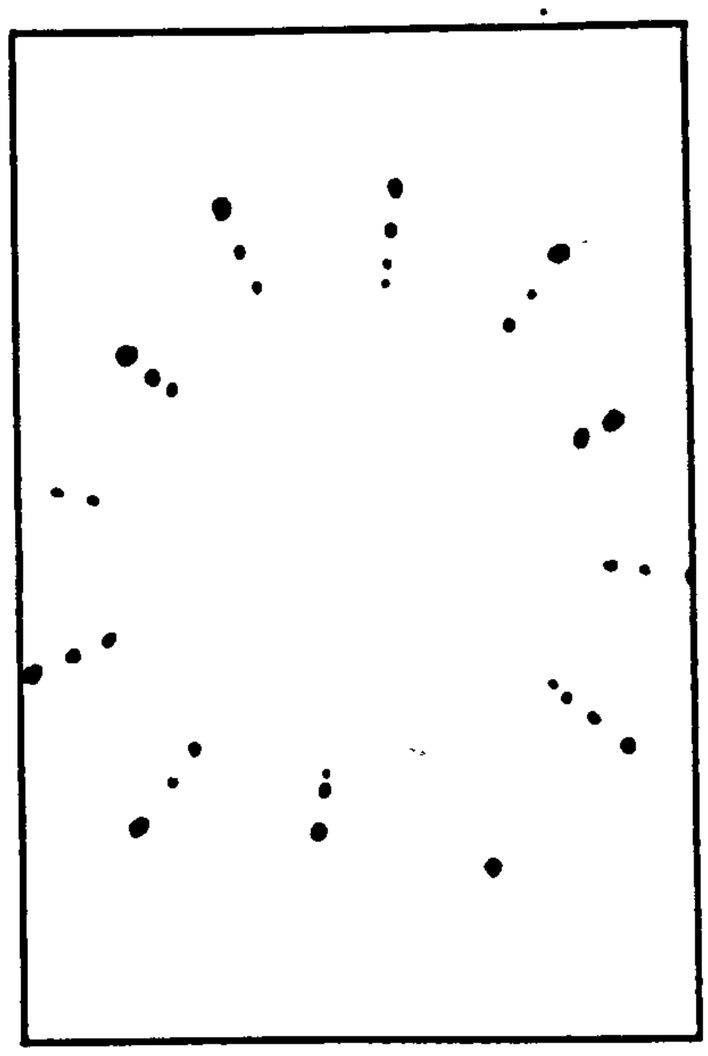

Laue diffraction of (111) spinel

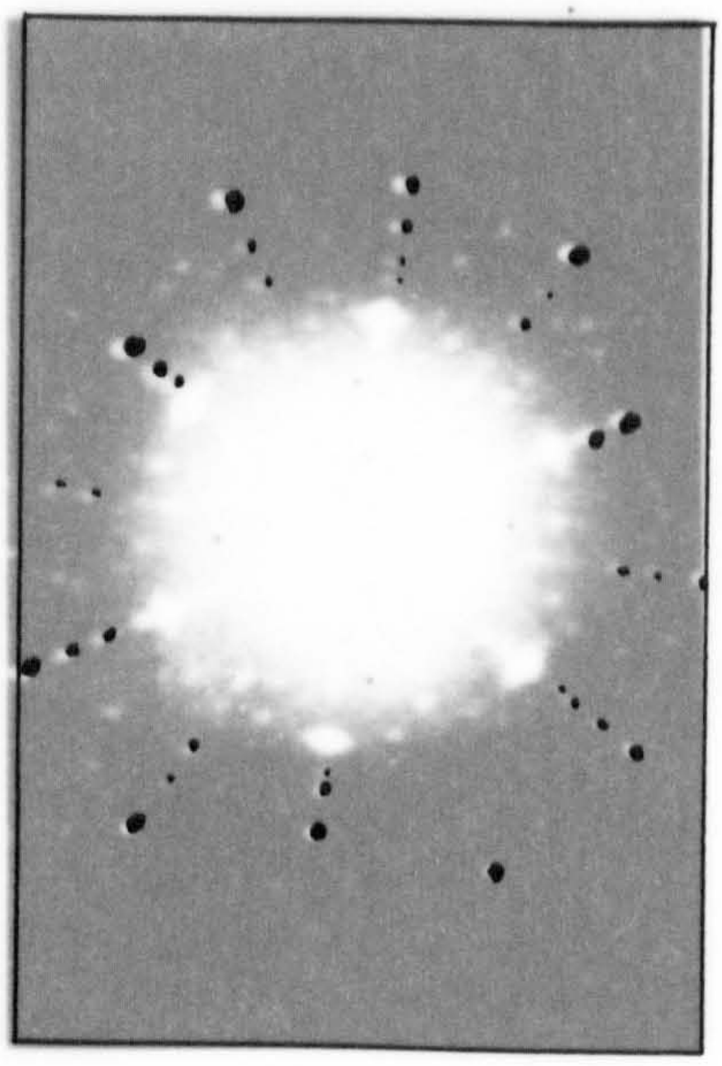

(a)

Cd flux = 0.5×10^{16} mol./cm^{2}s

S_2 flux = 1.7×10^{16} mol./cm^{2}s

Laue diffraction of (111) spinel

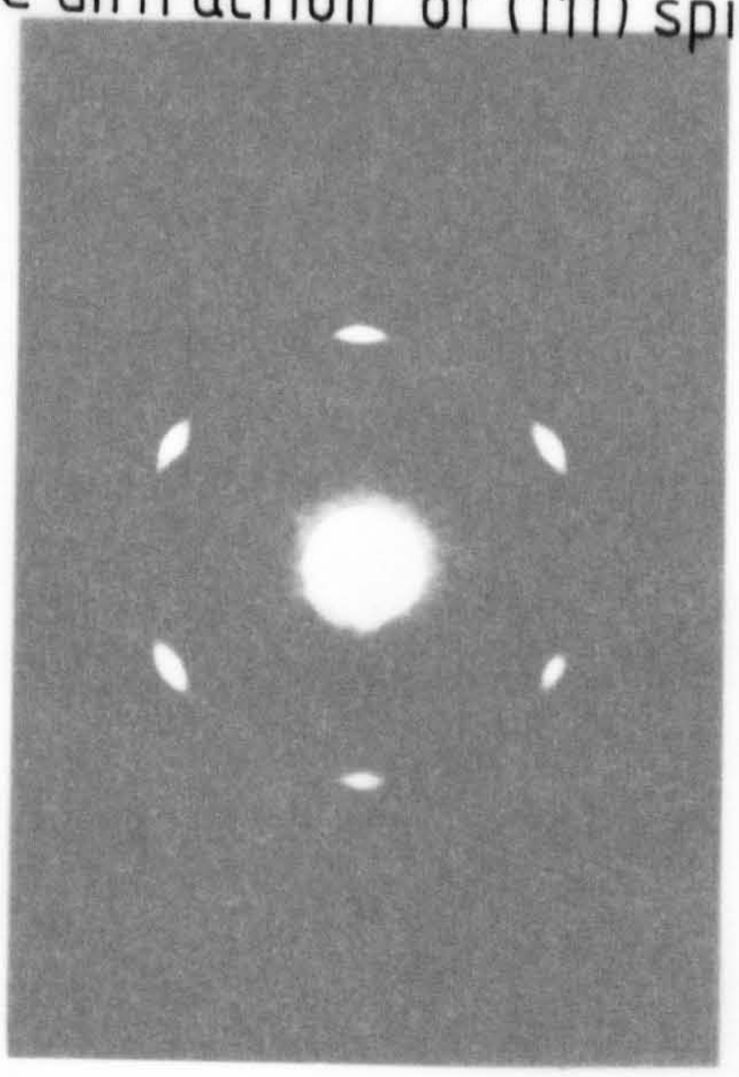

(b)

Cd flux = 1.4×10^{16} mol./cm^{2}s

S_2 flux = 1.7×10^{16} mol./cm^{2}s

(c)

Cd flux = 8.0×10^{16} mol./cm^{2}s

S_2 flux = 1.7×10^{16} mol./cm^{2}s

Fig. 4.5 X-ray Laue photographs of CdS films

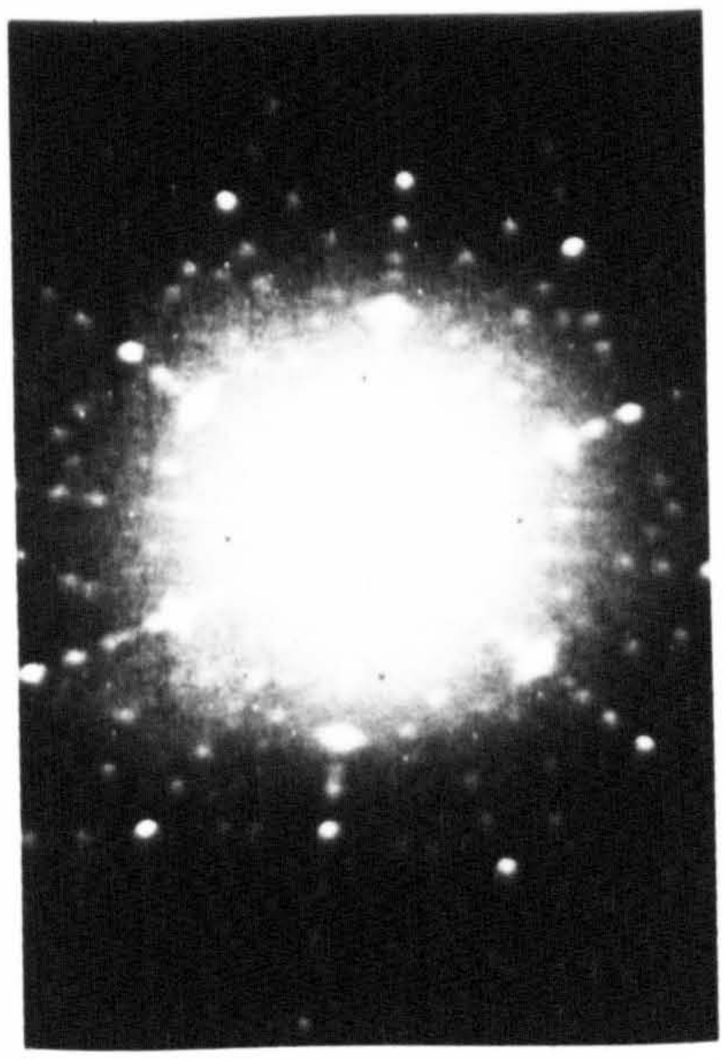

(a)

Cd flux = 0.5×10^{16} mol./cm^{2}s

S_2 flux = 1.7×10^{16} mol./cm^{2}s

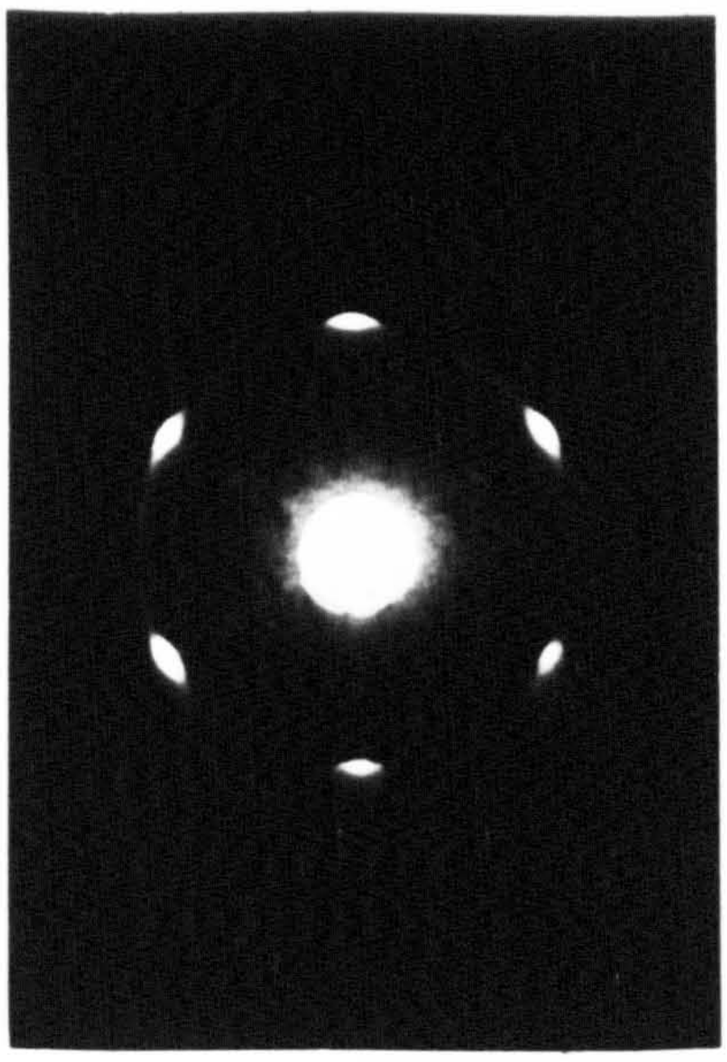

(b)

Cd flux = 1.4×10^{16} mol./cm^{2}s

S_2 flux = 1.7×10^{16} mol./cm^{2}s

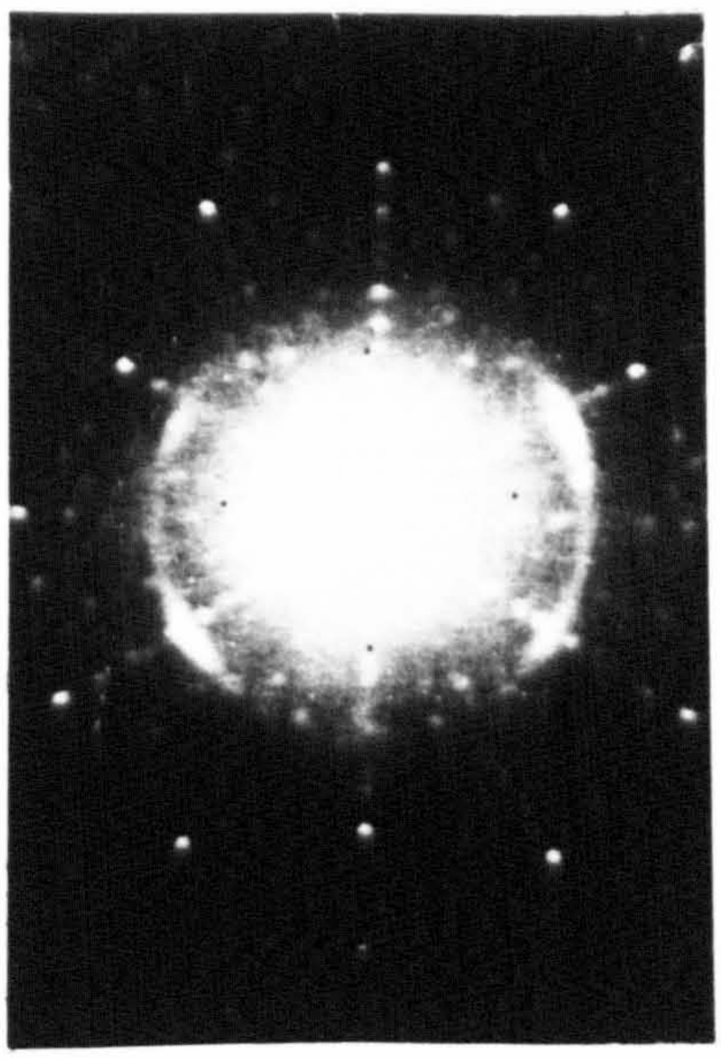

(c)

Cd flux = 8.0×10^{16} mol./cm^{2}s

S_2 flux = 1.7×10^{16} mol./cm^{2}s

Fig. 4.5 X-ray Laue photographs of CdS films

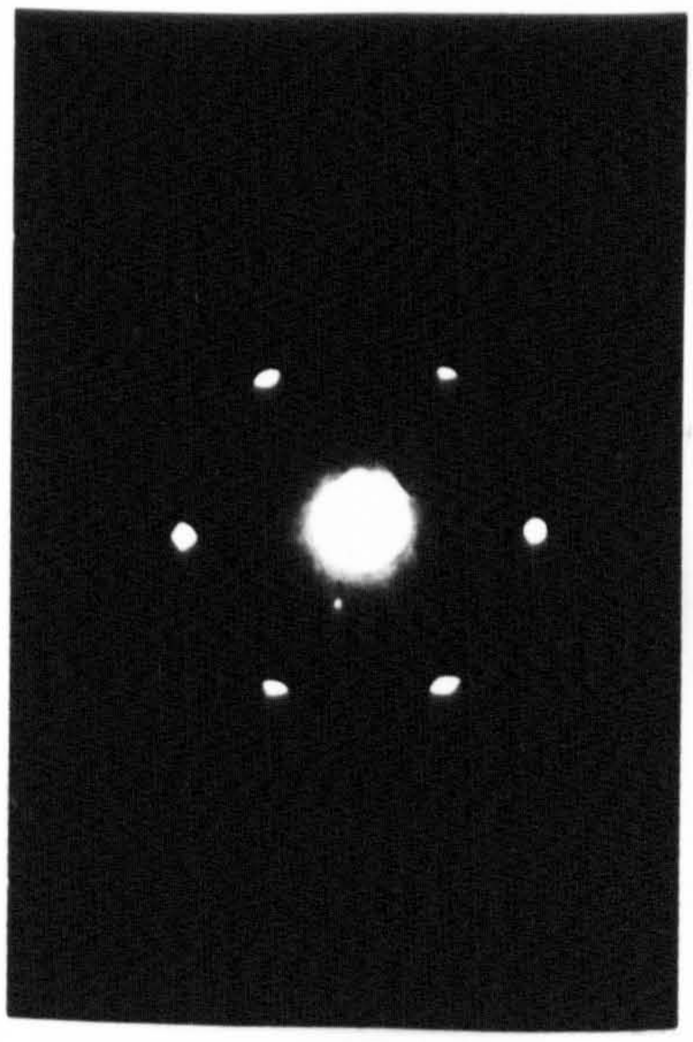

(a)

Cd flux = 2.6×10^{16} mol./cm^2.s

S_2 flux = 2.5×10^{16} mol./cm^2.s

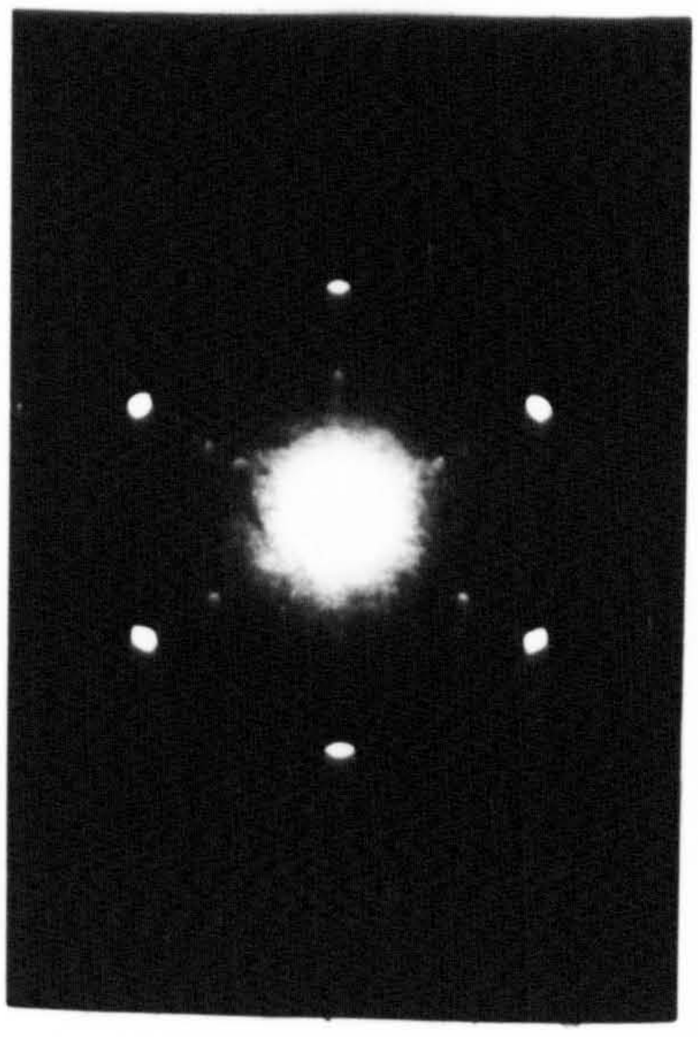

(b)

Cd flux = 4.0×10^{16} mol./cm^2.s

S_2 flux = 2.7×10^{16} mol./cm^2.s

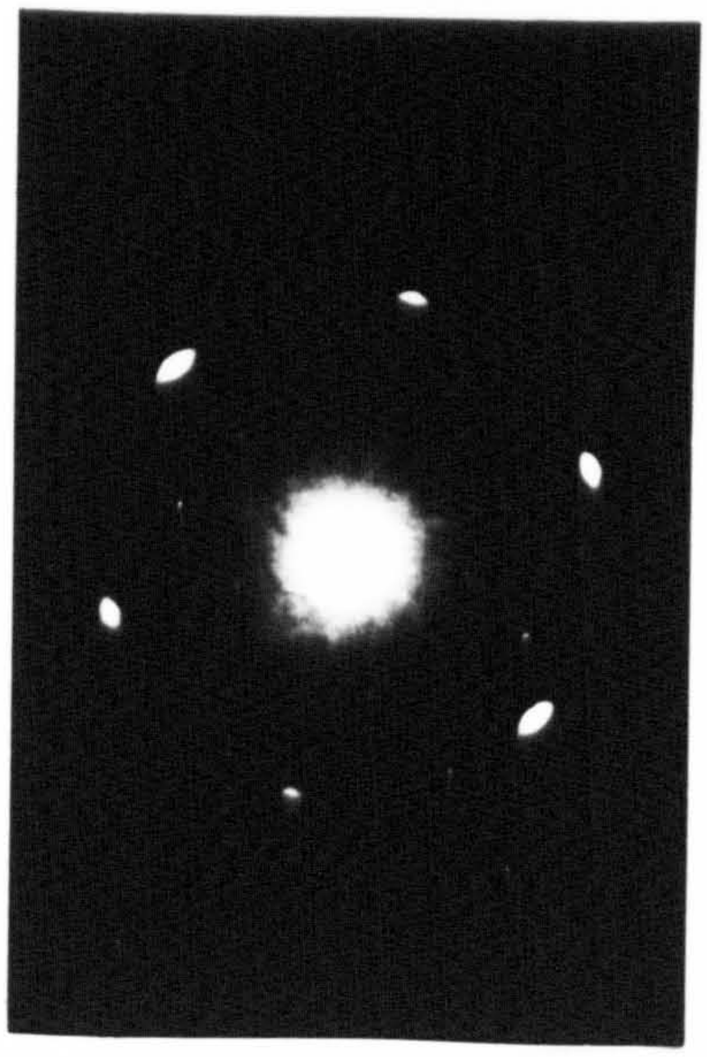

(c)

Cd flux = 8.0×10^{16} mol./cm^2.s

S_2 flux = 2.7×10^{16} mol./cm^2.s

Fig. 4.6 X-ray Laue photographs of CdS films

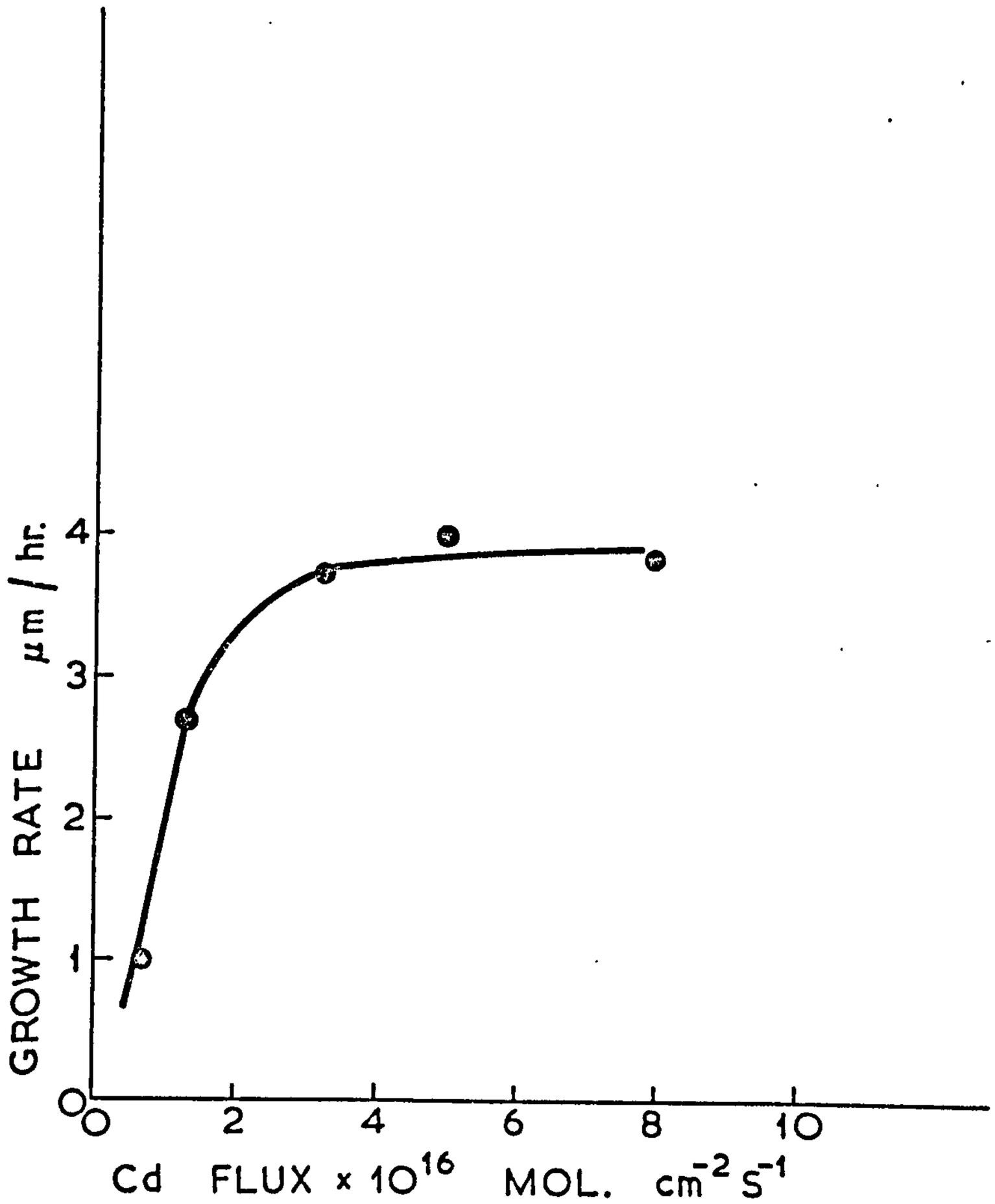

Fig.4.7 CdS growth rate as a function of Cd flux

polycrystalline region previously observed with Figure 4.5b does not exist in Figure 4.6b and in the case of 4.5c and 4.6c a significant improvement in structural order has been obtained by operating with a higher sulphur flux. Provided the ratio is maintained at about 1:1 film growth rates of 15 micron per hour have been obtained with structural order similar to that shown in Figure 4.6c.

The films were further analysed using the double diffractometer with a Ge (111) specimen as the first crystal and using Cu Kα radiation as shown in Figure 4.8. Shown in Figure 4.9 is the diffraction curve of specimen 4.5a which is Gaussian with a width at the half power points of 60 seconds. The diffraction associated with the (111) spinel substrate was similarly measured and found to be 60 seconds. This would seem to indicate that the degree of misorientation is determined by the structural imperfection of the polished substrate.

4.6 Transport properties

The properties of the epitaxial films studied were resistivity and its temperature dependence, mobility and photoconductivity. Shown in Figure 4.10 is the temperature dependence of resistivity of a film grown at about two microns per hour. The room temperature resistivity was about 10^5 ohm cm and exibited an exponential decrease in resistivity up to 300°C shown in curve A. The slope of the exponential was m=0.78 from which the activation energy of the deep donor can be determined. For a single donor state with no compensating acceptor the slope m = $E_d/2$ and as there is no evidence for such acompensating centre it has been concluded that the activation energy of this impurity is 1.6eV below E_c. Such an impurity is commonly found in

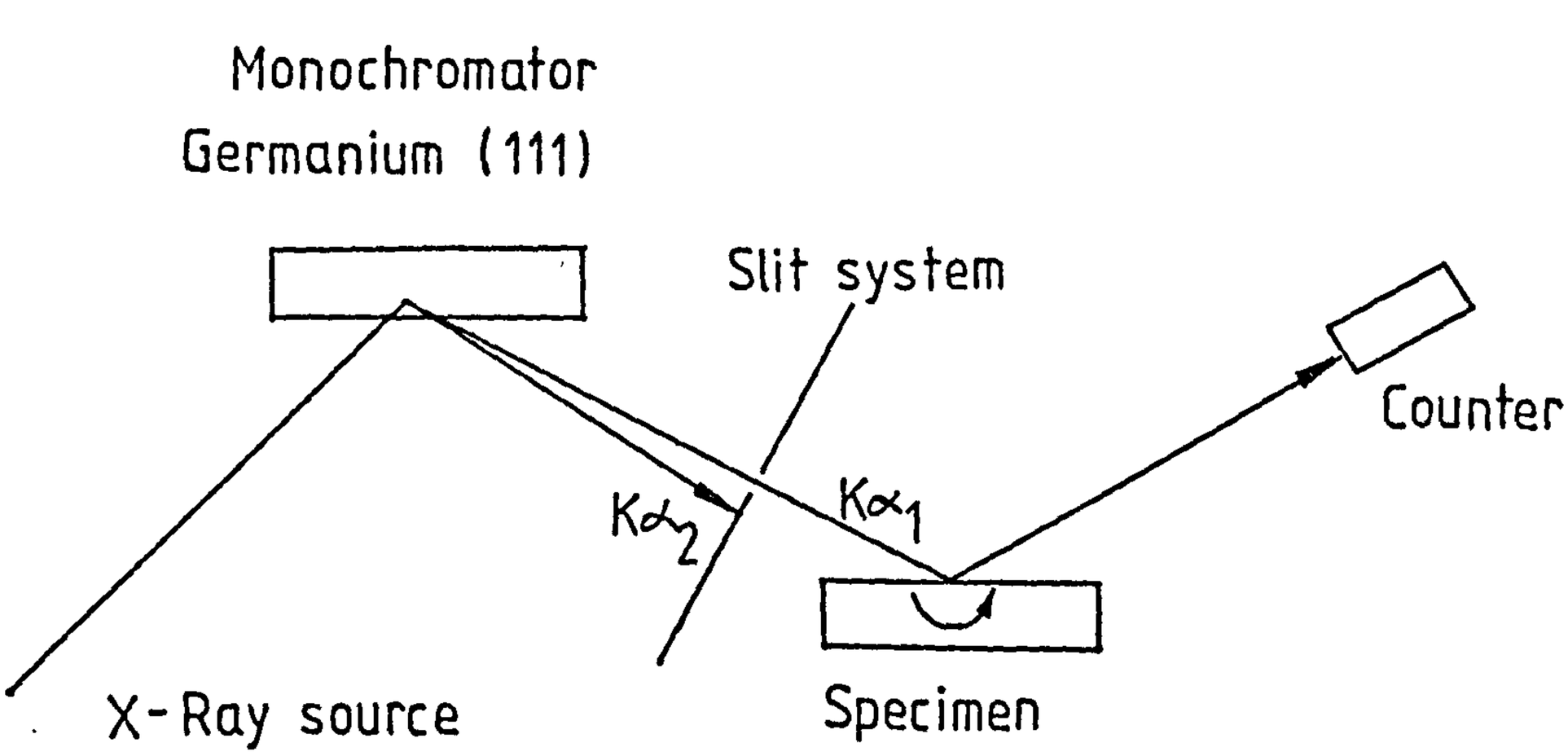

Fig. 4.8 Arrangement for double crystal diffractometry

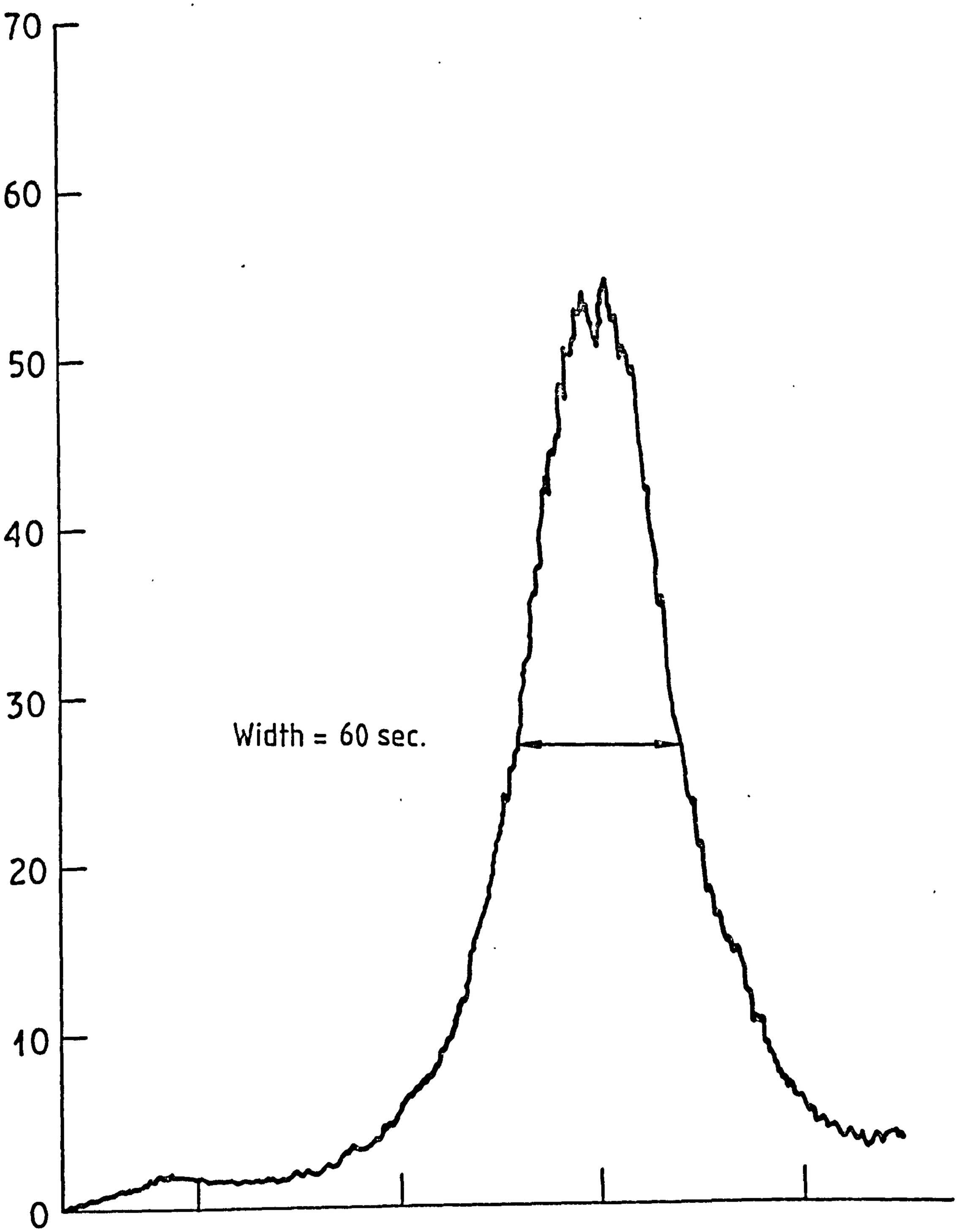

Fig. 4.9 Diffraction curve of specimen 4.5(a)

bulk CdS and considered to be due to a cadmium vacancy. The affect of annealing such a film at 600°C for 19 hours in argon is shown in curve B and it can be seen that a significant reduction in the concentration of this defect centre has been achieved. It was not possible to measure the mobility of these films because of the poor metal contacts viz. indium followed by aluminium evaporated contacts. Typically the maximum current injected was tens of nanoamps with a tens of volts applied.

Shown in Figure 4.11 is the spectral response of the photoconductivity and it is dominated by intrinsic photoconduction, i.e. band to band excitation of electron-hole pairs. However, a measurable absorption is observed at approximately 0.6 micron which would correspond to an electron trap with an ionisation energy of 2.0eV. This is in moderate agreement with the impurity defect at 1.6eV obtained from the resistivity data.

In the growth of bulk crystals of CdS or films grown by vapour transport, the resistivity can be controlled by using a relatively large excess of cadmium over sulphur. The excess cadmium or sulphur vacancies act as shallow donors with an activation energy of 0.03eV. It is evident from the results presented in the film growth rates that the deviation from stoichiometry must be small for good crystal structure and this method of n-type doping will not be satisfactory for controlling the resistivity.

4.7 Substitutional impurity doping with indium

For n-type films, substitution of cadmium by a group III impurity or a group VII for sulphur results in shallow donors. Obviously the group II impurities are more convenient and indium was used here. The indium molecular beam was evaporated from

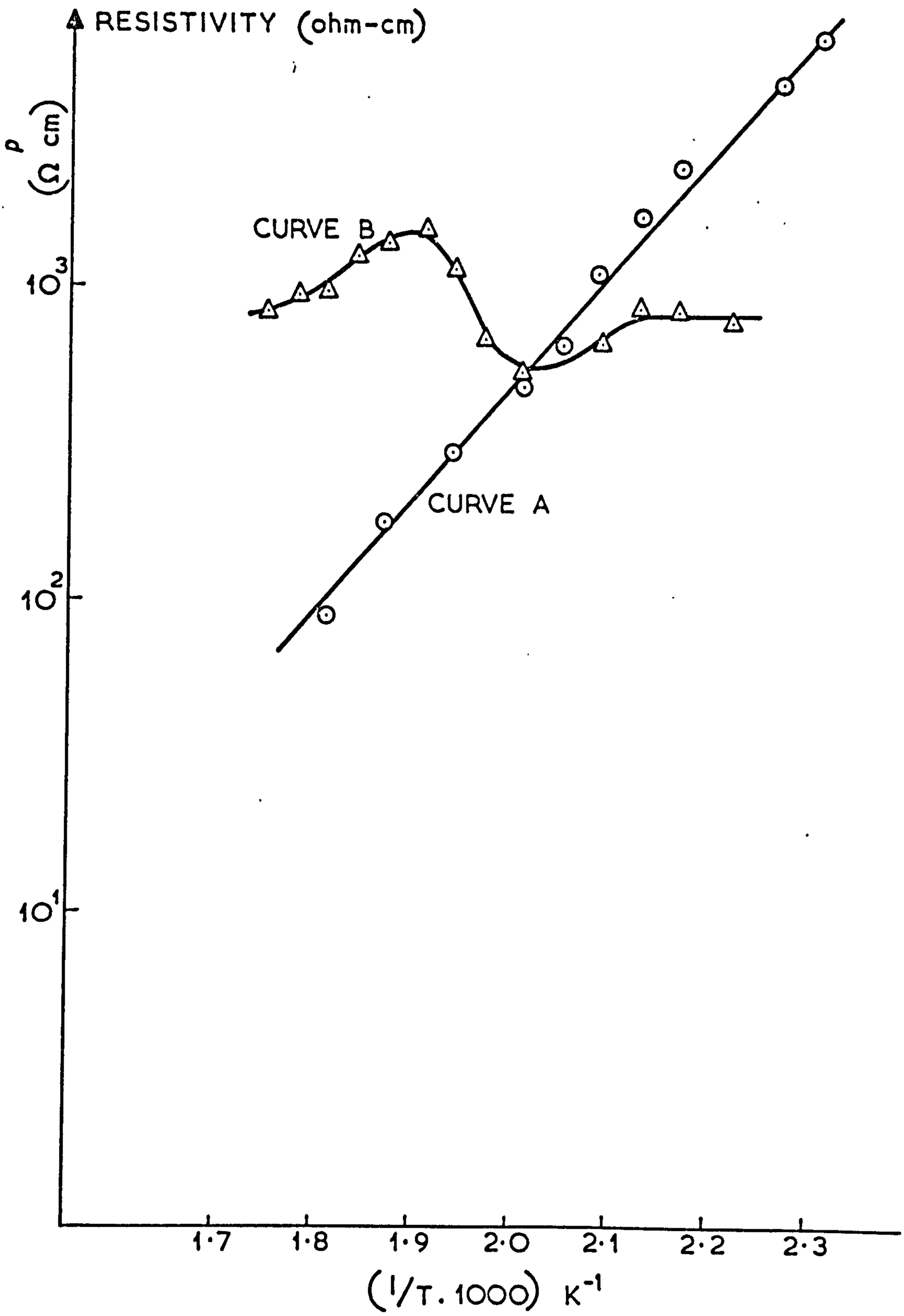

Fig. 4.10 Resistivity of CdS film vs reciprocal temperature

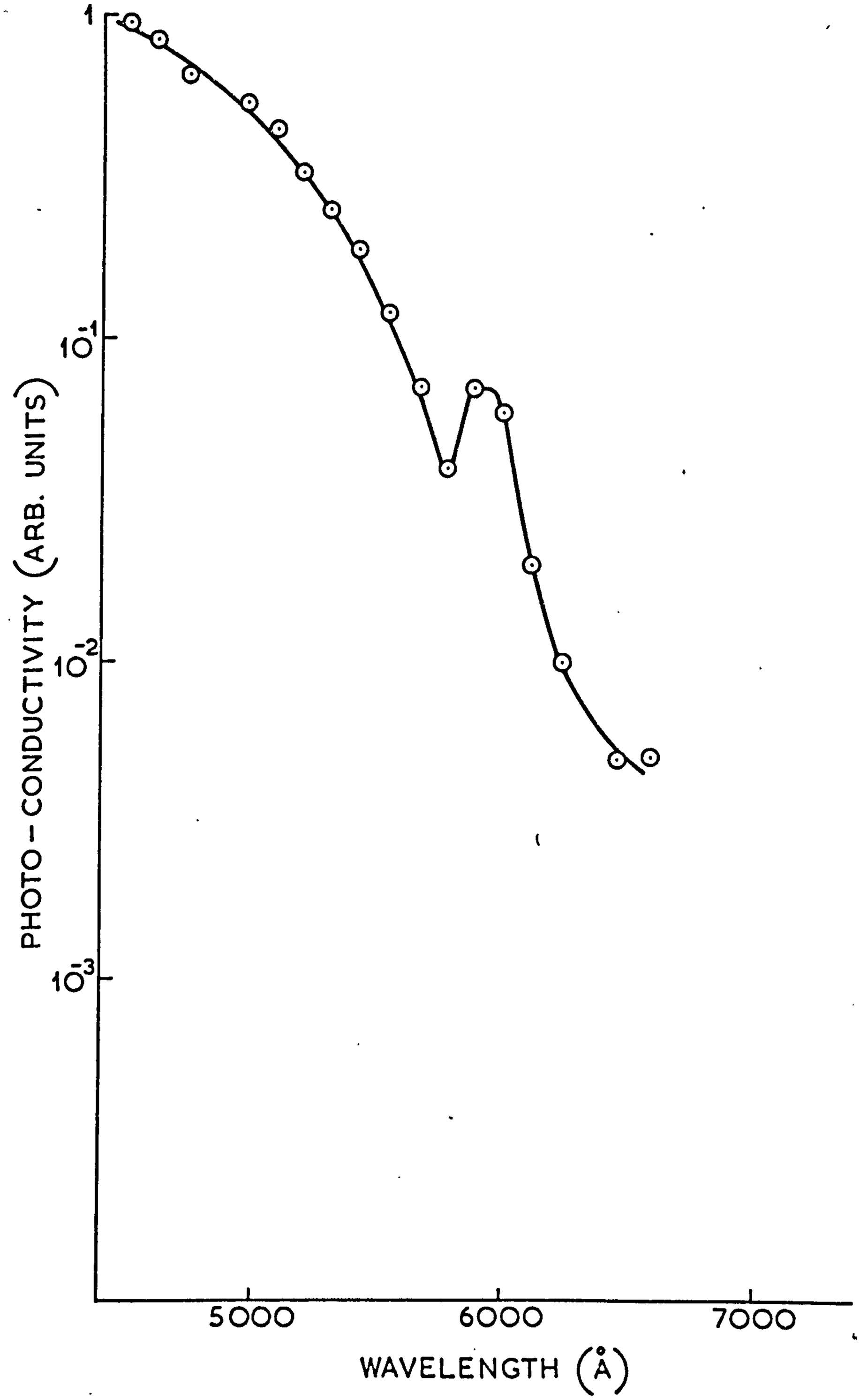

Fig. 4.11 Spectral response of photoconductivity

a graphite Knudsen cell of similar purity to the other cells. Shown in Table 4.2 are resistivity, Hall mobility, Hall constant, and donor concentration for different values of indium flux. Because of the relatively low levels of flux it was not possible to use the quartz crystal method for calibration. In this case the flux was computed[81] from the known temperature of the source and the geometry of the cell. It can be seen that in the case of specimens I, II and III, the dopant concentration varies by approximately a factor of three for a flux change of two orders of magnitude, which would seem to suggest that a saturated solution of indium is present. The Laue photographs in each case displayed a well defined spot pattern so it is unlikely that InS complexes are present. If a flux level an order of magnitude larger than that for specimen I was used, a disordered structure was found, and in this case complexes such as InS may be present. Thus in the case of specimen I, the flux level is probably the maximum to be used. The Hall mobility of these three specimens ($65 cm^2/V.s$) is reasonable as the dopant concentration N_d is N_c which for CdS is approximately $10^{18} cm^{-3}$. Thus impurity scattering will dominate for these degenerately doped films and limit the mobility. In the case of specimen IV a much reduced dopant concentration has been achieved, an order of magnitude less than that of specimen III. For all four specimens, the resistivity and Hall mobility were approximately constant over the temperature range $20^{\circ}C$ to $300^{\circ}C$ which is to be expected for such highly doped films.

4.8 Substitutional doping with phosphorus

It has been shown by Henry et al.[82] that the substitution of phosphorus for sulphur results in a deep acceptor state leV

Specimen	Indium flux mol.cm^{-2}s^{-1}	Resistivity ohm cm	Mobility cm^{2}V^{-1}s^{-1}	Carrier concentration cm^{-3}
I	4.7×10^{11}	48×10^{-2}	65	1.8×10^{18}
II	4.9×10^{10}	13×10^{-2}	65	6.1×10^{18}
III	5.1×10^{9}	20×10^{-2}	16	2.3×10^{18}
IV	5.3×10^{8}	1.3	30	1.5×10^{17}
V	8.4×10^{7}	75	40	2×10^{15}
Sulphur flux = 3×10^{16} mol. cm^{-2}s^{-1}				
Cadmium flux = 2×10^{16} mol. cm^{-2}s^{-1}				

Table 4.2 Indium doped CdS films

above the valence band edge. Obviously the thermal ionisation of such a deep acceptor will be negligible at room temperature. However, it was further shown by these workers that there is a shallow acceptor state associated with a phosphorus complex and the activation energy of this complex is approximately 0.1eV above the valence band edge. In this case a significant fraction of these states should be thermally ionised at room temperature. It was decided then to investigate the effect of substitutional doping of phosphorus on the electrical properties of the M.B.E. grown CdS films.

The phosphorus molecular beam was evaporated from a Knudsen cell identical to that used used for the cadmium and sulphur. As in the case of the indium it was not possible to measure the flux with the quartz crystal and it was computed[81] from the measured source temperature and cell geometry. The phosphorus flux levels used ranged from 2.5×10^{11} to 1×10^{13} molecules/cm^2.s and the structural quality of the films was similar to that shown in Figure 4.6c. A variety of metal contacts were used such as Ag, Au and Pt and in each case were non-ohmic. As in the case of the high resistivity films, the maximum circuit current was approximately 10nA for a few tens of volts applied. Although resistivity measurements were readily obtained, it was not possible to determine the Hall constant. Shown in Table 4.3 is the resistivity for three specimens grown with different phosphorus flux levels and the temperature dependence of resistivity is shown in Figure 4.12. The first point to note is that at room temperature, the measured resitivity voltage is negative, and shown in the insert in Figure 4.12 is the arrangement for resistivity measurements. The voltage is applied between contacts (1) and (2) and the resistivity voltage measured between

Specimen	Phosphorus $mol.cm^{-2}s^{-1}$	Resistivity ohm cm
VI	1×10^{11}	6.3
VII	2.1×10^{11}	1.0
VIII	3.5×10^{11}	2.0
Sulphur flux = 3×10^{16} $mol.cm^{-2}s^{-1}$		
Cadmium flux = 3.5×10^{16} $mol.cm^{-2}s^{-1}$		

Table 4.3 Phosphorus doped CdS films

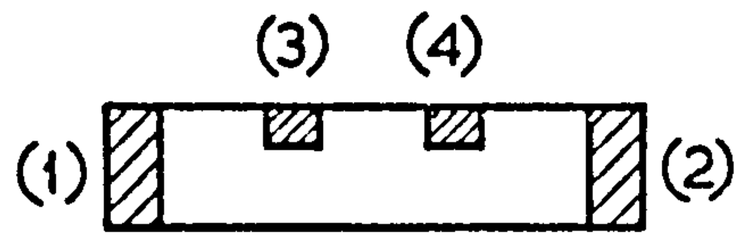

Fig.4.12 Resistivity of P doped CdS film vs reciprocal temperature

(3) and (4). If the polarity of the applied voltage is such that contact (1) is positive with respect to (2), then it was observed that (3) was negative with respect to (4). This is what is defined as a negative resistivity and is the opposite of what is normally observed. In all other resistivity measurements with n-type doping or undoped films the resistivity voltage was of the correct polarity with respect to the applied voltage. With increasing temperature the magnitude of V_p increases and at approximately 200°C it decreases rapidly and then becomes positive, increases and finally remains constant. When the temperature was reduced to 20°C, the resistivity remained positive and was an order of magnitude greater than the initial value. Such characteristics were obtained with the three phosphorus doped samples listed in Table 4.3. No explanation can yet be given for these curves, although they resemble the Hall constant versus temperature curves of two carrier conduction, i.e. electron and holes, in other semiconductors. However, in this case the sign reversal of the Hall constant is a basic conduction mechanism and does not apply to resistivity. The sign reversal observed here could indicate a two carrier conduction mechanism and that is probably due in part to the non-ohmic nature of the contacts.

Other group V impurities studied were nitrogen and antimony. For the former case operating with a residual nitrogen pressure of 5×10^{-6} torr there was no observable difference in the temperature dependence of resistivity compared with the undoped films. For antimony doped films polycrystalline films were obtained with antimony flux levels similar to those of phosphorus. Only with flux levels an order of magnitude less than that of the lowest phosphorus flux used were single crystal films obtained.

In this case the temperature dependence of the resistivity was similar to that of an undoped film.

An alternative method of determining the sign of free carriers in a semiconductor is from measurements of the thermo-electric power. For the n-type indium doped films the sign of the thermo e.m.f. was consistent with an n-type film, the exp-eriment being calibrated against known silicon specimens. Typically the thermal voltage was of the order of a few milli-volts for a temperature difference of 100°C. For the phosphorus doped films no thermal e.m.f. was observed.

4.9 Conclusion

The basic structrual and transport properties of M.B.E. grown CdS films on spinel have been examined. It has been shown that the deposition temperature, as well as the consti-tuent fluxes, have dominating effects on the structure of the films. Large lattice mismatch between the spinel substrate and CdS did not hinder the growth of epitaxial CdS films. The deposited films changed from polycrystalline at low depostion temperatures to highly oriented crystal, with a deviation of less than 60 seconds in orientation, at 400°C. A wide range of film growth rate was achieved, viz. from 2000Å per hour to 15 microns per hour. The resultant undoped films at room temperature exibit a resistivity of about 10^5 ohm cm. The significant trap defect occur at 1.6eV below E_c and are believed to be due to the cadmium vacancy. The X-ray Laue results confirmed Gunther's condensation model that a region existed where only stoichiometric CdS films are obtained. Substitutional doping with indium to produce n-type CdS has been achieved. The doping concentrations were from 6×10^{18} to 2×10^{15} cm^{-3}.

Hall mobility values obtained in such n-type films were of moderately high values indicating that ionised impurity scattering dominated the conductivity of heavily doped films.

Substitutional doping with phosphorus has been achieved, the films being of moderately low conductivity. The current carriers have not been identified because of the difficulty in fabricating ohmic contacts. The resistivity results are anomalous and no interpretation has been put upon them.

CHAPTER 5 MOLECULAR BEAM EPITAXY OF CdS FILMS ON EPITAXIAL GOLD, ALUMINIUM AND MgO SUBSTRATES

5.1 Introduction

The basic growth properties of CdS by M.B.E. on spinel have now been established (Chapter 4). The next stage in the investigation was the fabrication of simple thin-film diodes of the Schottky barrier type. Ideally the CdS film should be grown on a suitable single crystal metal substrate which is in a thin-film. An ohmic contact to the Schottky junction thus formed could be applied to the top surface, resulting in a thin-film Schottky barrier solar cell. However, the oriented growth of thin gold and aluminium films, as substrates for CdS film growth, require the use of substrate surfaces which are very smooth on the atomic scale. Systematic work[83] has been carried out with cleavage surfaces as substrates, but when metal single crystal substrates are required, cleavage is rarely possible. Metallic single crystal surfaces may be electropolished, but these are usually quite undulating, and is difficult to avoid small amount of surface contaminations which might cause gross imperfection in the films. In considering possible substrates in the present work, it seemed more promising to prepare the initial surface by an evaporation technique. An epitaxial (111) silver surface is easily prepared[84], and such a surface is very smooth on an atomic scale. But silver is unsuitable as a substrate for CdS growth because of its reaction with the sulphur flux. It is well known that chemical inertness is one of the more important substrate parameters for epitaxial film growth. Gold and aluminium (more precisely Al_2O_3), on the other hand, do not react with the incident fluxes.

The result of growth of CdS film on spinel described in Chapter 4 showed that large mismatch with the substrate did not hinder epitaxial film growth. (111) Au(a = 2.882Å) and (111) Al(a = 2.862Å)[97] have lattice mismatch with CdS in excess of 30% which are comparable to that of the spinel/CdS combination. Since similar structures exist between the (111) metals and spinel; epitaxial CdS film on metal substrates should be possible.

An investigation was therefore carried on the growth of metal substrates on mica, and a study made of the subsequent CdS film growth on the metals and its related characteristics. This work is described in detail in this chapter.

5.2 Epitaxial growth of metal films on mica

The method of growing single crystal metal films by evaporation onto mica is based on earlier works by Tull[85] and Pashley[83]. Epitaxial silver film were first evaporated onto mica, forming a substrate for gold and for aluminium deposition. The orientation between mica and silver has a fairly good fit, as shown in Figure 5.1. Along the mica [100] axis the misfit is only 4% and is the same along the mica [010], if a fit of three silver atom distances with the corresponding mica distance is considered. Silver is an ideal substrate for both gold and aluminium since the misfits for parallel orientations are only 0.2% and 0.9% respectively. Pashley[83] found that at substrate temperatures of 250°C to 300°C good single crystal silver films are formed on mica, and the surfaces of the deposited films are very smooth. Pashley also investigated the influence of the film thickness on the structure of the deposit. At its optimum substrate temperature of about 275°C it was found that in the very early stages the deposit consisted

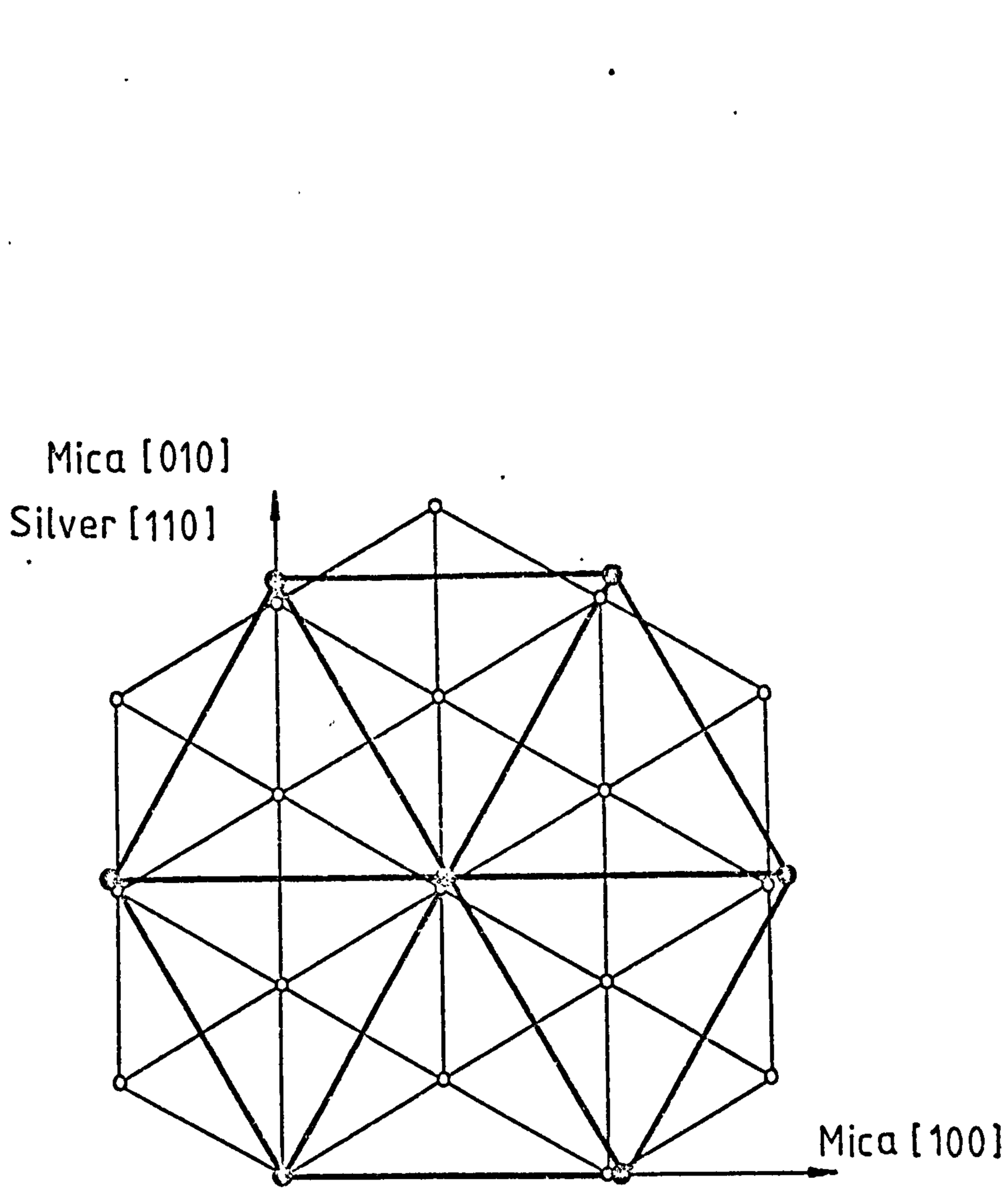

○ Silver atoms in (111) plane

● Potassium ion sites in mica (001)

Fig. 5.1 The fit of the main silver orientation on mica

of small isolated nuclei of a few tens of angstrom in linear dimensions. Many were oriented in the usual way, but some were randomly oriented, and prominant twinning occurred. Diffuse rings appeared in the diffraction pattern at the earlier stages (~50Å). As the thickness was increased, the orientation became more perfect and the rings disappeared from the diffraction pattern. The spots sharpened laterally. Further increase in thickness produced a continuation of these trends, together with a gradual weakening of the diffraction spots due to twinning. The twinning at the surface disappeared completely at a thickness of about 500Å. At a thickness of 1000Å a smooth well oriented surface was obtained.

5.2.1 The evaporation technique

The vacuum system used here for metal evaporation was carried out in an oil pumped coating unit (Edward E12) with a base pressure of 10^{-5} torr. The mica substrates were mounted below a quartz slide as shown schematically in Figure 5.2. Heating of the substrate was by a wide tungsten spiral. An iron-constantan thermocouple was placed on the surface of the mica substrate. Silver and gold were evaporated from graphite hearths heated by electron beams, and aluminium evaporated from a heated tungsten spiral mounted on top of the shutter as shown in Figure 5.2. The source materials used were of nominal purity of 99.9%. A quartz crystal thickness monitor placed adjacent to the substrate was used to monitor the growth rate and total thickness of the evaporated films.

The mica substrates were cleaved before mounted in the vacuum chamber. With the substrates in position and the required vacuum of less than 3×10^{-5} torr achieved, the substrate

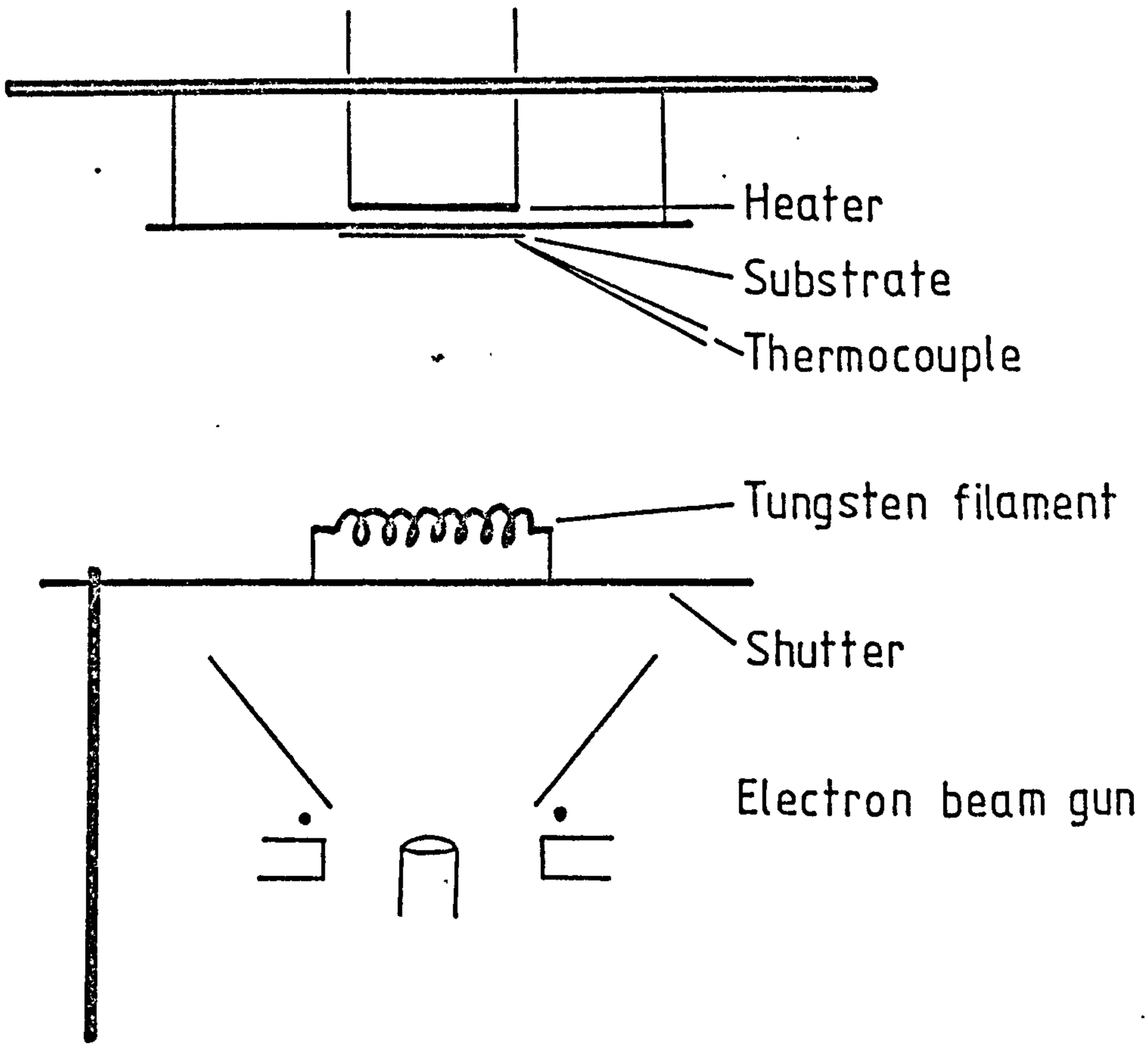

Fig. 5.2 Schematic diagram of vacuum chamber

temperature was brought up to 250-300°C and stabilised. The silver source temperature was then increased and reached evaporation temperature before the shutter was opened. A 2000Å layer of silver was then grown at a rate of 200Å per minute. During the period of evaporation the heat from the electron beam gun source tended to raise the substrate temperature. This was compensated by reducing the current to the substrate heater filament. In fact, during the gold evaporation, the substrate heater was finally turned off because the heat from the electron beam gun source was sufficient to maintain the required deposition temperature.

The epitaxial temperature for good single crystal growth was 250°C - 300°C. X-ray Laue photographs of a mica substrate and a silver film grown at 250°C on mica are shown in Figure 5.3a and Figure 5.3b respectively. Figure 5.3b clearly showed the well defined diffraction spots of the six fold symmetry of the (111) silver and this was confirmed by Bragg diffraction measurement. After the required thickness of epitaxial silver was achieved, a similar thickness of gold or aluminium was then grown onto the silver at the same growth rate of 200Å per minute. The substrate temperature was maintained throughout the entire evaporation at 250°C - 300°C. The structures of the gold and aluminium films were analysed* by transmission electron diffraction in an electron microscope. For this purpose the gold and aluminium films, which were specially grown to 200Å thick, were removed by dissolving the silver in dilute HNO_3 or NH_3/H_2O_2 mixture. Figures 5.4a and 5.4b give the diffraction pattern and TEM of gold respectively, and show perfect (111) orientation.

* J. Fryer, Chemistry Department

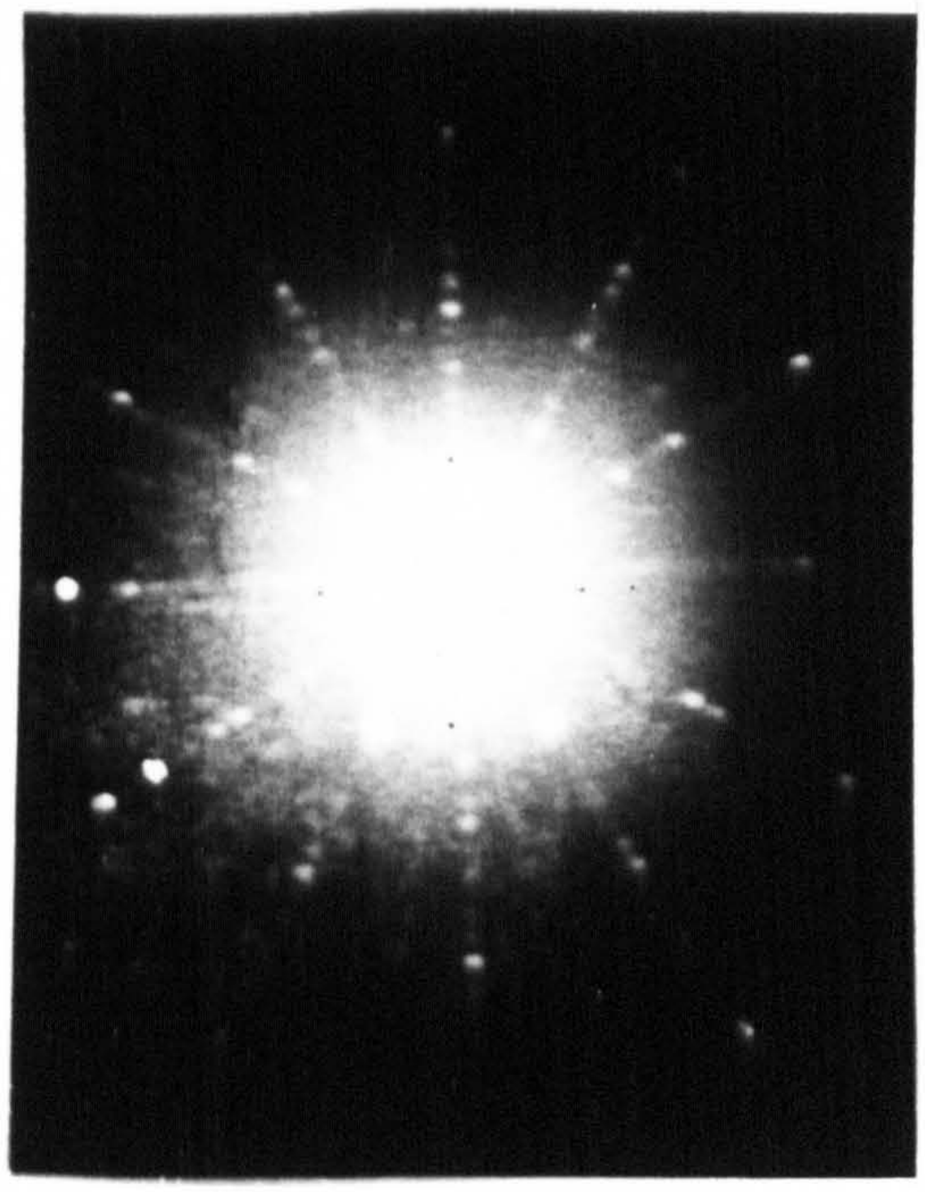

(a)

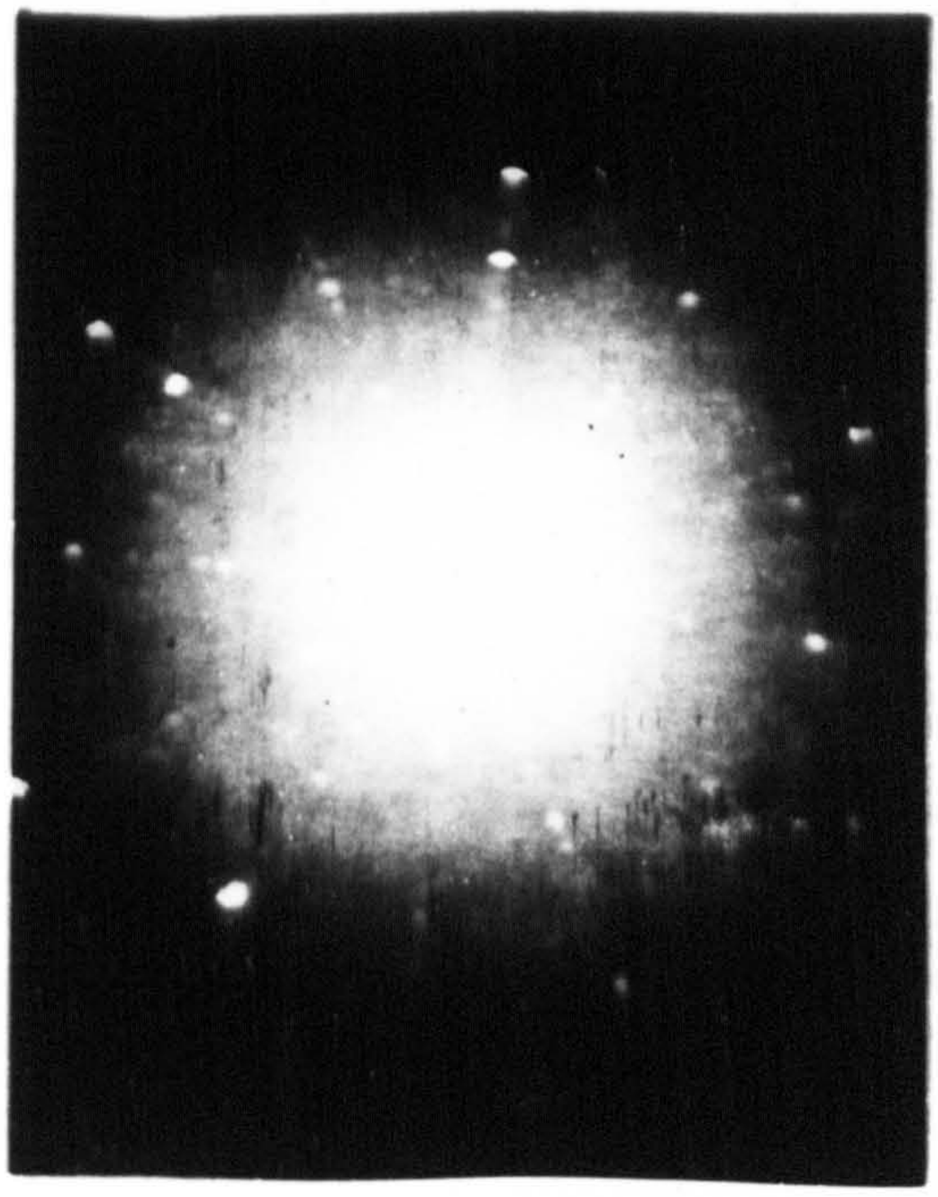

(b)

Fig. 5.3 X-ray Laue photographs of (a) mica and (b) silver on mica

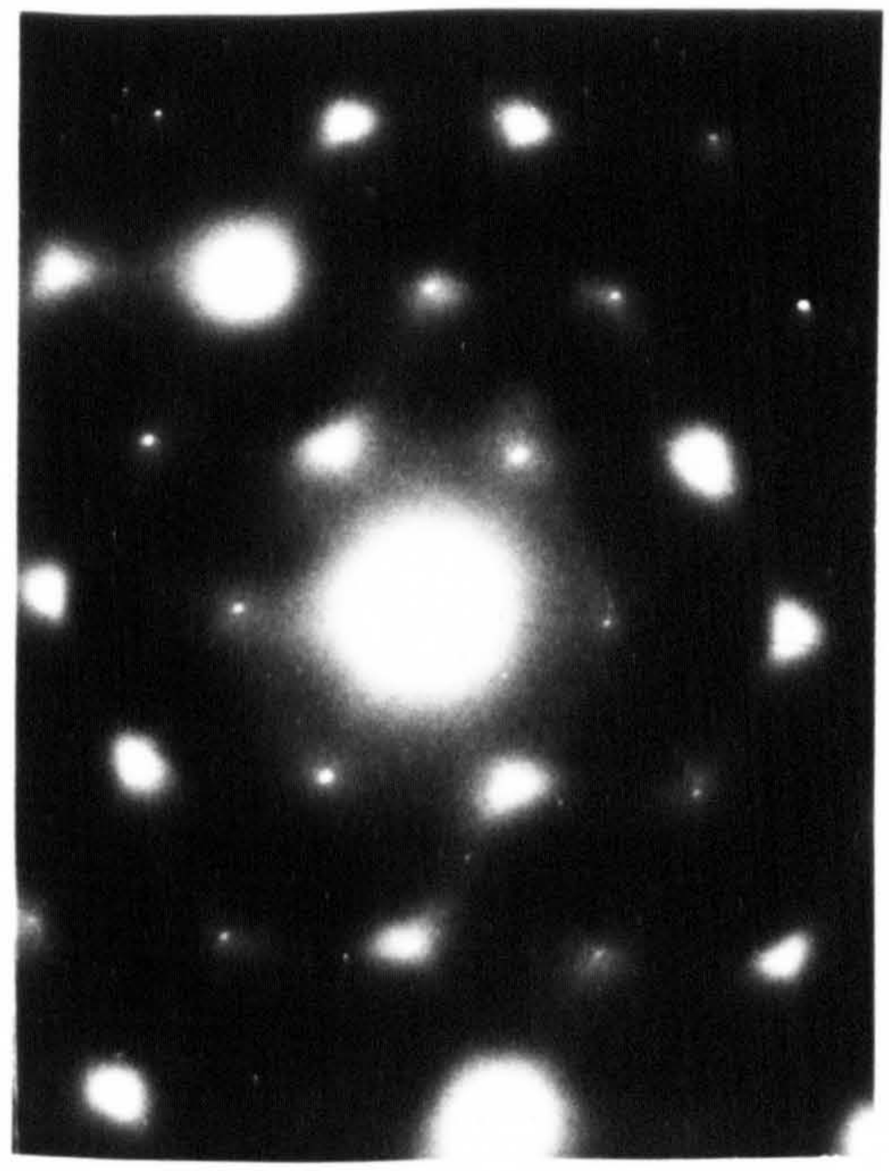

(a)

(b)

Fig. 5.4 (a) Transmission diffraction pattern and

(b) TEM (× 10,000) of a gold film

The corresponding diffraction pattern and TEM of aluminium are given in Figure 5.5a and Figure5.5b respectively. The diffraction pattern of the aluminium film was taken from a small selected area. Al_2O_3 was present and was analysed as ionic γ-Al_2O_3[86].

5.3 Growth of epitaxial CdS films on epitaxial metal substrates

CdS films were deposited on the metal substrates in the U.H.V. plant used for CdS deposition on spinel, as described in Chapter 4. The epitaxial metal films were transferred from a separate vacuum system as there was no provision to grow the metal in the U.H.V. plant. This arrangement resulted in the formation of an oxide layer of approximately 20Å[87] on the aluminium surface. Although no such reaction occurs with the gold film, the absorption of impurities takes place on exposure to the atmosphere. The metal substrates were mounted similarly to that of spinel except for a molybdenum piece placed on the back of the substrate in order to spread the heat distribution from the tungsten spiral mounted above.

When silver was first used as substrate for CdS deposition, a dark polycrystalline structure was produced, which was predominantly Ag_xS_{1-x} with very little trace of CdS. This result was not unexpected as the silver reacts rapidly with sulphur and the formation of silver sulphide occurs in preferance to that of CdS, similar to that found with copper.

The substrate deposition temperature, as with CdS deposition on spinel, was found to play an important role in the growth of the CdS film on the metal substrates. In the case of the gold substrate, no noticeable film growth occurred above $300^{o}C$ with cadmium and sulphur beam fluxes of 3×10^{16} mol./cm^2.s.

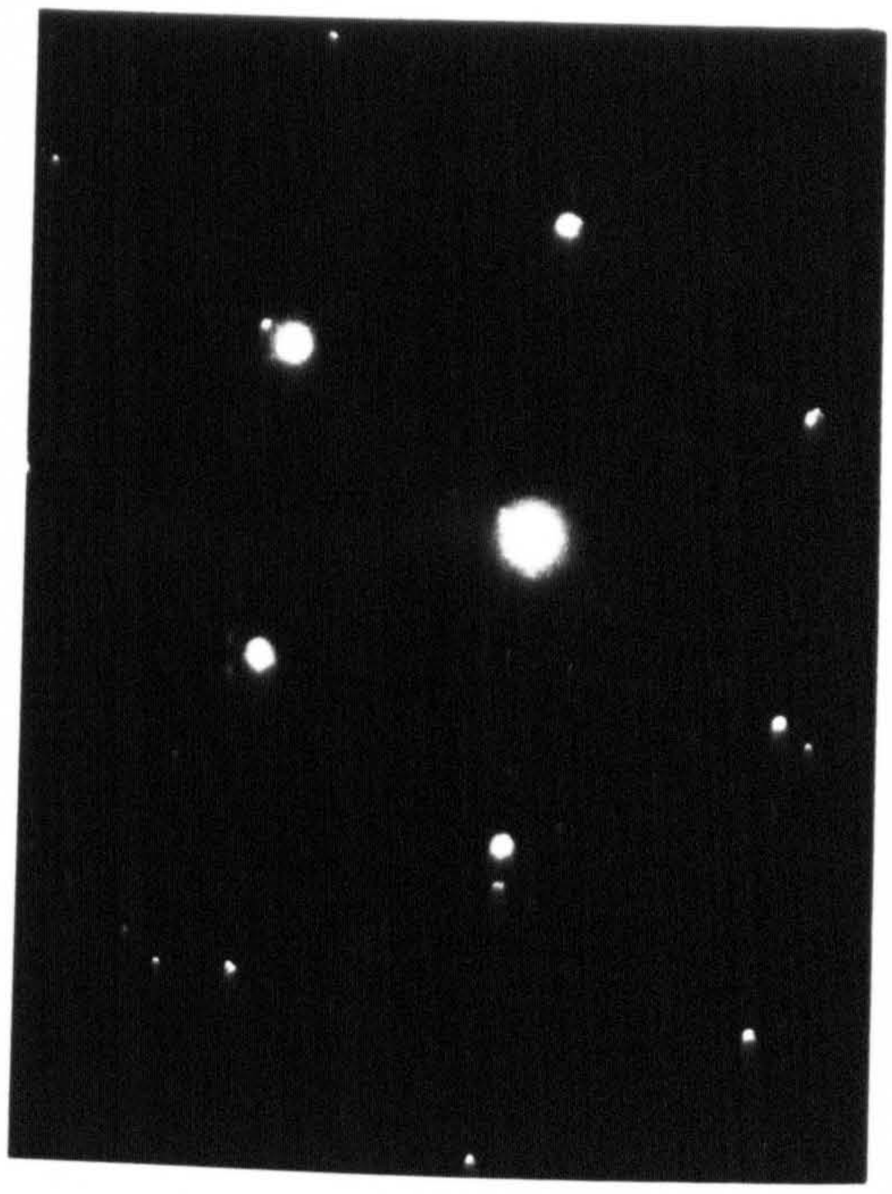

(a)

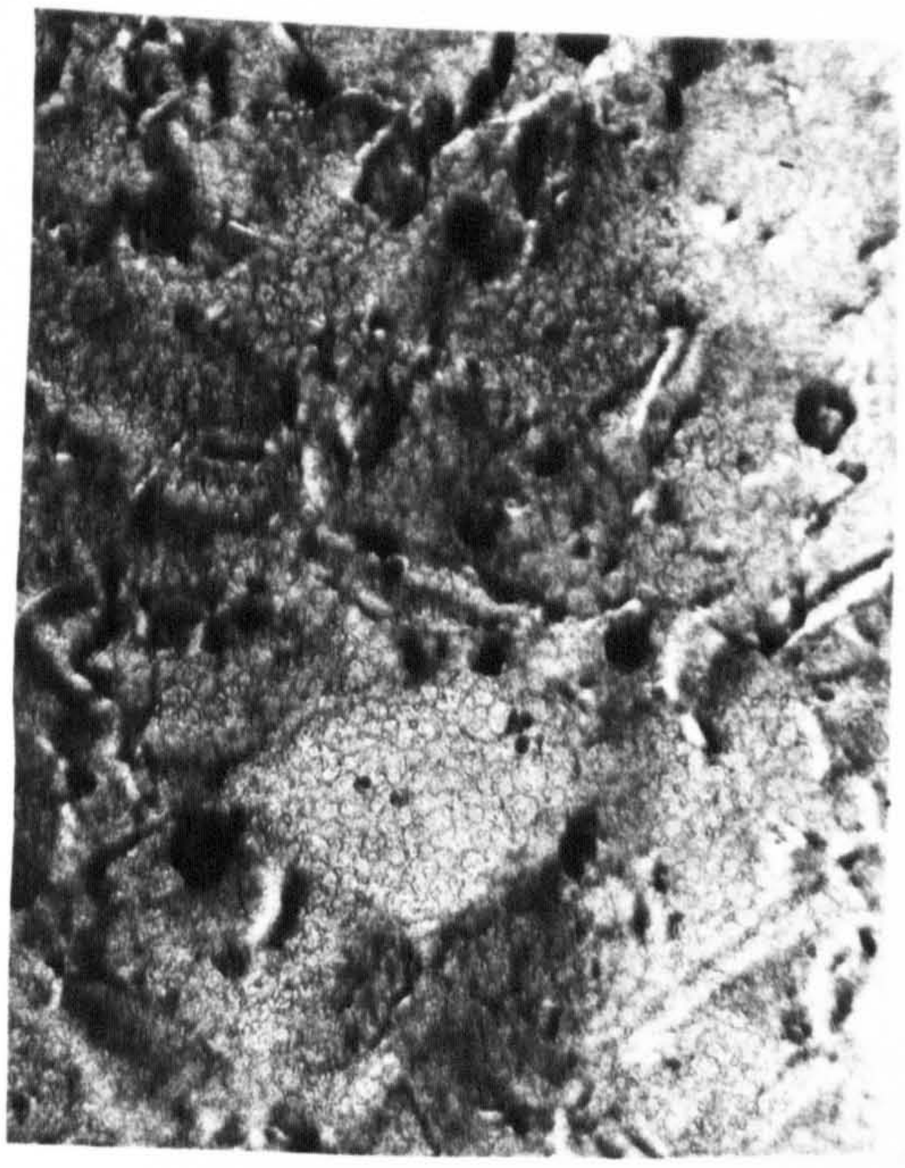

(b)

Fig. 5.5 (a) Transmission diffraction pattern and

(b) TEM(× 100,000) of an Al film

Below approximately 200°C polycrystalline hexagonal films were obtained; only over the substrate temperature range of 240°C to 300°C were epitaxial films obtained. An X-ray Laue photograph of a CdS film grown on gold at 300°C is shown in Figure 5.6. The CdS films deposited were of the wurzite structure (2θ = 26.40) as determined by Bragg diffraction using Cu Kα radiation with a nickel filter[80]. For CdS film growth on epitaxial aluminium, a cut-off temperature of 320°C was observed for similar flux levels and the corresponding epitaxial temperature range was 200°C to 320°C. Shown in Figure 5.7a is an X-ray Laue photograph of a 4 micron thick CdS film grown at 300°C with a film growth rate of 8 microns per hour. Two points are of note, firstly the film consists of an epitaxial cubic phase with the (111) orientation, and secondly a polycrystalline hexagonal phase is also present. When another film was grown on aluminium substrate under similar conditions but for a reduced time period, giving a film thickness of approximately 1μm, no trace of the polycrystalline region was evident, only the epitaxial cubic phase was present, as shown in Figure 5.7b. This suggests that the film growth proceeds as a single crystal cubic structure which transforms to the polycrystalline hexagonal structure as the film thickness increases. This deduction is supported by Figure 5.8a and 5.8b which showed the X-ray Laue photographs of a 3μm CdS film grown at 300°C on aluminium substrate photographed from the substrate (back) and the free growing (front) ends respectively. Figure 5.8b clearly shows spots of the cubic phase as well as rings of the hexagonal structure, while Figure 5.8a shows only well defined diffraction spots. In CdS, with Cu Kα radiation, it can be demonstrated that 63% of the diffracted radiation comes from the 1μm layer of the surface[80],

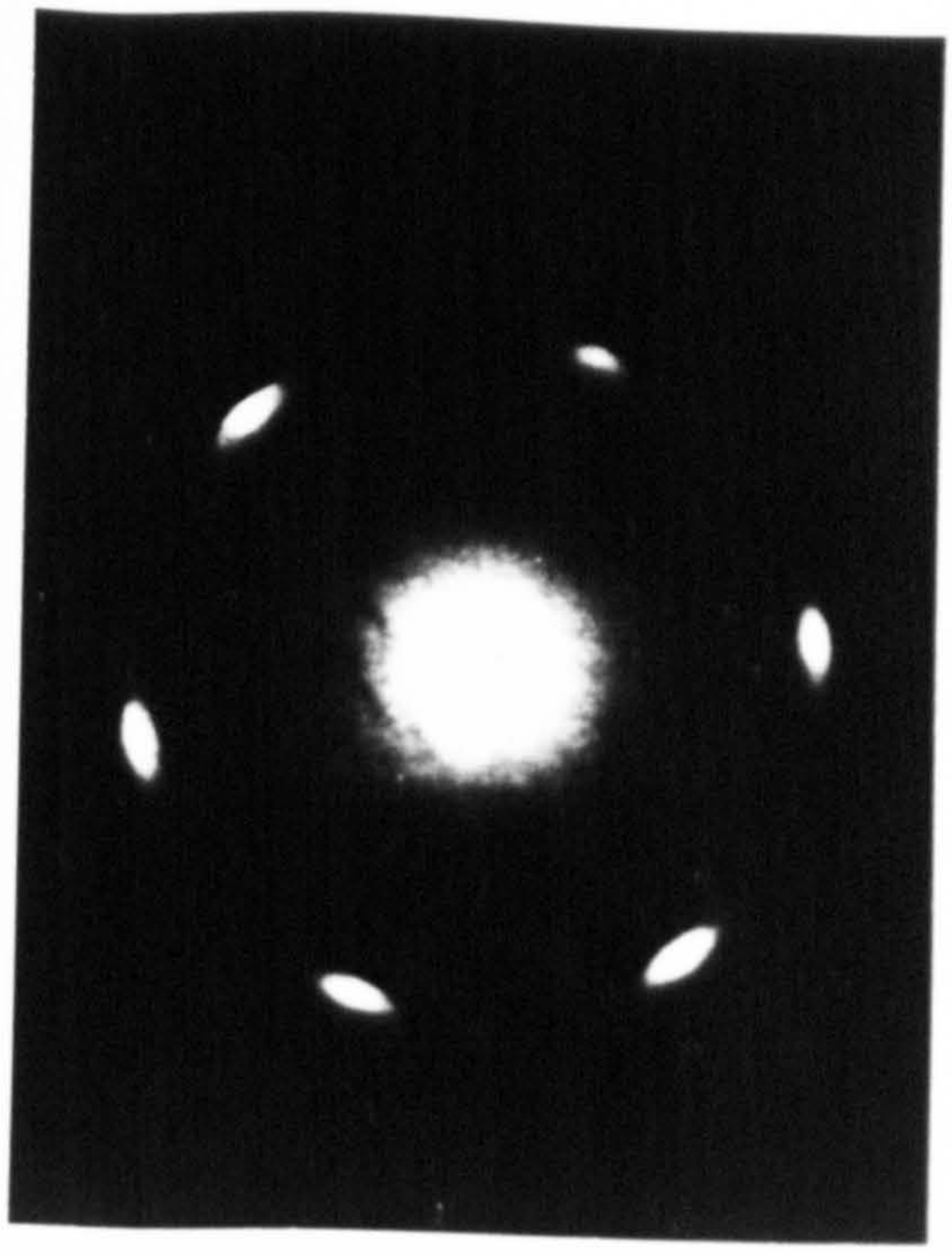

Fig. 5.6 X-ray Laue photograph of a CdS film on gold substrate

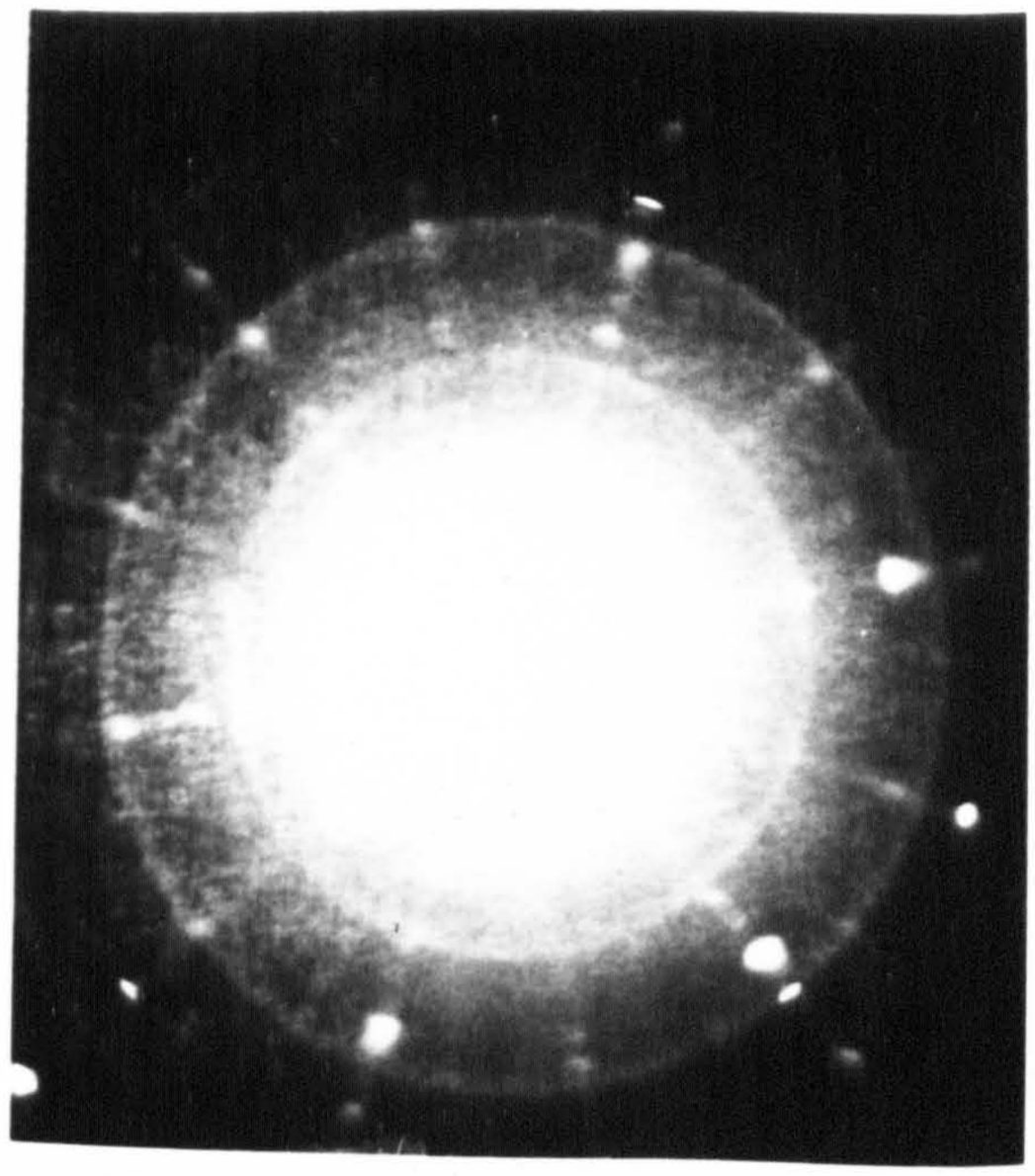

(a)

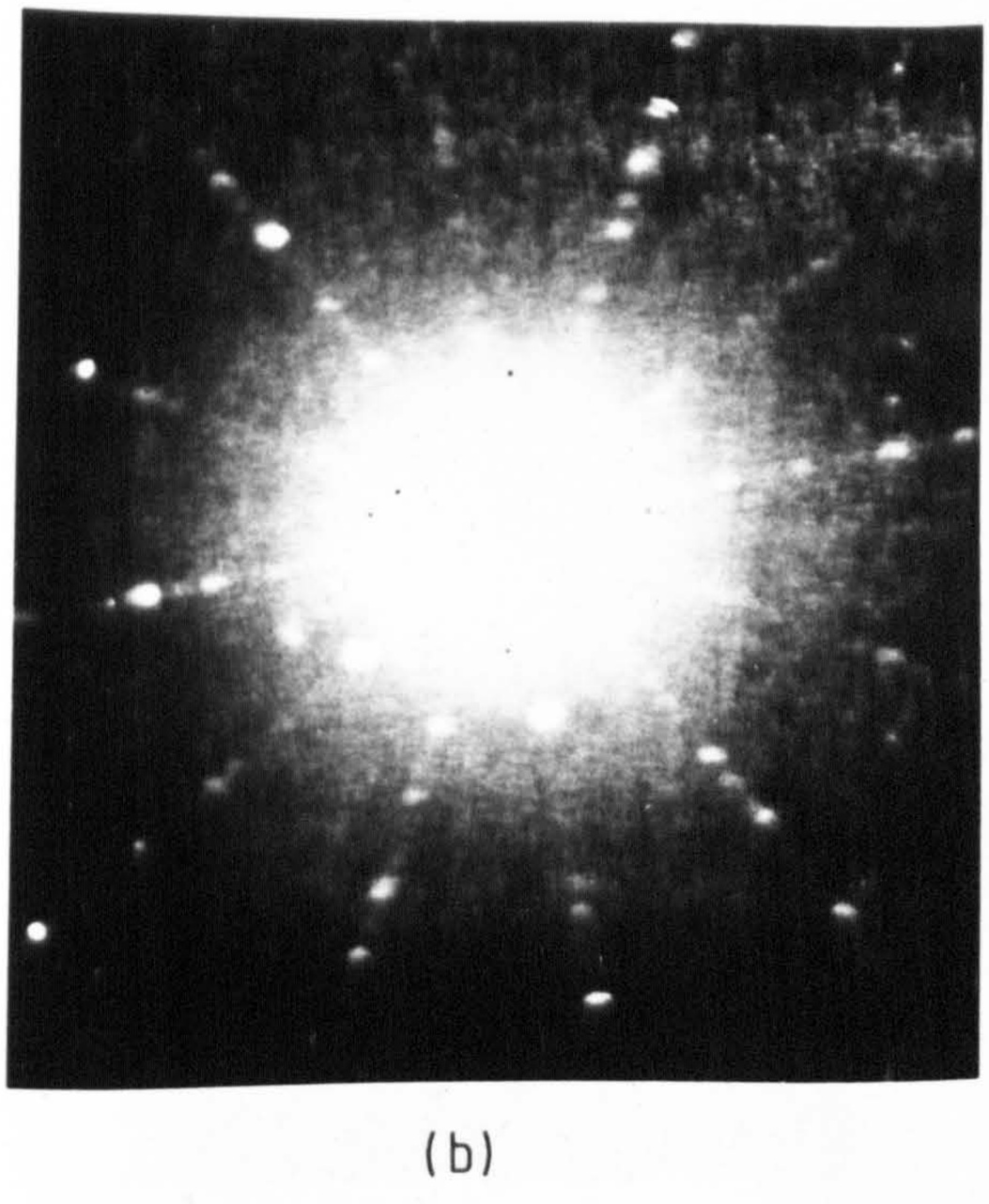

(b)

Fig. 5.7 X-ray Laue photographs of (a) a 4 μm and (b) a 1 μm thick CdS film grown at 300 °C

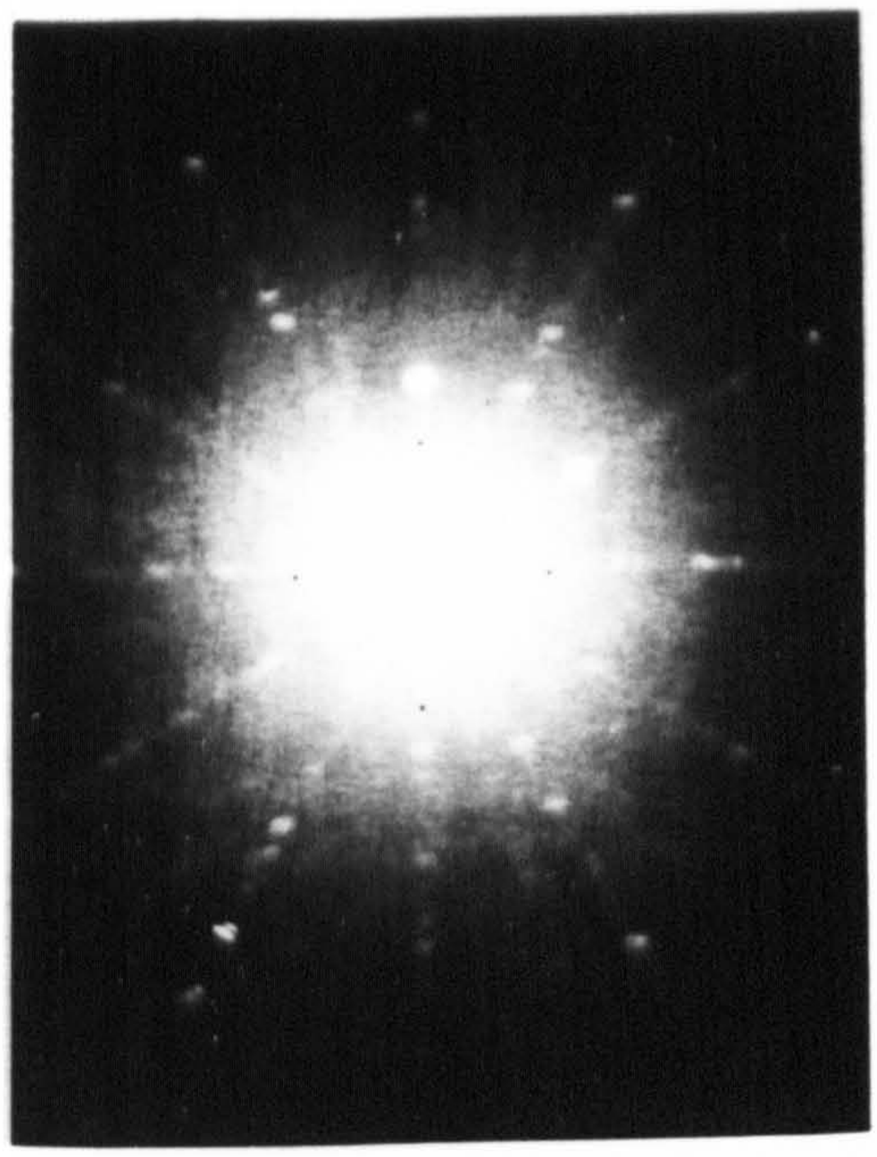

(a)

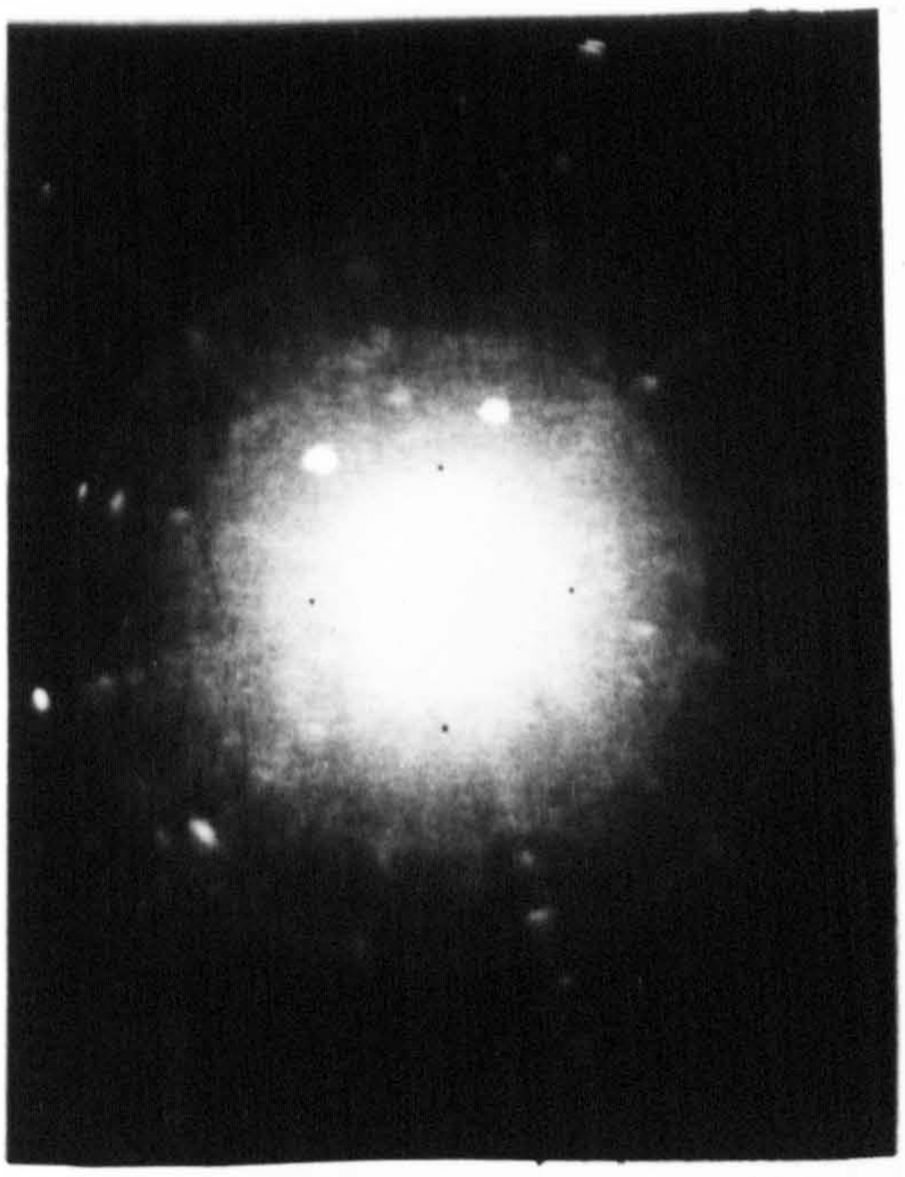

(b)

Fig. 5.8 X-ray Laue photographs of a CdS film on aluminium substrate photographed from (b) the front and (a) the back

and that the beam intensity has decayed to 1% of its initial value on penetrating 4.7μm.

From the investigations of CdS films deposited on spinel reported in Chapter 4, it was found that the epitaxial hexagonal CdS film grew at about 400°C. In contrast, the results obtained using aluminium substrates showed that polycrystalline hexagonal CdS film was present at the higher deposition temperatures. Attempts were therefore made to grow the CdS film on aluminium in such a way that the film would convert from the initial epitaxial cubic structure to the epitaxial hexagonal phase. This was achieved by growing the CdS film initially at 300°C for 5 minutes, this having been shown to produce epitaxial cubic CdS (Figure 5.7b), followed by further growth at substrate temperature of 400°C. The constituent fluxes were shuttered off between the two growth conditions. An X-ray Laue photograph of a 1.5μm CdS film grown by this technique is shown in Figure 5.9. The picture clearly shows no trace of polycrystalline CdS; clear diffraction spots at the position of the hexagonal ring indicating the presence of epitaxial hexagonal CdS.

5.4 Characteristics of deposited CdS films

5.4.1 Piezoelectric polarity measurements

Cadmium sulphide, in the hexagonal form, is typical of the hexagonal semiconducting compounds from elements in Group II and Group VI of the Periodic Table. It posses a unique polar axis (the C-axis). Piezoelectric polarity measurement[88-90] by compression or extension along this axis produces opposite charges on the basal faces, which also differ in their response to etching and other properties[91]. A negative polarity is

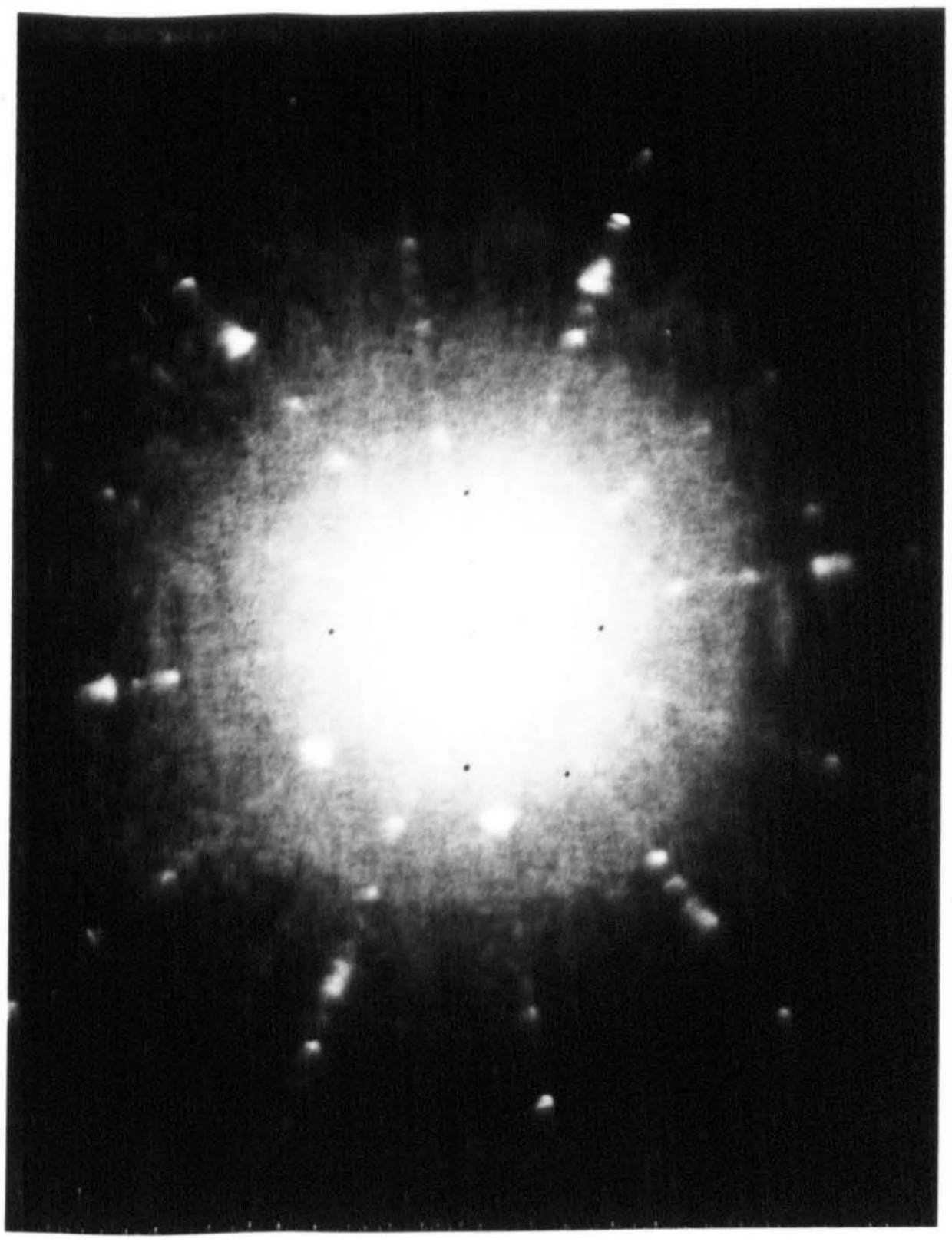

Fig. 5.9 X-ray Laue photograph of a CdS film grown at 300°C followed by 400°C

observed on compression, indicating that the film is oriented with the cadmium face at the free-growth surface and the sulphur face next to the substrate. The crystal structure of hexagonal CdS as shown in Figure 5.10 shows the polarity clearly. Viewed normal to the C-axis, pairs of closely spaced cadmium-sulphur layers are seen. The "cadmium face" and the "sulphur face" are defined in Figure 5.10.

Piezoelectric measurements were made on deposited CdS samples by a pressure point contact probe applied to the top surface of the film. The piezovoltages generated between the metal substrates and the top contact were determined. Typical piezovoltages measured on CdS grown on gold substrate were approximately 4 volts with the top surface negative with respect to the substrate surface, indicating that the films were oriented with the cadmium face at the free-growth surface. On the other hand, the piezovoltages induced on CdS films grown on aluminium substrates were only of the order of millivolts and of opposite polarity to those found with CdS on gold. The top surface was positive with respect to the substrate surface, indicating the surfaces of the films were of the sulphur face. The piezovoltage induced on the CdS films grown on aluminium substrate, which were (111) cubic (Section 5.3), were weak by virture of the fact that it does not have a centre of inversion.

5.4.2 Thermo-e.m.f. measurements

Smith[92,93] has shown that an e.m.f. is set up in a temperature gradient along a conductor even when no electric current flows. The thermo-electric power of semiconductors is high, of the order of 1 mV/^{o}C, whereas for metals the thermo-electric power is of the order of a few μV/^{o}C. For a semi-

Cadmium face

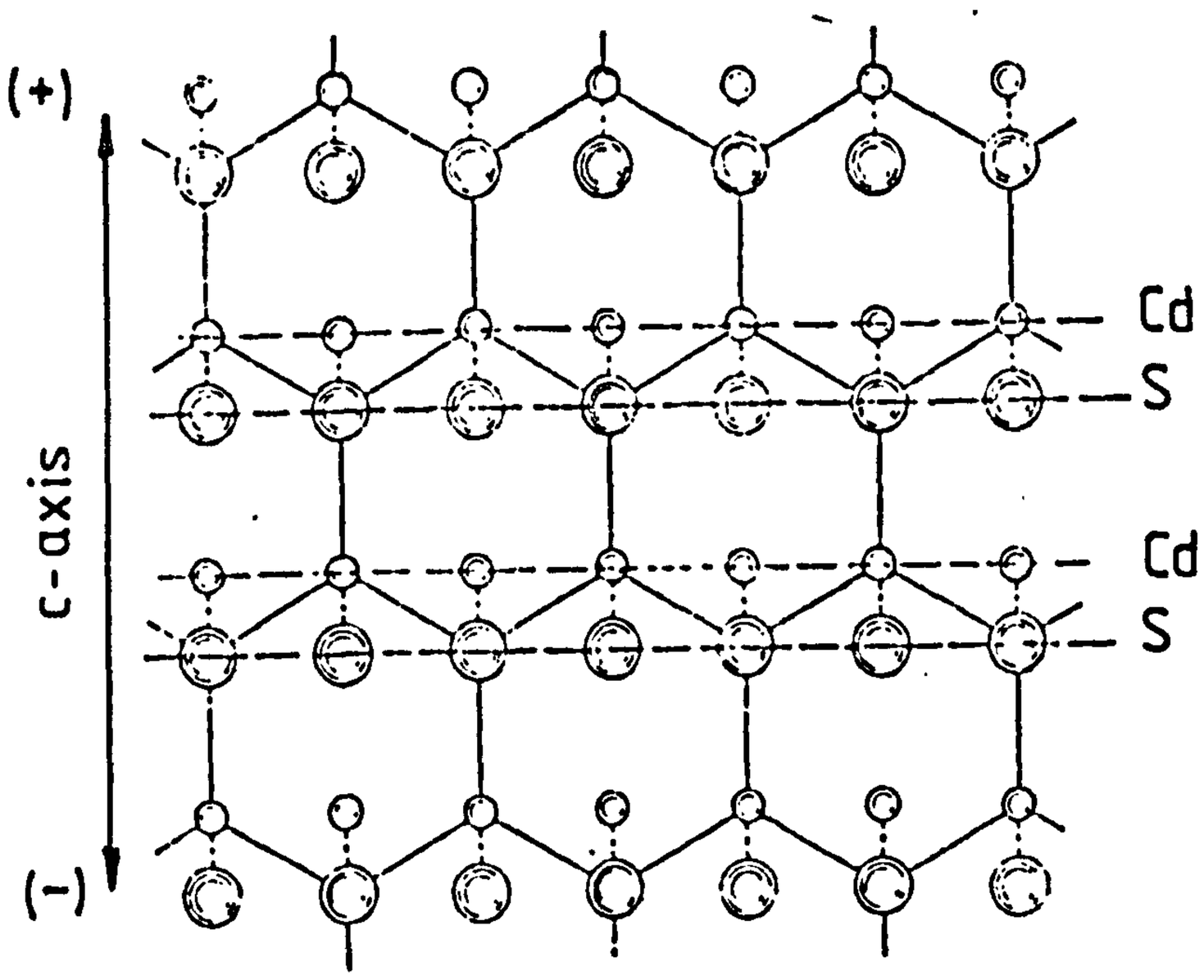

Sulphur face

Fig. 5.10 Alternate layers of Cd and S parallel to the (0001) surfaces

conductor-metal junction the thermo-electric power is approximately equal to the absolute thermo-electric power of the semiconductor. Furthermore, the sign of the thermo-e.m.f. of a p-type semiconductor is opposite to that of a n-type semiconductor. The sign of the thermo-e.m.f. therefore gives a simple direct test as to whether a semiconductor is n-type or p-type.

The thermo-e.m.fs of CdS films were measured by mounting one end of the substrate on a heater block with the other end maintained at room temperature. The thermo-e.m.fs measured as a function of temperature for CdS films grown on gold and aluminium are shown in A and B of Figure 5.11 respectively. The signs of the voltages, which were calibrated against silicon specimens, corresponded to that of n-type for CdS grown on gold and p-type for CdS grown on aluminium. The p-type CdS was observed for all CdS films grown on aluminium over the epitaxial temperature range, although variations in the magnitude of the voltage were observed. It was confirmed that the thermovoltage was not due to the metal substrate itself, this was found to be over more than two orders of magnitude smaller, which is to be expected.

5.4.3 Summary of CdS films deposited on gold and aluminium substrates

CdS films deposited on gold substrates were found to be of hexagonal structure, while those deposited on aluminium substrates were of the cubic phase. Thermo-e.m.f. measurements indicated n-type conduction in CdS films deposited on gold while p-type conduction existed in CdS films on aluminium. Piezoelectric measurements indicated that sulphur face grew initially on gold substrates whereas cadmium was the first to

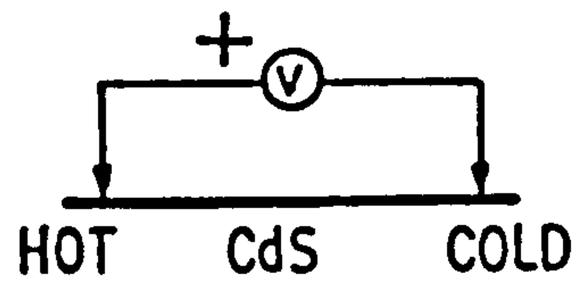

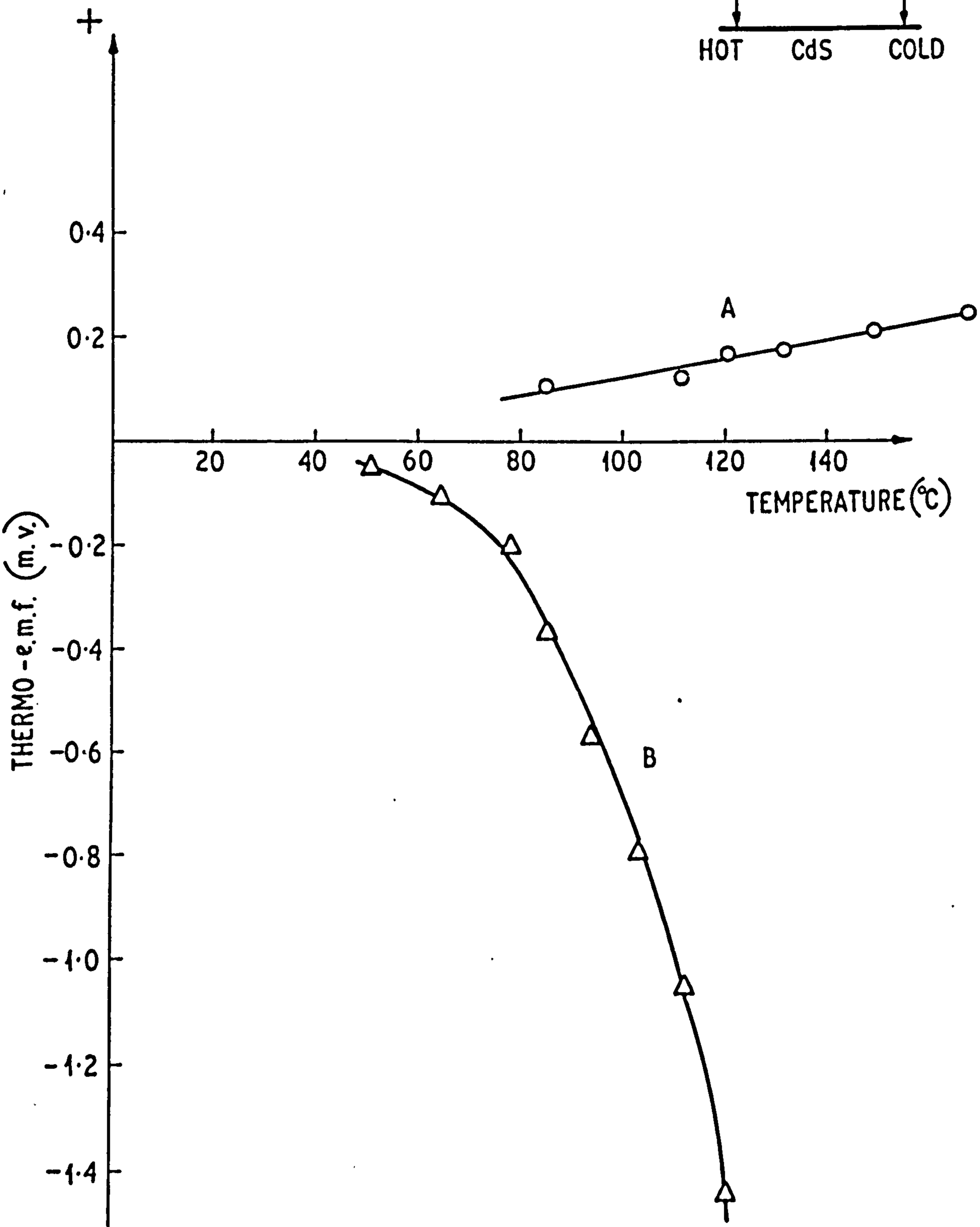

Fig. 5.11 Thermo-e.m.f. vs. Temperature of CdS films grown on (A) gold and (B) aluminium substrate

nucleate on aluminium. The above differences in the CdS film characteristics deposited on aluminium substrates indicated that the thin layer of ionic Al_2O_3 of the order 20Å to 30Å thick on the surface of the aluminium may have played an important role, and that a MIS structure existed consisting of Al-Al_2O_3-CdS.

5.5 Epitaxial CdS growth on MgO

Thin-film MgO was considered to be a suitable substitute for Al_2O_3. The epitaxial growth of thin-film MgO has been established by numerous workers[94]. However, before initiating work on thin-film MgO, some preparatory studies were carried out on bulk crystals to establish the epitaxial growth conditions for this substrate.

5.5.1 Single crystal (100) MgO substrate

The deposition procedure of CdS on single crystal (100) MgO was as described in Section 5.3. The substrate was first polished and then cleaned in organic solvent before mounted in the U.H.V. plant for CdS deposition. The substrate was thermally cleaned at 600°C for 15 minutes before the substrate temperture was stabilised for film deposition. The CdS films were grown over a wide range of deposition temperature. With the substrate temperature at 220°C, polycrystalline cubic films were observed. At 300°C epitaxial cubic films were produced. An X-ray Laue photograph of a 1.5μm thick CdS film deposited at substrate temperature of 300°C on single crystal (100) MgO is shown in Figure 5.12. The four-fold symmetry observed in the photograph on (100) plane can only be of the cubic structure. (A hexagonal structure would have six-fold symmetry). Both the cubic and

hexagonal structure have six-fold symmetry on the (111) plane. The film was deposited with cadmium and sulphur fluxes at 5×10^{16} molecules/cm^2.s. Comparison of the diffraction spots with those of the MgO substrate showed that the substrate diffraction spots were not present in Figure 5.12. Diffractometer readings confirmed that the intensity of the substrate signal was 100:1 down. A series of CdS films were deposited at a range of cadmium fluxes ranging from 2.6×10^{16} to 9×10^{16} molecules/cm^2.s. The sulphur flux was maintained at a value of 4×10^{16} molecules/cm^2.s. Growth rates from 0.2μm/hr at a cadmium flux of 2.6×10^{16} molecules/cm^2.s to 6μm/hr at a cadmium flux of 9×10^{16} molecules/cm^2.s were found. The structure of the deposited film was to deteriorate at growth rates higher than 1.5μm/hr.

5.5.2 Thin-film (111) MgO substrate

A freshly cleaved mica was used as the base. A 2000Å film of silver was first deposited followed by 2000Å of aluminium or gold, and then MgO. The MgO was evaporated from an electron beam gun source. The deposition temperature was maintained at about 250°C throughout. In order to minimise any oxide formation on the aluminium in the vacuum of $<10^{-5}$ torr during deposition, the MgO source was heated to evaporation point before the aluminium deposition was completed. The base that held the aluminium source also acted as a shutter for the MgO source below. Movement of the base/shutter therefore resulted in a rapid and smooth transition from aluminium to MgO deposition. The thickness of the MgO, as with the metals, was measured by a quartz thickness monitor. Film thickness of 40Å to 1000Å were obtained. A TEM of a 100Å film of (111) MgO deposited on

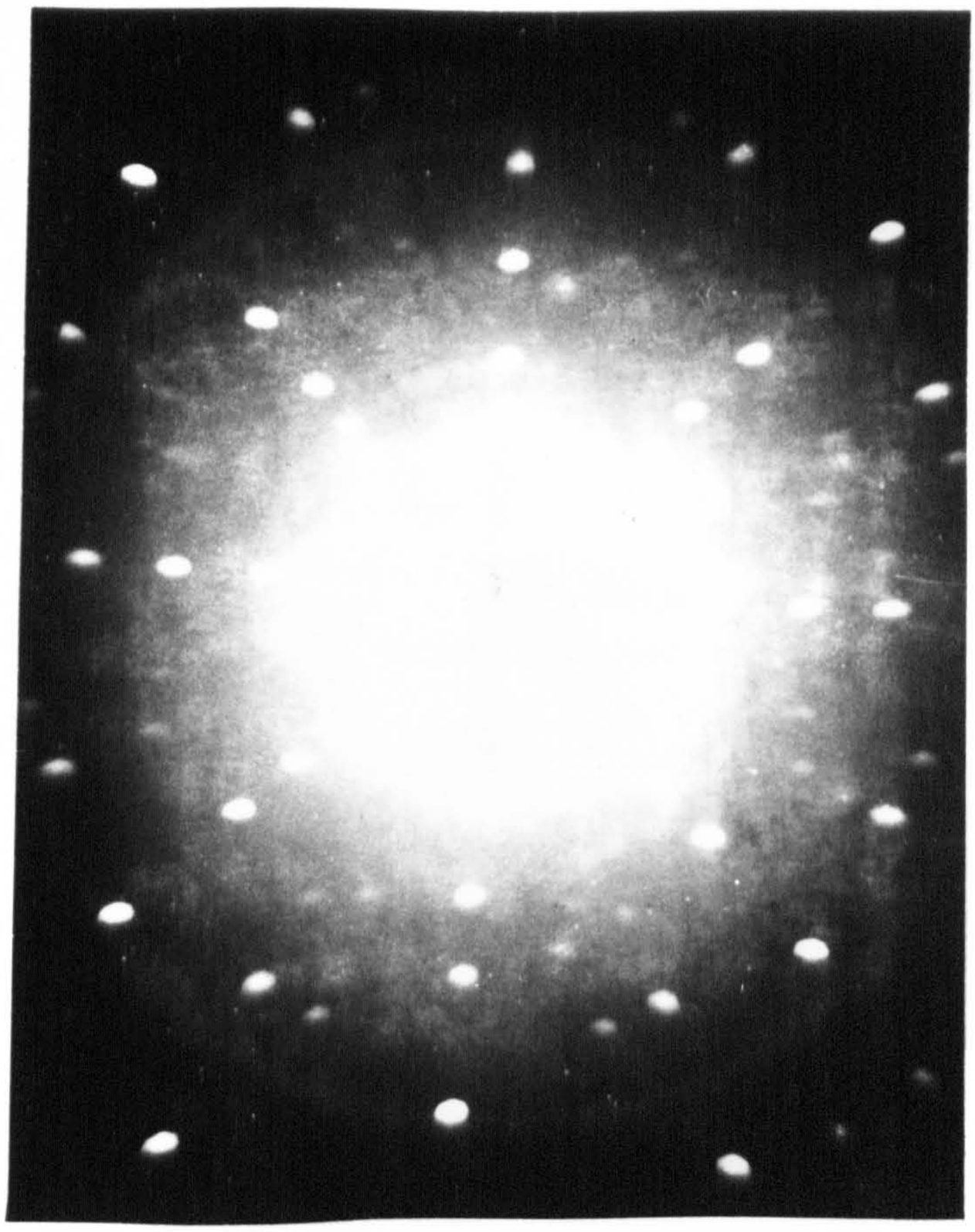

Fig. 5.12 An X-ray Laue photograph of a CdS film deposited on single crystal (100) MgO

200Å film of gold is shown in Figure 5.13. The diffraction pattern shown in Figure 5.13 is identical to that obtained from a thin epitaxial gold film(Figure 5.4). This was due to close lattice match of the MgO and Au in the (111) plane.((111) Au(a = 2.88Å and (111) MgO(a = 2.97Å)). Figure 5.13 is therefore consist of two identical diffraction patterns, of Au and MgO, superimposed on top of one another, and not of gold alone.

The deposition of CdS on thin-film MgO substrate was carried out as described in Section 5.3 for deposition on metal substrates. At a substrate temperature of 300°C with cadmium and sulphur fluxes at 4×10^{16} molecules/cm^2.s, the growth rate was 1.5μm/hr. An X-ray Laue photograph of a CdS film deposited in the above condition on thin-film epitaxial (111) MgO is shown in Figure 5.14. Measurements of the positions of the diffraction spots and diffractometer readings confirmed that the structure of the CdS film was cubic. Thermo-e,m.f. which were made by the method described in Section 5.4.2, (shown in Figure 5.15), confirmed p-type conduction. Positive piezovoltages of the order of millivolts indicated the presence of sulphur face on the free-growth surface.

5.6 Conclusion

The growth of metals on mica, and CdS films on metals and MgO were investigated by X-ray Laue diffraction, Bragg diffraction, Piezovoltage and thermovoltage techniques. Epitaxial growth of silver film on mica substrate was obtained at growth temperature of 250°C - 300°C. The silver film was of (111) orientation. In-situ evaporation of gold and aluminium on deposited silver film resulted in epitaxial (111) oriented gold and aluminium film respectively. The epitaxial temperature range was 250°C - 300°C.

CdS films deposited on gold substrates were found to be

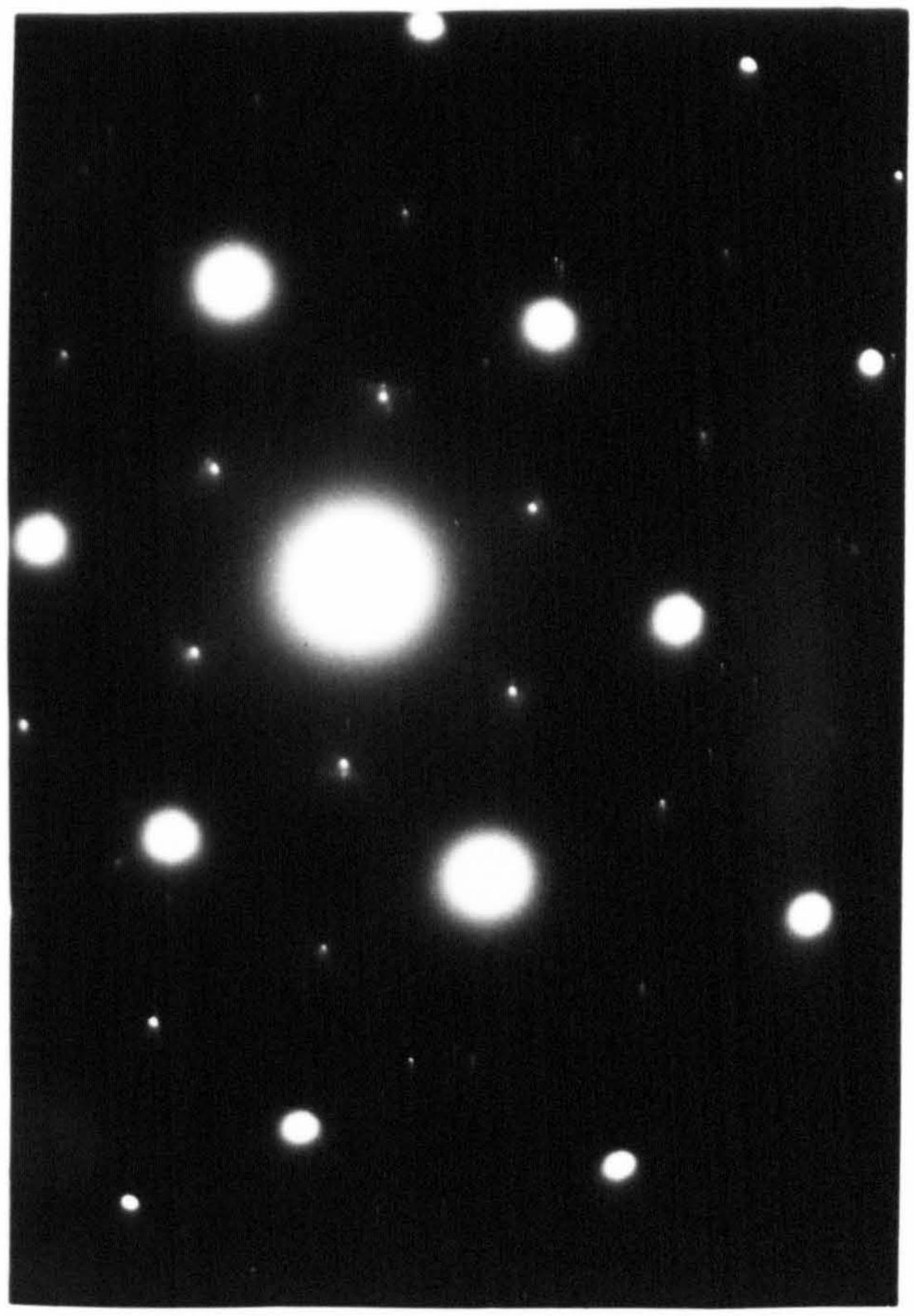

Fig. 5.13 Transmission diffraction pattern of a MgO film

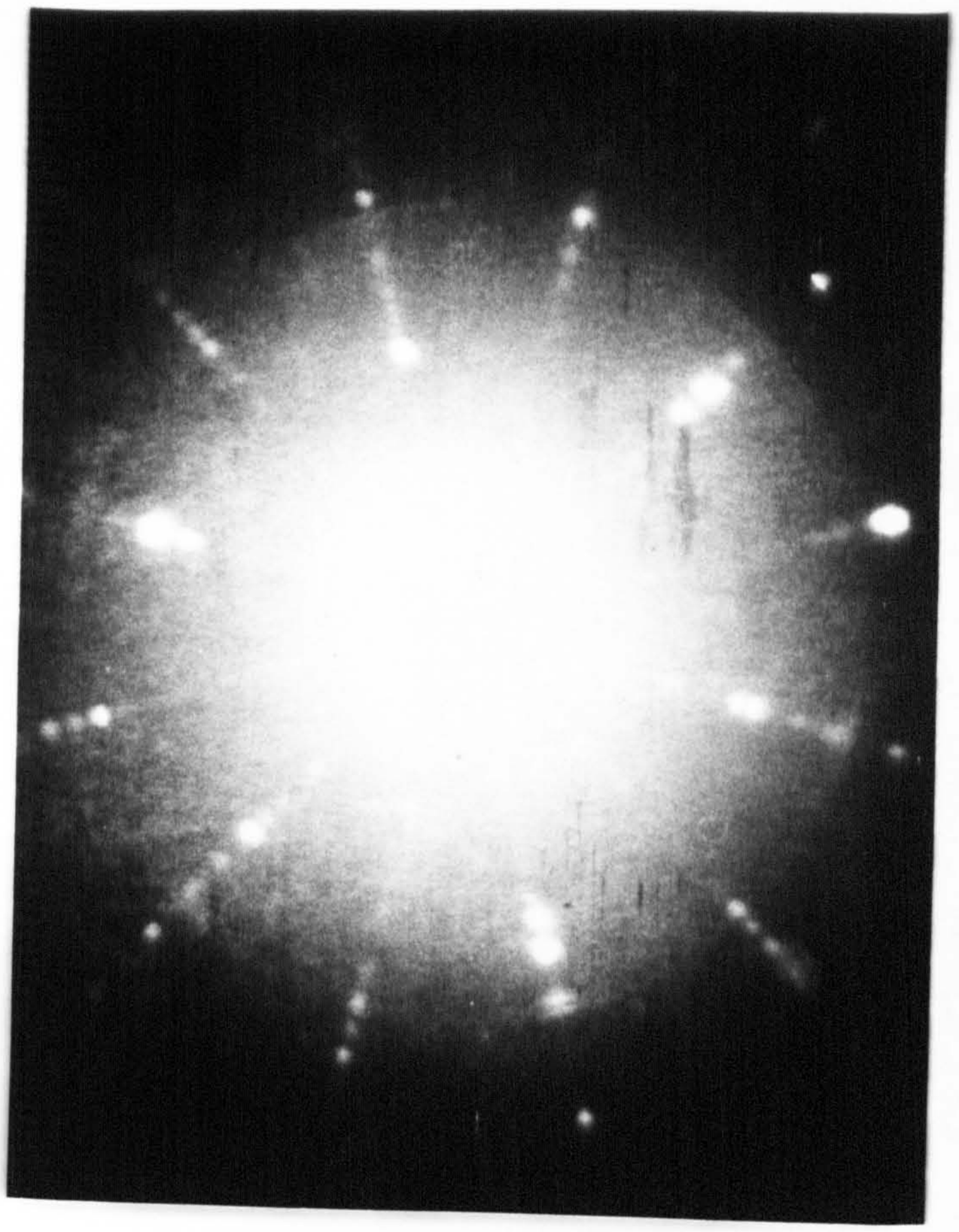

Fig. 5.14 An X-ray Laue photograph of a CdS film deposited on thin-film (111) MgO

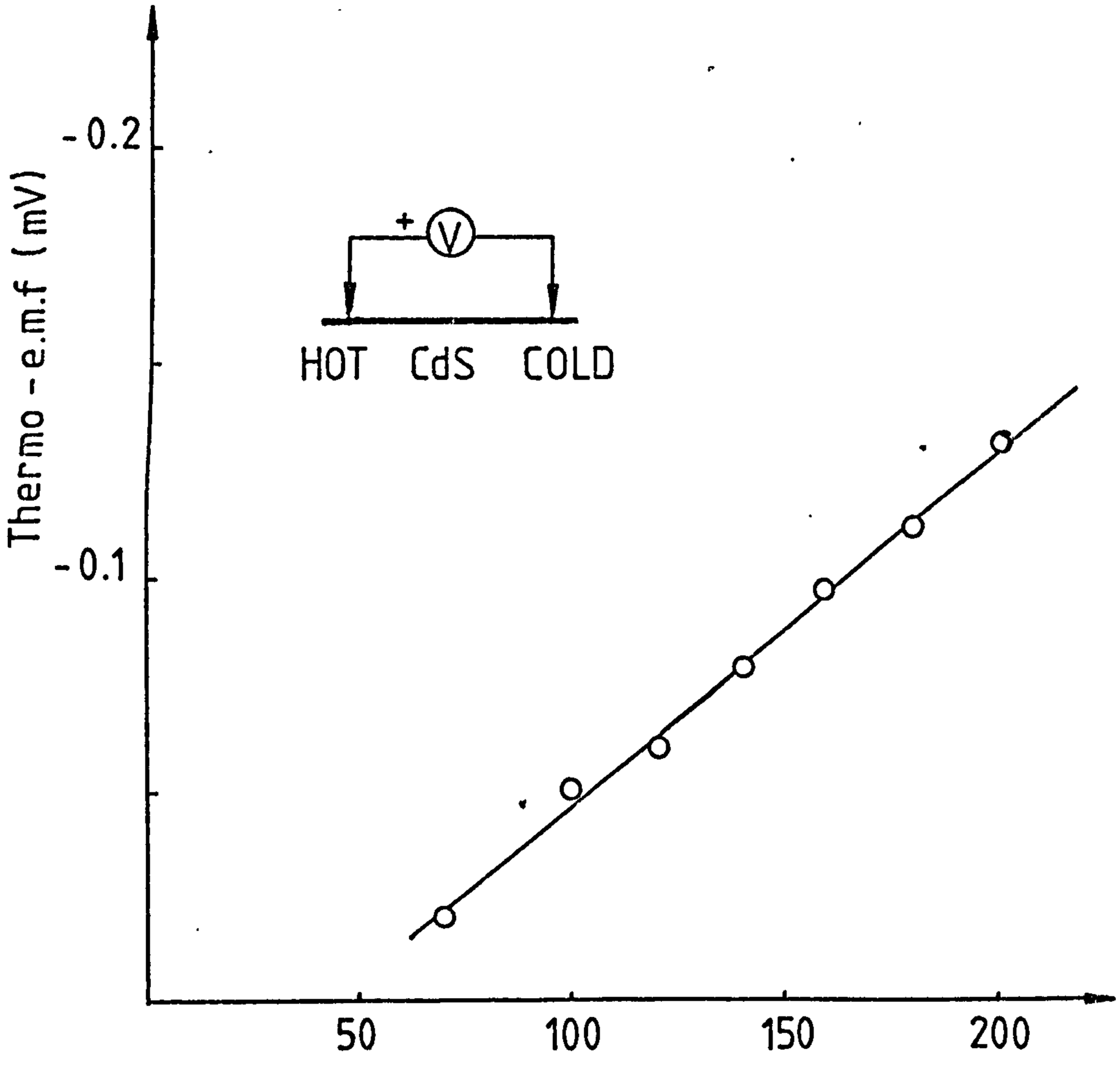

Fig. 5.15 Thermo-e.m.f. vs. Temperature of a CdS film grown on MgO substrate

of hexagonal structure, while those grown on aluminium substrates were found to proceed in the cubic phase initially, and then changed to a polycrystalline hexagonal structure as the thickness of the films increased. The polycrystalline region was later eliminated by a two stage evapration process at substrate temperature of 300°C and 400°C respectively. Thermo-e.m.f. measurements showed that CdS grown on gold was n-type, and on aluminium p-type. Unintentional doping by residual gas, nitrogen and carbon monoxide is not thought to be responsible for the different "doping" of the CdS films. Also it is well known that the self compensation mechanism in the wide bandgap II-VI compound applies to both hexagonal and cubic structures, consequently substitutional impurity doping is not thought to be the likely mechanism.

An alternative method whereby n- and p-type conductivity can be achieved is by using a MIS structure. This has been attempted by numerous workers[95] using II-VI compounds. A thin layer of Al_2O_3 of the order of 20 to 30Å thick is present on the surface of the epitaxial aluminium and as has been previously mentioned was observed on the TEM, and the MIS structure then consists of Al-Al_2O_3-CdS. The other known work on cubic CdS is that of Cardona et al.[96] These workers observed that CdS films grown by C.V.D. on GaP, films grown on the phosphorus face were cubic whereas those grown on the gallium face were a mixture of both structural phases. It was suggested that the growth of the cubic phase proceeds by nucleation of the cadmium with phosphorus forming Cd^+P^-. The results of the present work suggest that a similar bonding structure exists, in this case the cadmium being ionically bonded to the oxygen to form a Cd^+O^- bond. The Cd^+ ions at the interface could then act as deep

surface state acceptors thereby causing a depletion of conduction band electrons and creating a p-type inversion layer channel adjacent to the interface. Such a structure could act as a p-n junction, hole injection taking place by electrons tunnelling from the valence band of the CdS into the conduction band of the metal. The observed thermo-e.m.f. is considered to be due to the flow of holes along the p-type inversion layer channel when a temperature gradient exists along the length.

CdS films deposited on (100) single crystal MgO and thin-film MgO showed identical structural characteristics to CdS films grown on aluminium substrates. Thermo-e.m.f. measurements of Al-MgO-CdS and Au-MgO-CdS structures confirmed similar p-type conduction. The earlier suggestion that CdS deposited on aluminium substrate, which had been exposed to atmosphere, resulted in a MIS Al-Al_2O_3-CdS structure was therefore confirmed.

CHAPTER 6 JUNCTION CHARACTERISTICS OF METAL-CdS DIODES FABRICATED BY MOLECULAR BEAM EPITAXY

6.1 Introduction

The fabrication of Au-CdS, Al-Al_2O_3-CdS and Au-MgO-CdS structures have been presented in the previous chapter. The experimental measurements of current and capacitance as a function of applied voltage, and the photovoltaic characteristics of these devices are presented in this chapter. The results of these measurements have been used to determine the effect of various thin-film deposition procedures, and in particular, the effect of insulator thickness on the device characteristics as solar cells.

6.2 Au-CdS junction

The I-V characteristics of epitaxial hexagonal CdS film grown on epitaxial gold substrate have been measured. The measurements were carried out using In-Ga alloy or evaporated aluminium contacts to the top surface of the n-type CdS film and a pressure contact to the gold substrate. The current was found to be linear function of voltage for both bias voltages.

The ideal Schottky model of metal-semiconductor junction predicts that ohmic contact will result if the work function of the metal is less than that of the n-type semiconductor. The work function, ϕ, for gold is 4.8eV[98] and for CdS $\phi = x \pm E_f$, where x is the electron affinity and E_f the Fermi energy. For CdS, x = 4.8eV[98], and for non-degenerate CdS, i.e. $N_D < 10^{18}_{cm}{}^{-3}$, $\phi_m < \phi_s$. The condition of non-degeneracy is most likely to apply to the films under consideration, therefore on the basis of the ideal model the Au-CdS should be an ohmic junction.

6.3 Al-Al_2O_3-CdS junction

It has been shown in chapter 5 that epitaxial cubic films of CdS with the (111) orientation grown by M.B.E. on epitaxial aluminium exibit a thermo-e.m.f. appropriate to p-type material. It was proposed that the result obtained with CdS on aluminium substrates was due to a p-type inversion layer within a narrow region of the CdS adjacent to the substrate. A thin insulating layer of Al_2O_3, approximately 20Å thick, was always present on the surface of the aluminium and was sandwiched between the metal and the CdS. Thus the structure is essentially that of the MIS type, i.e. Al-Al_2O_3-CdS. The inversion is considered to be due to high density of surface Cd^+ ions associated with a Cd^+O^- bond between the CdS and oxide. A schematic representation of the potential band model of this structure is shown in Figure 6.1. Provided that the CdS film is sufficiently thick to ensure that the top surface of the film is n-type, the structure should behave as a p-n junction. Furthermore, hole injection into the CdS should be feasible by electron tunnelling through the thin oxide from the valance band of the CdS into the conduction band of the metal, and electron injection at the ohmic contact to the top surface.

6.3.1 I-V characteristics

The I-V characteristics of the Al-Al_2O_3-CdS structures were measured using either In-Ga alloy or evaporated aluminium contacts to the top surface and a pressure contact to the aluminium substrate. The forward conducting I-V characteristics are shown in Figure 6.2a and for comparison purposes those of a commercial p-n junction silicon diode are also given. In Figure 6.2b is shown a Laue photograph of the CdS film; the

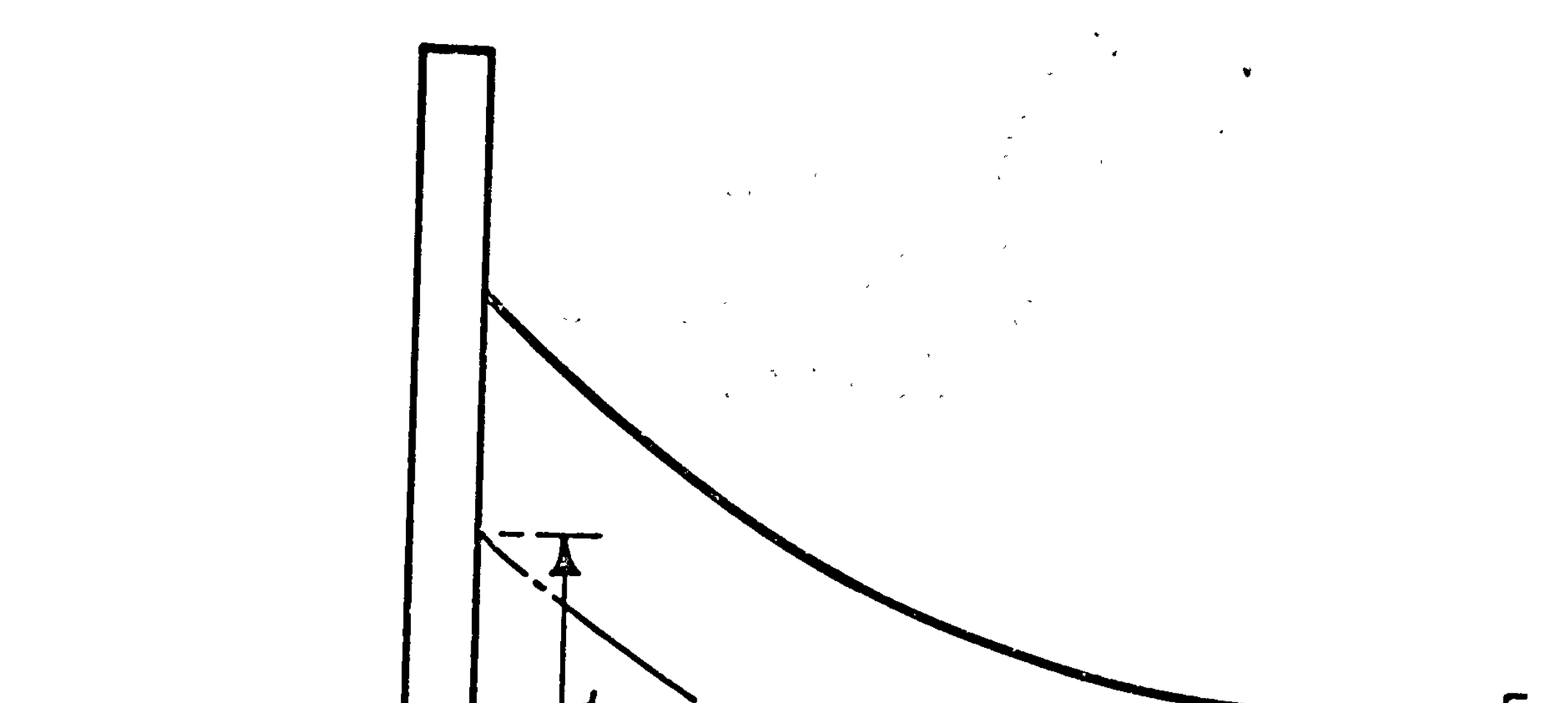

Fig. 6.1 Schematic band model of Al-Al_2O_3-CdS structure

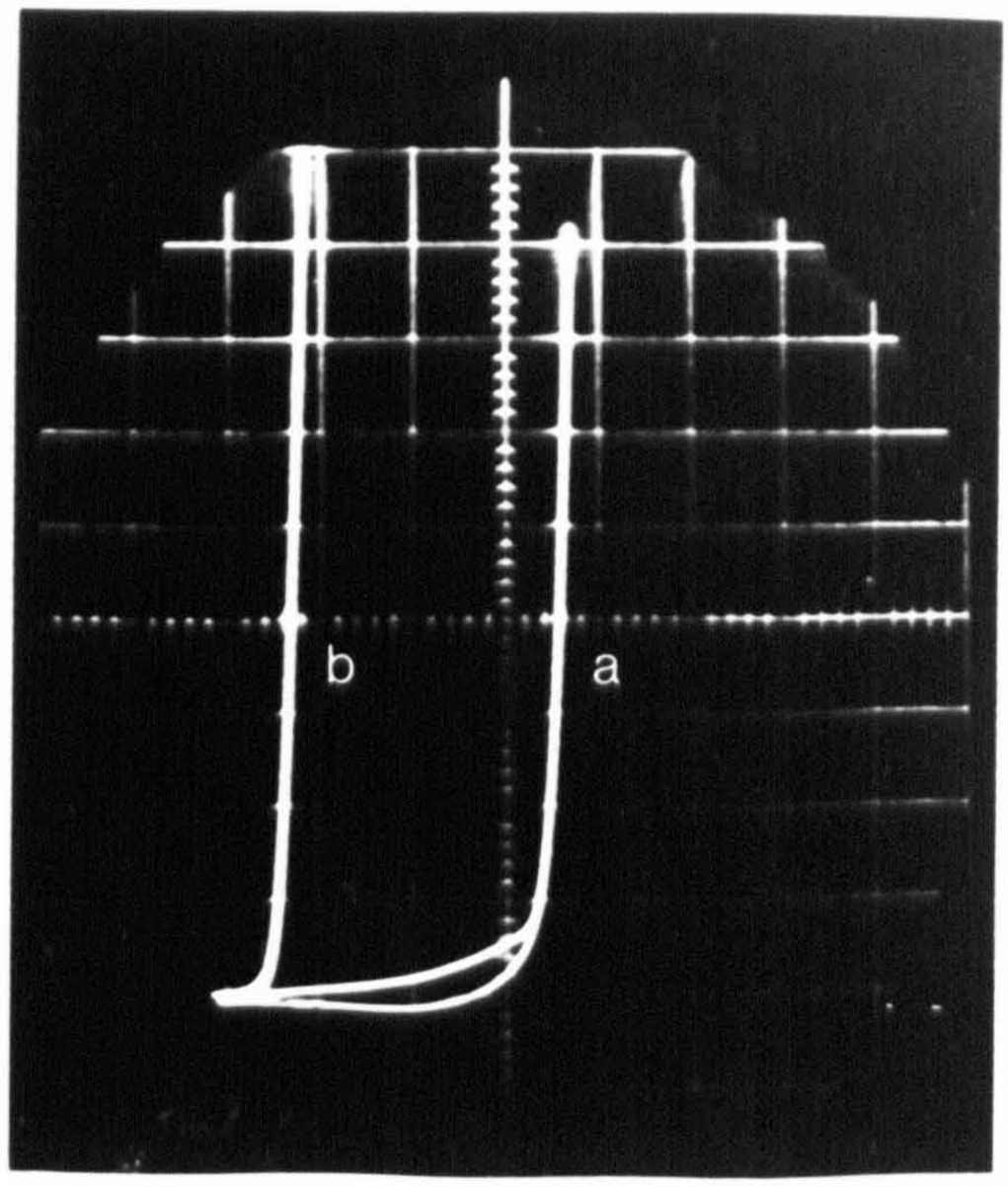

Fig. 6.2a Forward biased I-V characteristics of

(a) an Al-Al_2O_3-CdS diode and

(b) a commercial silicon p-n diode

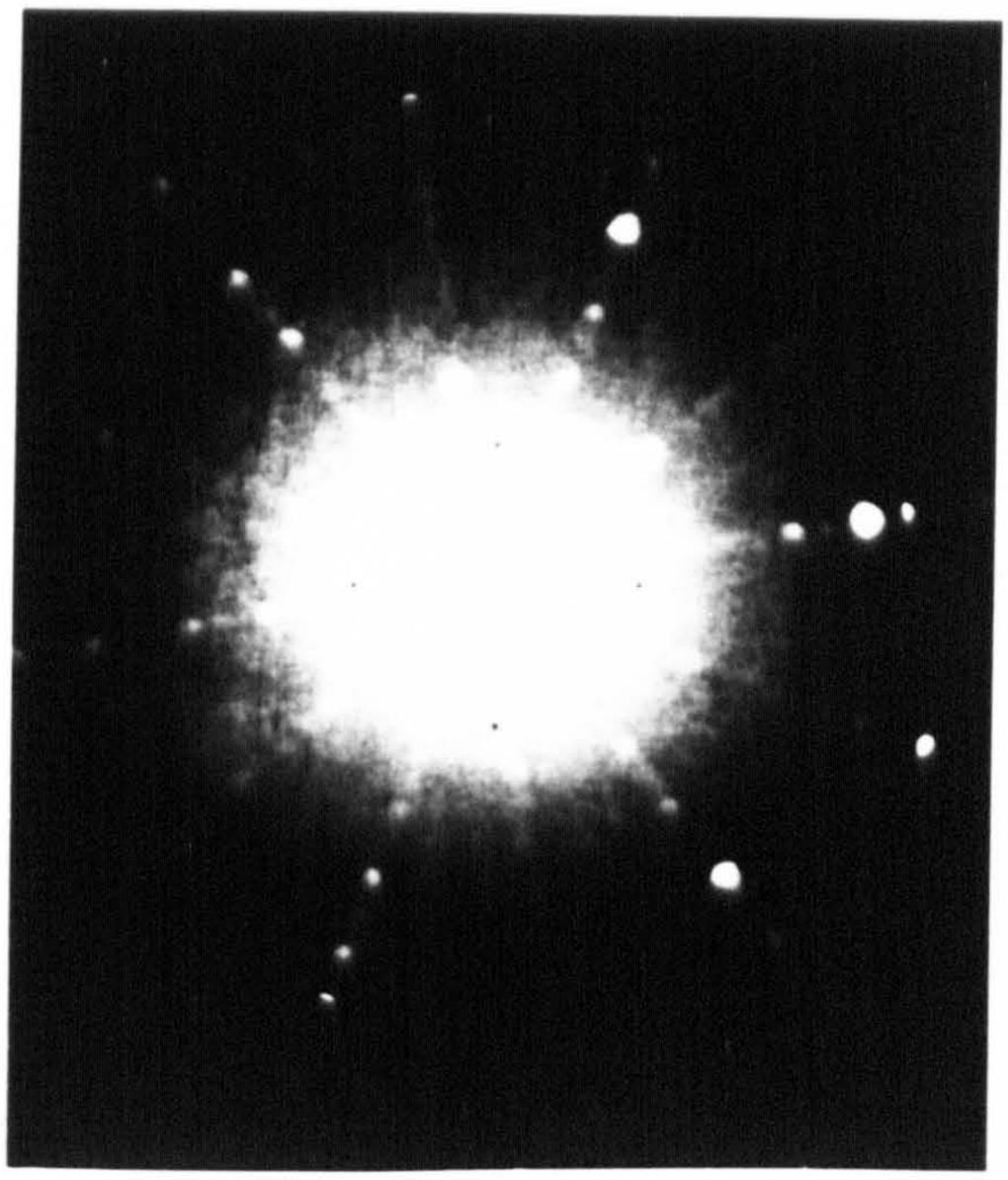

Fig. 6.2b X-ray Laue photograph of CdS film used in Fig. 6.2a

(111) cubic orientation is clearly evident. The details of the fabrication of this diode are listed in Table 6.1 as diode type A. The characteristics display two exponential regions. Below 1.7 volts the bias current is proportional to exp(qV/nkT), where n = 18 and above 1.7 volts the exponential coefficient n reduces to a value of 2.2. The reverse saturation current is not shown in Figure 6.2a but is approximately 3×10^{-8}A and only weakly dependent on bias voltage up to -3 volts. The important feature of this diode is that for forward conduction the aluminium substrate electrode is positive with respect to the top In-Ga contact, and this is the required polarity for forward conduction of a p-n diode. Thus the basic I-V characteristics are consistent with the model shown in Figure 6.1, but do not provide a conclusive verification of it. If the junction characteristics described are not those of an inversion type of p-n junction, they must be of the metal-semiconductor or Schottky junction.

For a Scottky junction

$$J = AT^2 \exp(-\frac{q\phi_{Bn}}{kT}) \exp \frac{qV}{nkT} \qquad (6.1)$$

where $A = 100 A.cm^{-2}K^{-2}$ is the Richardson constant, $\phi = 0.7eV$ [76, 100] the zero-field asymptotic barrier height, and n = 2.2 the diode factor for bias voltage in the range 1.7V to 2V, this being the range for which n = 2.2 was obtained. The calculated values of current for the above values were at least four orders of magnitude greater than that observed and only for $\phi = 1.2eV$ was good correlation obtained.

The exponential coefficient n is indicative of recombination processes[99] within the depletion region, and for wide band-gap semiconductors with a single recombination centre at the

	Substrate temperature T_s ^oC	Film growth rate $\mu m.hr^{-1}$	Film thickness μm	Turn-on voltage V	n value
A*	420	6	1.5	1.7	2.2
B	300	3	0.3	1.0	5.5
C	270	18	3.0	2.5	31
D	250	24	3.9	4.6	100
E	220	24	3.9	6.7	100

* An initial layer 2000Å thick grown at 300°C with a growth rate of $2\mu m.hr^{-1}$ followed by deposition at 420°C with a growth rate of $6\mu m.hr^{-1}$.

Table 6.1 Characteristics of Al-Al_2O_3-CdS diodes

midgap n = 2 [99]. The value of n = 2.2 obtained is in fair agreement with this. The exponential coefficient was observed to be strongly dependent on the film growth conditions, particularly on the substrate deposition temperature. Listed in Table 6.1 are the respective values of n and the turn-on voltages of a number of diodes fabricated with substrate deposition temperatures in the range 220°C to 300°C. As described in the previous chapter, epitaxial cubic films were obtained with substrate deposition temperature, T_s, in the range $200^{\circ}C < T_s < 320^{\circ}C$, those formed below 200°C were wholly polycrystalline and above 320°C no film growth occurred. For the films listed in Table 6.1 the X-ray Laue photographs were similar to that shown in Figure 6.2a. Comparing diodes B to E, it can be seen that both the n-values and turn-on voltages increase with a reduction in the substrate deposition temperature. If the n-value is dependent on the density and type of recombination centres, this implies that such defects increase as the deposition temperature is reduced. Shown also in Table 6.1 are the film growth rates as a function of the substrate temperature, these rates range from 3μm/hr to 24μm/hr. The growth rate depends on the respective beam fluxes and the substrate deposition temperature and in each case both the cadmium and sulphur beam fluxes were maintained at approximately 10^{17} molecules/cm^2.s. It has been shown in Chapter 4 that epitaxial CdS film growth rates ranging from 0.2μm/hr to 15μm/hr can be obtained on spinel, provided that the ratio of the Cd:S beam fluxes are approximately unity. If this ratio exceeds by more than two-fold, structurally disordered films are observed with the X-ray Laue. For this reason, during the growth of the CdS films used here the respective fluxes were maintained at the above value. It is a generally held view that

the degree of structural quality of M.B.E.[32] grown films is better under conditions of low film growth rates. Consequently it is to be expected that the density of centres such as cadmium vacancies and vacancy complexes increases as the film growth rate is increased. To obtained the characteristics shown in Figure 6.2a with an n value of 2.2 it was necessary to grow the film at a higher temperature than 320°C, the cut-off temperature for film growth. An initial epitaxial growth layer thickness of approximately 1000Å was grown at 300°C, the shutter was then closed to isolate the substrate from the Kudsen cells and the substrate temperature increased to 400°C. Films grown by this method were found to result in diodes with n values of slightly in excess of 2, as shown in Figure 6.2a. The Cd:S beam flux ratio was found to affect critically the n values of the diodes, even though no appreciable differences were observed in the X-ray Laue photographs. Reproducibility in the M.B.E. system used here was poor, since the actual evaporating fluxes could not be monitored. As described in Chapter 4, the constituent fluxes were measured by the respective cell temperatures which have been previously calibrated under steady state conditions. The actual evaporation rate of the respective fluxes were therefore not known exactly particularly as the source temperatures drifted from its stabilised conditions.

The main problem associated with the Al-Al_2O_3-CdS diodes was instability. The diodes brokedown easily and show no photovoltaic effects. The main cause is thought to be the thin and uncontrollable thickness of the Al_2O_3 layer. This layer was further complicated by being polycrystalline and contained large amount of defects.

6.3.2 C-V characteristics

The depletion-layer capacitance per unit area is defined as $C = dQ/dV$, where dQ is the incremental increase charge per unit area upon an incremental change in applied voltage dV. For one-sided abrupt junctions the capacitance per unit area is given by[98]:

$$C = \frac{dQ}{dV} = \frac{\varepsilon_s}{w} = \left(\frac{q\varepsilon_s N_b}{2(V_{bi} \pm V)}\right)^{\frac{1}{2}} \tag{6.2}$$

$$\text{or} \quad \frac{1}{C^2} = \frac{2}{q\varepsilon_s N_b}(V_{bi} \pm V) \tag{6.2a}$$

$$\frac{dC^{-2}}{dV} = \frac{2}{q\varepsilon_s N_b} \tag{6.3}$$

where w is the depletion width, N_b the impurity concentration, V_{bi} the built-in potential and $\pm$ signs are the forward and reverse-bias conditions respectively. The C-V characteristics* of a low n value diode were measured at a frequency of 10KHz with a $1\,mm^2$ contact on the CdS surface. The C and C^{-2} characteristics as a function of applied voltage are shown in Figures 6.3 and 6.4 respectively. From the value of zero bias capacitance the depletion width was calculated to be 3000Å. From equation 6.3 an approximate value of impurity concentration $N_b \sim 2 \times 10^{16}\ cm^{-3}$ at 20°C was obtained from a linear interpolation in Figure 6.4 assuming a contact area of $1\,mm^2$. However, because the area of the substrate electrode is $1cm^2$ the assumed junction area of $1\,mm^2$ may be somewhat low because of the associating fringing fields. It was difficult to measure the capacitance with a forward bias in excess of 0.5 volt because of the forward bias conduction of the diode.

* measured by D. C. Cameron

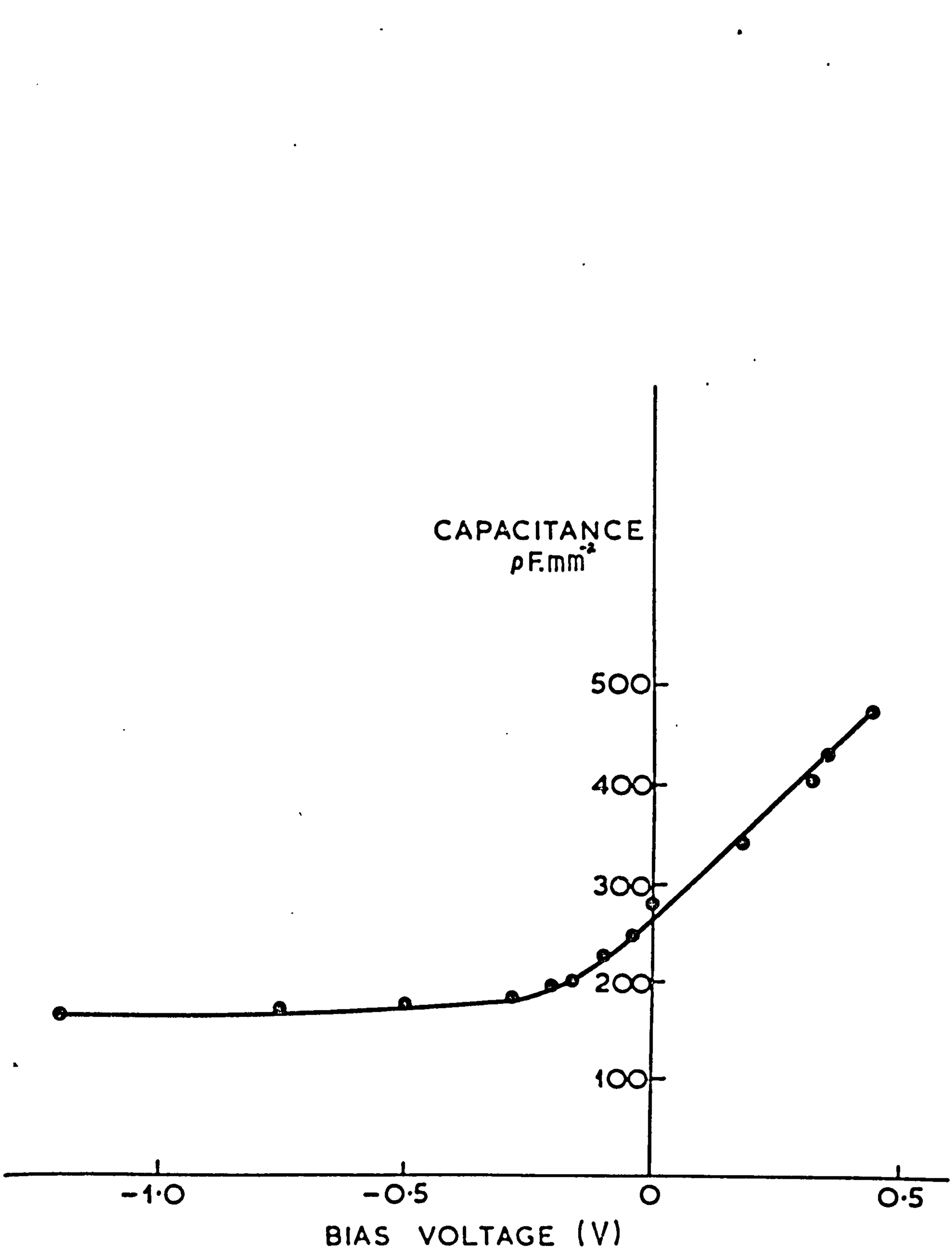

Fig.6.3 C-V characteristics of an Al-Al_2O_3-CdS diode

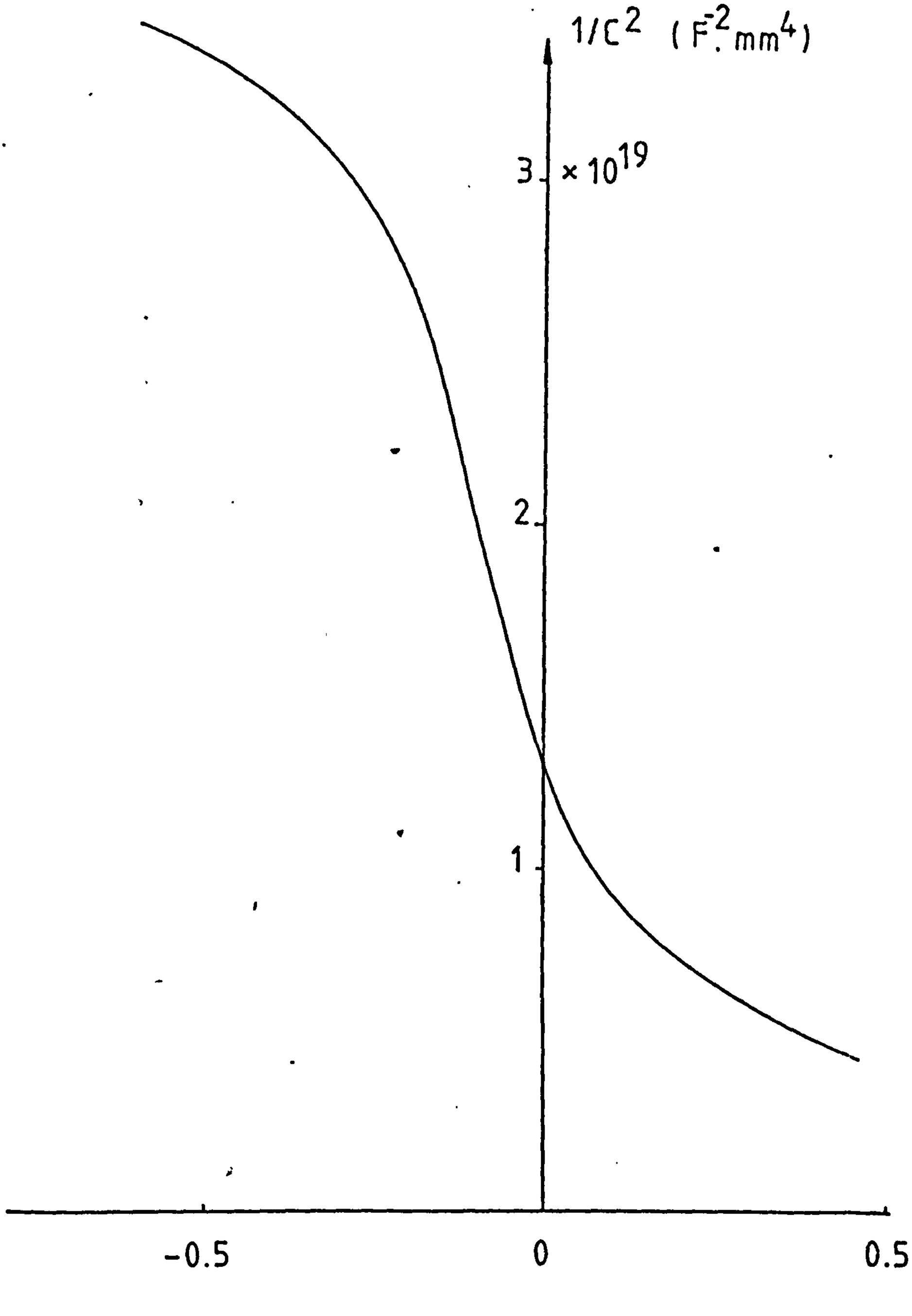

Fig. 6.4 C^{-2} vs. V for an $Al-Al_2O_3-CdS$ diode

6.4 Au-MgO-CdS junction

There were several problems associated with the Al-Al_2O_3-CdS structure. The Al_2O_3 layer was thin and uncontrollable. Furthermore, it was polycrystalline and contained many defects. The reproducibility of diodes was poor and frequent breakdowns were common.

Many of the above problems were overcome by the use of MgO in place of the Al_2O_3 layer. The thickness and epitaxy of MgO, as shown in Section 5.5, were easily controlled. The purity of the aluminium film deposited in a vacuum of 10^{-5} torr was always in question. This uncertainty was eliminated by the use of gold as a substrate for the MgO layer.

Thus the structure investigated was Au-MgO-CdS. Ohmic In-Ga alloy or evaporated aluminium contacts on the CdS surface completed the diode structure. The fabrication procedures for the Au-MgO-CdS have been presented in detail in the previous chapter.

6.4.1 I-V characteristics

The I-V characteristics of the Au-MgO-CdS structure were measured using either In-Ga alloy or evaporated aluminium contacts to the CdS surface and a pressure point contact to the gold substrate. The I-V characteristics of a typical Au-MgO-CdS diode fabricated with MgO thickness of 40Å are shown in Figure 6.5 and are similar to those of the Al-Al_2O_3-CdS diodes. One significant improvement over the Al-Al_2O_3-CdS structure was found. The Au-MgO-CdS diodes fabricated with MgO thicknesses in excess of 40Å were not prone to breakdown. The diode n values were similarly found to increase with decrease in CdS deposition temperature, T_s. It decreased from n = 15 at T_s = 240°C

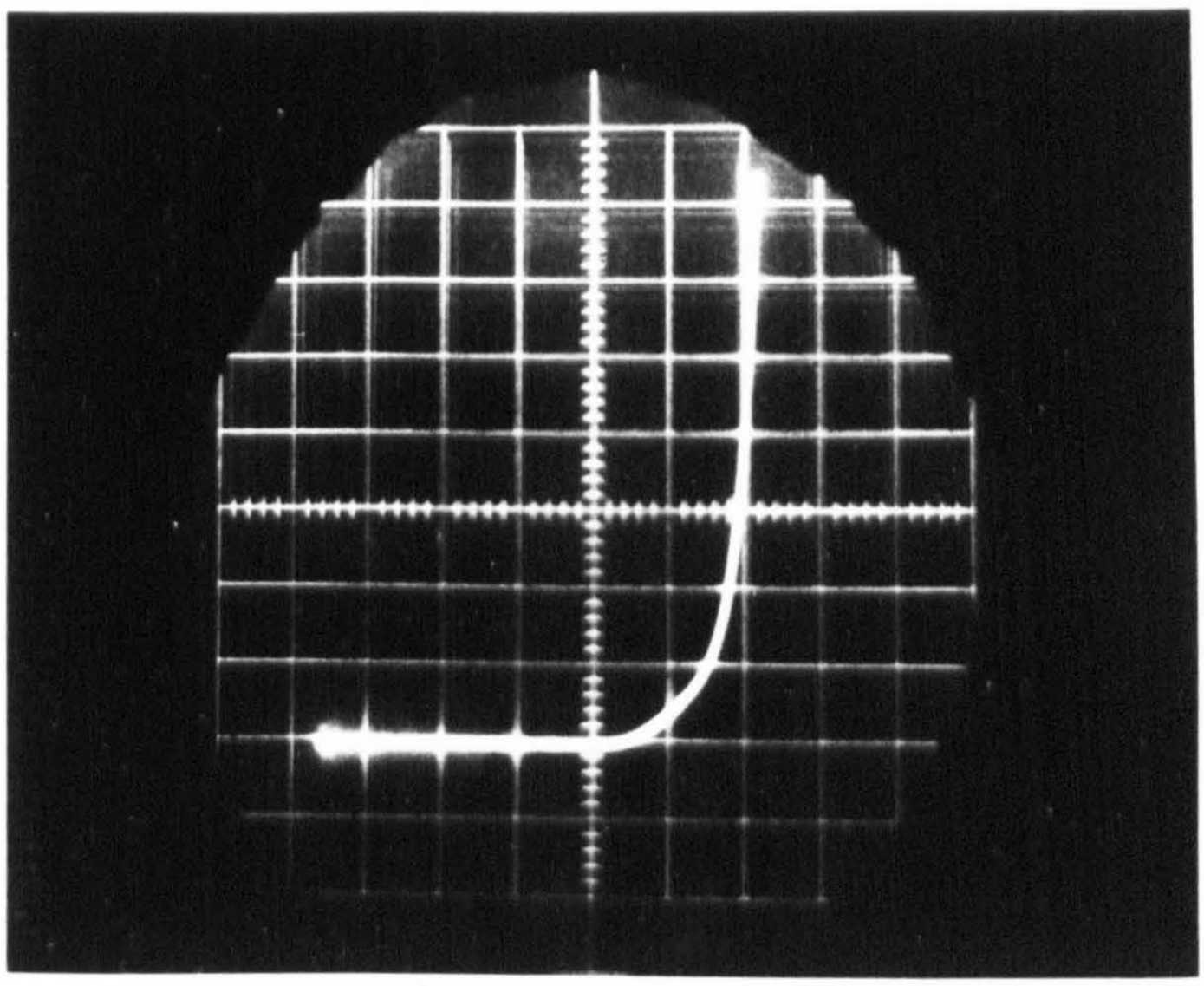

Fig. 6.5 I - V characteristics of an Au-MgO-CdS diode

$V_x = 1{\cdot}0 \ \ V\,cm^{-1}$

$I_y = 0{\cdot}1 \ \ mA\,cm^{-1}$

	MgO thickness (Å)	Voc (V)	Isc
A	80	0.24	< 1μA
B	60	0.32	< 1μA
C	50	0.70	< 1μA
D	40	1.1	2mA
E	30	Ohmic	

Table 6.2 Photovoltaic characteristics of Au-MgO-CdS cells

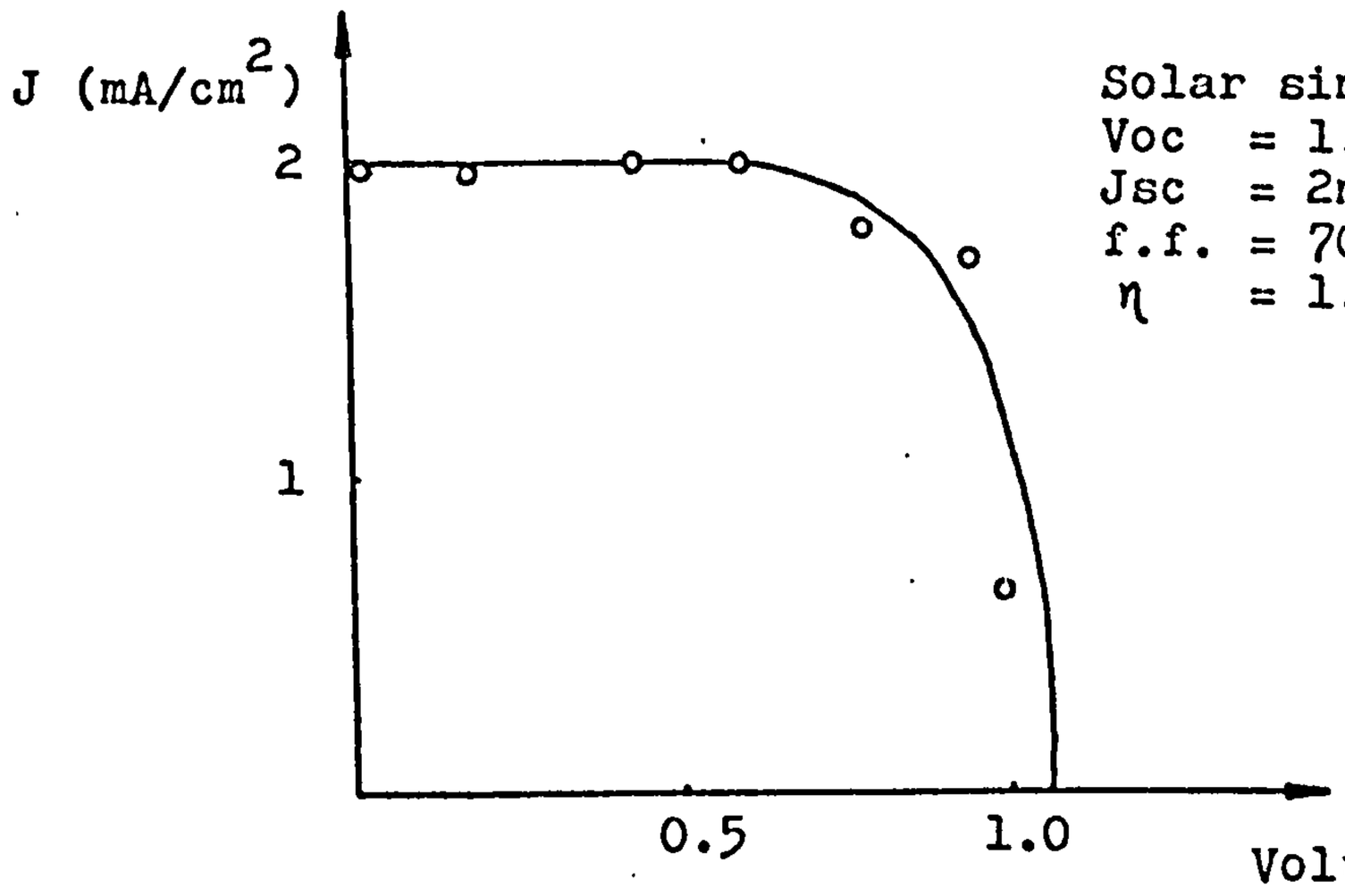

Figure 6.6 Photovoltaic response of an Au-MgO-CdS cell

to $n = 3$ at $T_s = 380^{o}C$. Although no abrupt cut-off temperature was found during CdS depositions on MgO substrate, no significant improvement in diode characteristics was observed above $T_s = 380^{o}C$.

6.4.2 Photovoltaic characteristics

The photovoltaic effect was evident in the Au-MgO-CdS structure. It was found to vary with the thickness of the MgO layer. Listed in Table 6.2 are the respective open circuit voltages, Voc, and short circuit current, Isc, of a number of Au-MgO-CdS diodes fabricated with MgO thickness in the range of 80Å to 30Å . All the diodes were fabricated under the same conditions of substrate and CdS deposition. The CdS deposition temperature was $380^{o}C$ and the respective cadmium and sulphur fluxes were approximately 7×10^{16} molecules/cm^2.s . The CdS Films were two microns thick and were deposited at a rate of two microns per hour. Evaporated aluminium grid contact, as shown in Figure 3.6, was used to complete the devices. The open circuit voltage was found to increase as the thickness of the MgO layer was decreased from 80Å to 40Å. The short circuit current was also at its highest with MgO = 40Å. The illuminated I-V characteristics of the diode with MgO = 40Å is shown in Figure 6.6. Ohmic conduction was observed when MgO thickness was decreased to approximately 30Å.

6.5 Summary

The characteristics of Au-CdS, Al-Al_2O_3-CdS and Au-MgO-CdS junctions have been investigated. The Au-CdS junction was established to be ohmic as expected on the basis of the ideal Schottky model of metal-semiconductor junction. Diode blocking

was found in the Al-Al_2O_3-CdS configuration. This was attributed to the presence of an inversion layer. A potential band model of the MIS structure was proposed; and I-V characteristics measured were consistent with the model presented. The Al-Al_2O_3-CdS diodes were found to breakdown easily and show no photovoltaic effects. The main problem is thought to be due to the uncontrollable thickness of the Al_2O_3 insulating layer. Attempts have been made to overcome this instability problem by the use of a controlled layer of MgO in place of the Al_2O_3. Similar diode blocking action was found in the Au-MgO-CdS configuration. The Au-MgO-CdS diodes were not prone to breakdown, and photovoltaic effects were observed for MgO thickess of less than 40Å.

CHAPTER 7 MINORITY CARRIER METAL-INSULATOR-SIMICONDUCTOR (MIS) TUNNEL DIODE FOR SOLAR ENERGY CONVERSION

7.1 Introduction

The metal-insulator-semiconductor (MIS) solar cells are Schottky barrier devices with a non-conducting interfacial layer between the metal and semiconductor. Several recent papers[9, 101,102] indicate that the addition of such an interfacial layer improves solar cell performances. These insulating layers are generally reported to be in the range of 10-100Å. The semiconductors investigated so far are principally silicon and gallium asenide. Stirn and Yeh[9] have reported a photovoltaic efficiency of 15% with GaAs, and Kipperman and Omar an efficiency as high as 12% with silicon[102]. The exact role of the interfacial layers has been the subject of considerable theoretical study in recent literature[103-105]. In an analysis given by Fonash[104, 105] it is suggested that surface states at the semiconductor-oxide interface play a central role in shaping the field in the semiconductor and thus altering the I-V characteristics. Green et al.[105] have examined in detail an alternative explanation which may account for all or part of the experimental observations-namely, that the mechanism for current conduction is tunnelling through the insulator of a MIS diode which is formed when these interfacial layers are introduced. Basically, the field effect induces a p-n junction at the surface of the semiconductor facing the insulating layer. Coupling to this junction is achieved by tunnelling, allowing the metal to be connected to the induced junction.

7.2 Theoretical background

Investigations by Green et al.[105,106] have shown that when the insulator in a MIS diode is less than a critical thickness (60Å for Al-SiO_2-Si) significant tunnel currents can flow between the metal and the semiconductor. These currents are initially of such small magnitude that the semiconductor is essentially in thermal equilibrium. If the insulator thickness is further decreased, the tunnel currents increase to the point where they are sufficiently large to disturb the semiconductor from thermal equilibrium. This occurs at around 28Å for Al-SiO_2-(p-type)Si. Thus, in general, below some critical value of insulator thickness, "non-equilibrium" tunnel MIS diodes are formed. Over a certain bias range, the MIS tunnel diode in this non-equilibrium mode where the diode current is semiconductor limited (due to generation-recombination in the bulk) and the tunnel current merely provides an ohmic contact. Such non-equilibrium diode can be further classified as majority, surface state or minority carrier devices depending on whether the dominant tunnel current flow near zero bias is between the metal and the majority carrier band, surface states or the minority carrier band. Which type of diode is formed depends on whether the semiconductor-insulator interface at zero bias is accumulated, depleted or in strong inversion. The work function of the contact metal is the most important parameter in determining which of these states exists[106].

The schematic energy band diagrams of an n-type semiconductor at zero bias for two values of the metal-to-insulator barrier height are shown in Figure 7.1 The insulator layers are assumed to be thin, so that tunnel current can flow between the metal and the semiconductor. The main difference between the two

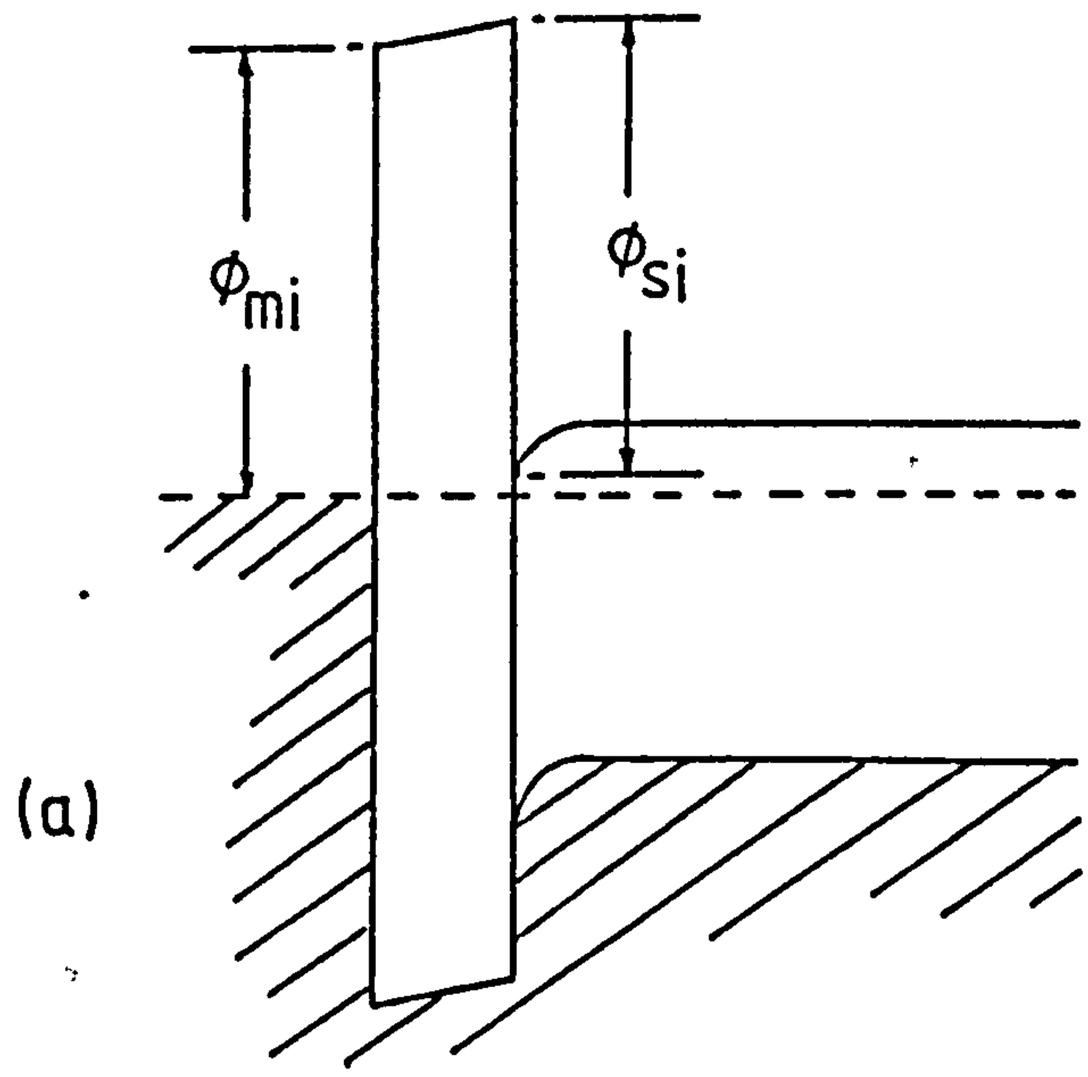

(a)

$$\phi_{mi}(a) < \phi_{mi}(b)$$

$$\phi_{si}(a) = \phi_{si}(b)$$

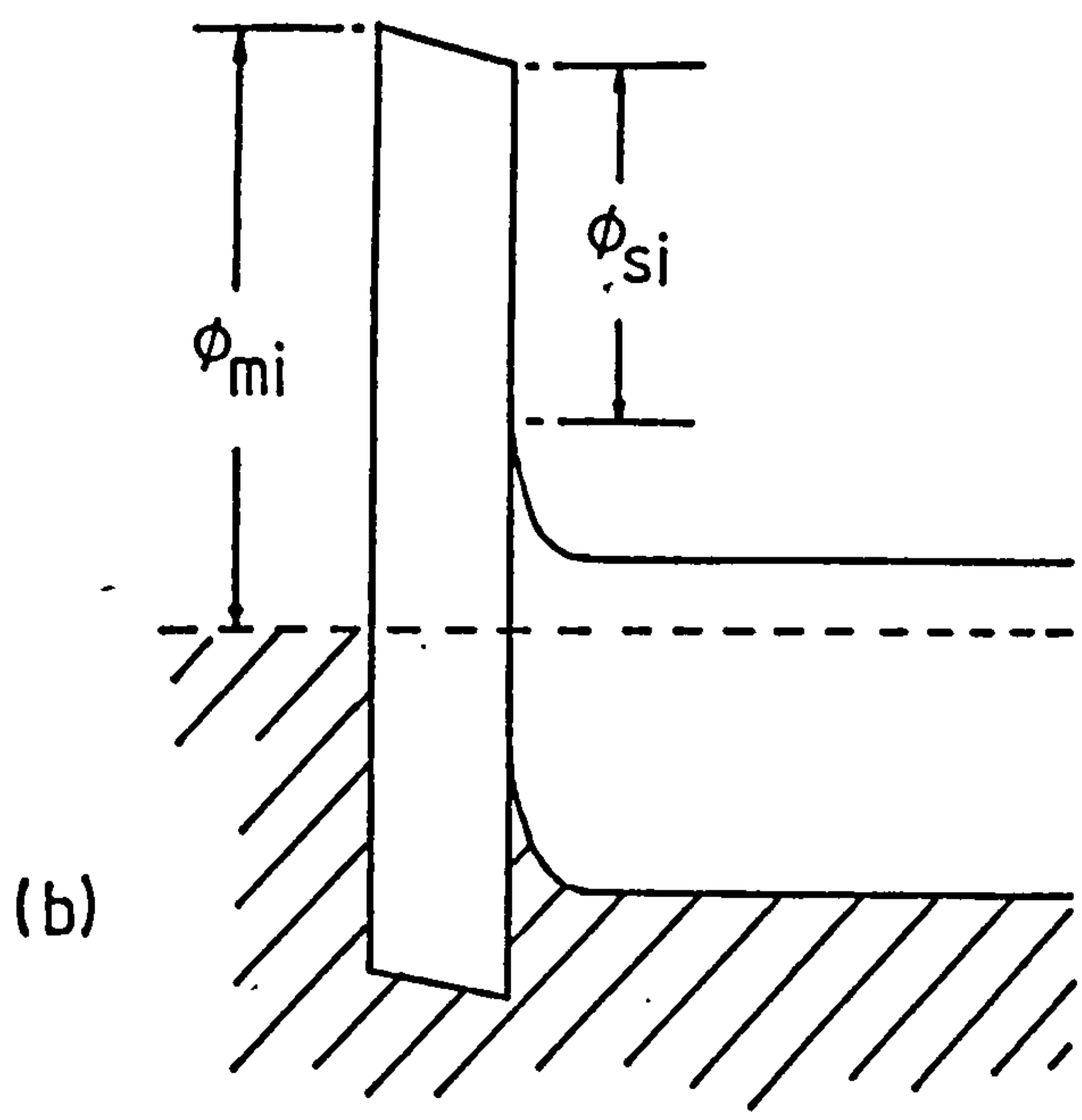

(b)

Fig.7.1 Schematic energy band diagram at zero bias for MIS diodes.

cases is that the surface is inverted for the higher value of ϕ_{mi}, while it is accumulated for the lower value. The transition from minority to majority carrier device occurs at an intermediate value of ϕ_{mi} and in this region tunnelling via surface states can dominate. Majority carrier tunnel diodes show current multiplication properties and are not necessarily suitable for photovoltaic purposes but are useful in transistor-type devices[106]. Minority carrier devices, on the other hand, can show I-V characteristics which obey the ideal Shockley diode equation[105] and are suitable for photovoltaic conversion[101].

Obviously, the key parameter which controls the conversion efficiency of tunnel MIS solar cells is the insulator thickness. The results of calculations of conversion efficiency, open circuit voltage and short circuit current as a function of insulator thickness for the case of Al-SiO_2-(p-type)Si[107] are shown in Figure 7.2. The open circuit voltage, V_{oc}, is seen to vary very slowly with insulator thickness and in a linear fashion. The short circuit current, I_{sc}, on the other hand, does not become appreciable until the insulator thickness of less than about 23Å is reached and then a rapid rise of current to an almost saturating plateau at around 19Å. In the region between 15Å and 20Å, the rapid decrease in efficiency is thought to be due to an increasing effective series resistance, as the tunnelling current changes exponentially with thickness, and because of changes in the I-V characteristics which arise from the transition from the semiconductor limited mode to the tunnelling limited mode.

7.3 Discussion of results

The present work has shown that the thickness of insulating

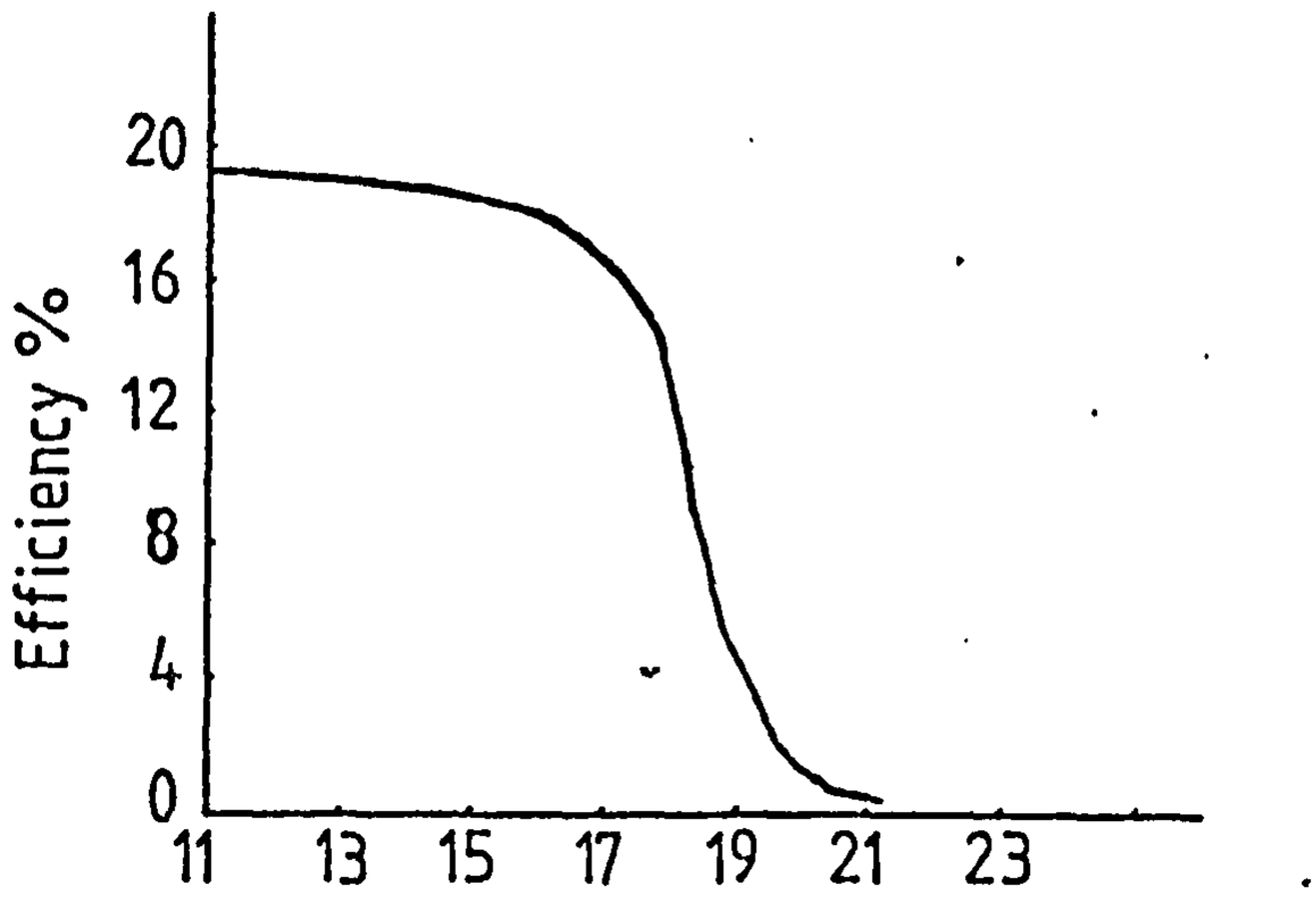

Fig.7.2a Computed effect of insulator thickness on conversion efficieny of an Al-SiO_2-Si (p-type) diode

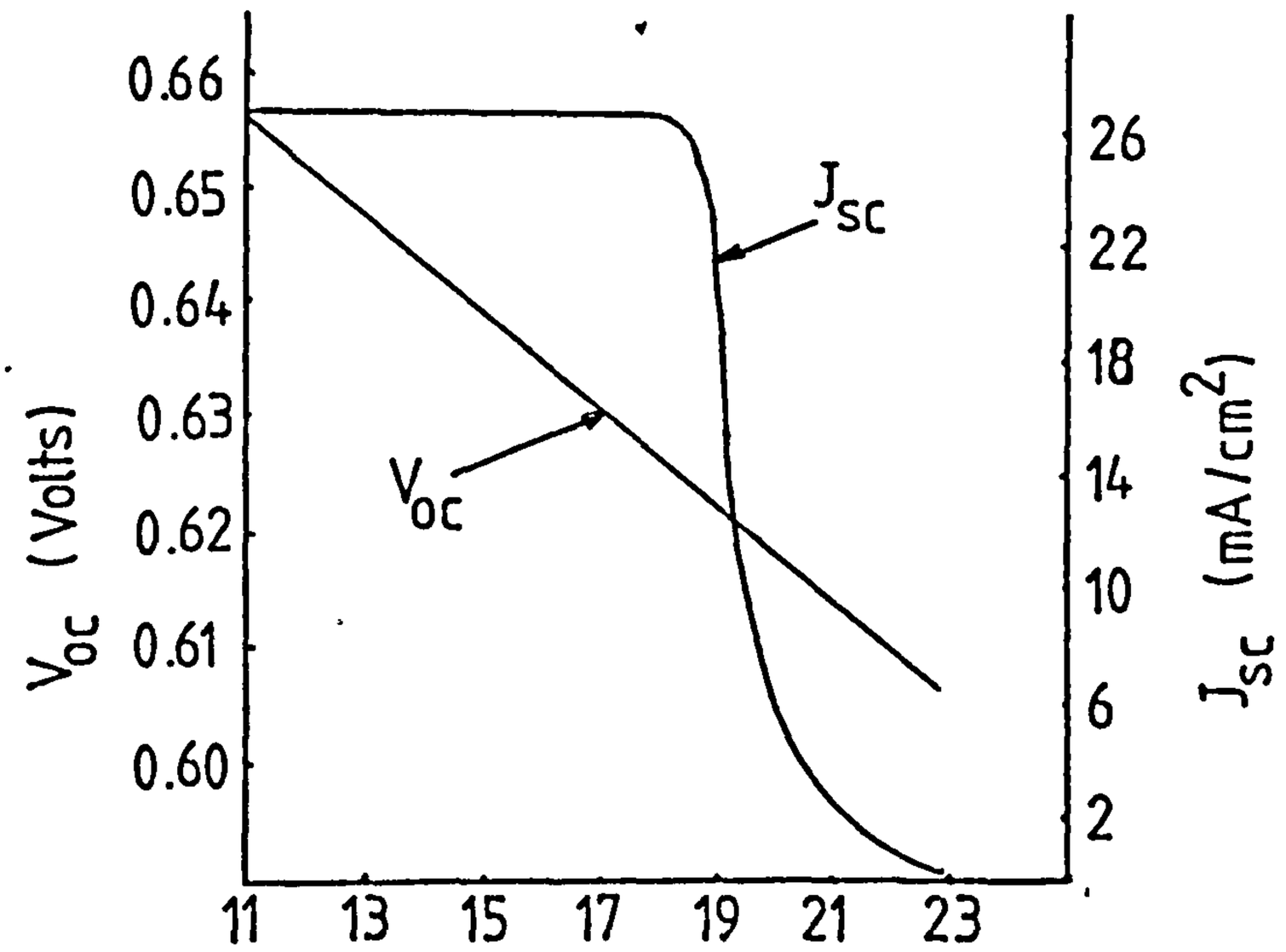

Fig.7.2b The variation of J_{sc} and V_{oc} as a function of insulator thickness of an Al-SiO_2-Si(p-type) diode

region plays a significant role in the photovoltaic characteristics of the Au-MgO-CdS structure. The thickness of the insulating oxide requires to be around 40Å before significant photovoltaic currents are observed. Oxide layers of comparable thickness are also required for the Al-SiO_2-CdS solar cells[107]. It was suggested[107] that the insulating layer presents an effective series resistance to current flow and only when the tunnelling current is greater than the diffusion or generation-recombination current will this effective series resistance be negligible.

The tunnel current density J_T between a metal and semiconductor through an insulating region is given by[52]

$$J_T = \frac{q^2(m^*)E}{2\pi^2\hbar^2(m^*E_g)^{\frac{1}{2}}} \; T.D \qquad (7.1)$$

where T is the tunnelling probability,

$$T = \exp - \frac{\pi(m^*)^{\frac{1}{2}}E_g^{\frac{3}{2}}}{2\sqrt{2}\, q\hbar E} \qquad (7.2)$$

where $m^* = m_c m_s/(m_c+m_s)$, m_c is the conduction effective mass of the metal and m_s is the effective mass in the semiconductor as defined below, E_g is the semiconductor bandgap, E is the junction field, and D is the overlap integral which is approximately unity. For majority carrier tunnelling, when electrons flow from the metal into the semiconductor conduction band, m_s is the conduction band mass. However, for the structure being considered here, where an inversion layer exists within the semiconductor as shown in Figure 6.1 the mass appropriate is that of the hole mass. The effective hole mass for CdS is $m_s = 0.6m_c$[59]. The value of J_T for the Au-MgO-CdS diode can be determined as all the relevant quantities are known. Shown in

Figure 7.3 are the values of J_T as a function of insulator thickness for an applied voltage of one volt.

The p-n junction current flow consists of two components, the minority carrier diffusion current and the generation-recombination current. The diffusion current density is

$$J_d = J_s(\exp \frac{qV}{kT} - 1) \qquad (7.3)$$

$$\text{where} \quad J_s = q\frac{D_p}{L_p}p_{no} + q\frac{D_n}{L_n}n_{po}, \qquad (7.4)$$

D_p and D_n are the diffusion coefficient for holes and electrons respectively, and L_p and L_n are the corresponding diffusion length. The value of J_d is proportional to n_i^2 because $p_{no} = n_i^2/N_D$ and $n_{po} = n_i^2/N_A$.

The generation-recombination current density is

$$J_r = (\frac{qW}{2}\sigma v_{th} N_t n_i) \exp \frac{qV}{2kT} \qquad (7.5)$$

where σ is the capture cross section, v_{th} is the thermal velocity, N_t is the trap density, n_i is the intrinsic carrier density, and W is the depletion layer width. It is evident that the generation-recombination current dominates in wide bandgap semiconductors because n_i^2 is very small and hence only at large forward bias voltage does the diffusion current becomes significant. In the case of CdS $n_i^2 \sim 10^{-4}cm^{-6}$. The factor n in the exponent of J_r takes account of recombination; and for a single recombination at $E_g/2$, $n = 2$. When more complex trapping mechanism are involved, $n > 2$. For efficient photovoltaic generation the tunnel current must be sufficiently large to disturb the semiconductor from thermal equilibrium i.e. $J_T > J_r$. Insufficient data exists to

calculate J_r for such junctions. However, using an experimental value of $n = 3$ and $J_s \sim 10^{-8}$ A/cm^2 in the equation

$$J = J_s \exp \frac{qV}{nkT} \qquad (7.6)$$

gives $J \sim 6 \times 10^{-3}$ A/cm^2. A tunnel current density of this magnitude, as shown in Figure 7.3, is produced for an insulator thickness of approximately 75Å. This compares with insulator thickness of about 60Å for the Al-SiO_2-Si diodes[101,105,106] when tunnel currents are measurable. As discussed in Section 7.2, large tunnel currents are required so that they can significantly disturb the semiconductor from thermal equilibrium. This condition occurs at around 30Å for Al-SiO_2-Si diodes. For the Au-MgO-CdS structure investigated here, a similar insulator thickness of less than 40Å was required before significant photovoltaic currents are observed.

7.4 Summary

The effect of insulator thickness on the diode properties has been investigated. The insulator thickness was found to have dominating influences on the photovoltaic characteristics of the MIS diodes. An insulator thickness of less than 40Å was required for the Au-MgO-CdS structure before significant photovoltaic effects were observed. The experimental results were in good agreement with the theoretical description, which was presented in Section 7.2, of the device operation[105].

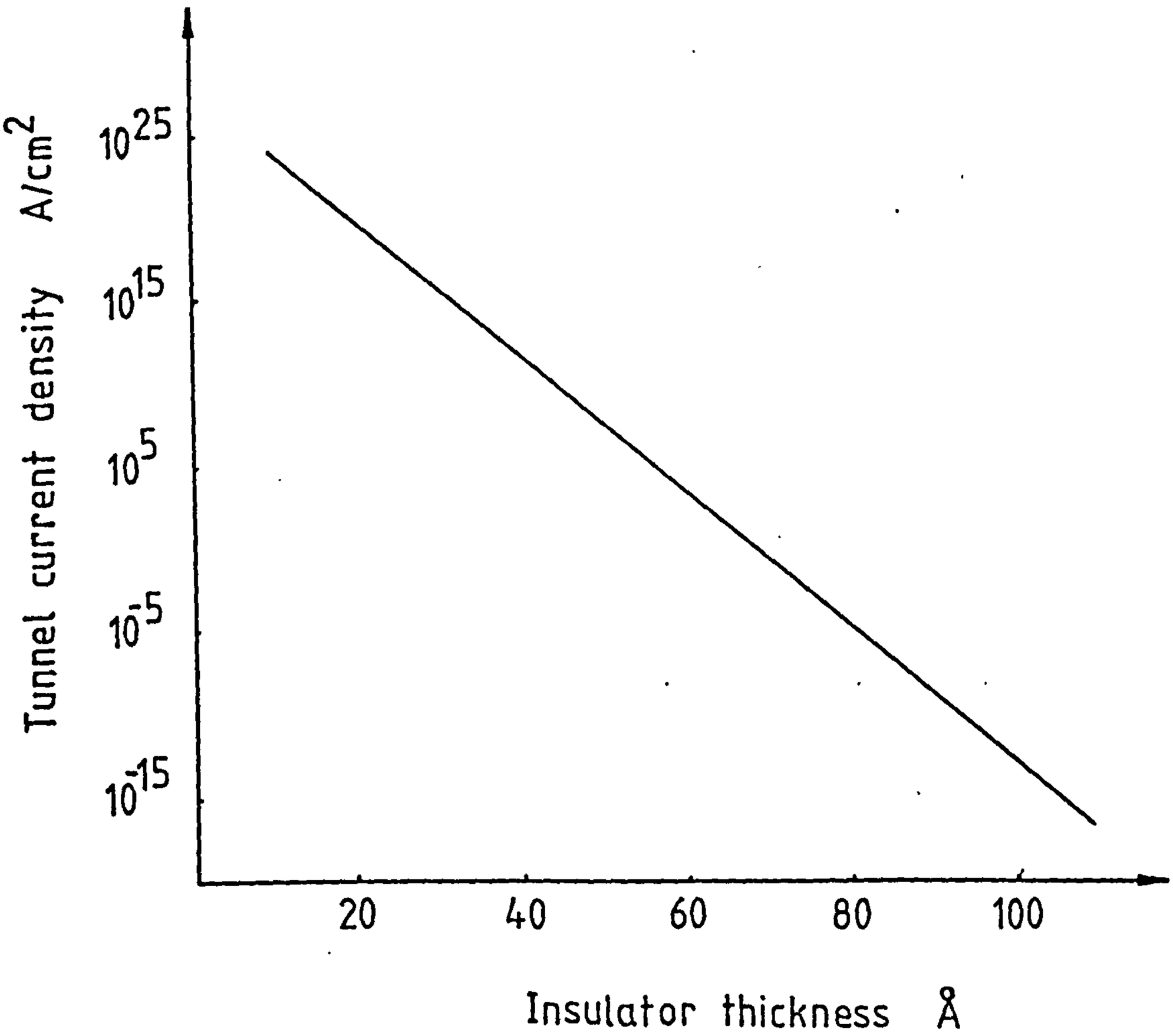

Fig. 7.3 Tunnel current density vs Insulator thickness

CHAPTER 8 CONCLUSIONS

A wide range of p-Si/n-CdS heterojunction devices has been studied in order to determine the optimum fabrication condition for the use of these devices as solar cells. The efficiencies of the cells produced, without antireflection coatings, of 1 to 2% were clearly insufficient even for terrestrial applications. The cells were found to be insensitive to substrate resistivity. This was attributed to unknown interfacial states at the heterojunction and to the density of traps in the evaporated CdS film.

Substrate cleaning was found to have a dominant influence on both the cell characteristics and the crystallographic structure of the evaporated film. Devices fabricated with substrate cleaning in vacuum were found to produce much more consistent characteristics, and improvement of the CdS crystal structure at higher growth temperature was clearly evident.

Annealing of the comleted device significantly improved the performance of the Si/CdS solar cells. This was attributed to the improvement of crystal structure of the CdS film, and reduction of the interfacial states at the heterojunction.

No further improvements in the CdS film, electron beam evaporation of compound CdS, on silicon substrate was thought possible, mainly because of the lack of control of the constituent fluxes evaporated from the source material. In addition, there was evidence of chemical attacks on the silicon surface by cadmium and/or sulphur vapours. The Si/CdS structure was found to be unsuitable for low cost solar cells for terrestrial applications, and a new approach was therefore adopted. An investigation of wholly thin-film devices of both the Schottky barrier and the MIS configuration were carried out. Molecular

beam epitaxial growth of CdS was studied in an attempt to improve the structure of the evaporated film.

The M.B.E. studies of CdS films on (111) oriented spinel substrate showed that both the deposition temperature and the constituent fluxes have dominating effects on the structure of the CdS films. A unique feature of the co-evaporation method is that CdS films with good stoichiometry and high degree of C-axis orientation could be deposited. A large lattice mismatch of about 28% between the spinel substrate and CdS did not hinder the growth of epitaxial CdS films, provided the constituent flux ratio of cadmium and sulphur was maintained at about 1:1, and the substrate was sufficient clean and its temperature sufficiently high. A wide range of film growth rate was achieved, ranging from 2000Å/hr to 15 m/hr. The resultant CdS films at room temperature exibit a resistivity of about 10^5 ohm cm. The significant trap defect occur at 1.6eV below the conduction band and is believed to be due to the cadmium vacancy.

Substitutional doping with indium to produce n-type CdS has been achieved. The doping concentration were from 2×10^{15} to $6 \times 10^{18} cm^{-3}$. Moderately high Hall mobility values in such n-type films were obtained, indicating that ionised scattering dominated the conductivity of heavily doped films.

Substitutional doping with phosphorus has been achieved. The films being of moderately low conductivity. The current carrier has not been identified because of the difficulty in making ohic contacts.

The growth of metals on cleaved mica has shown that epitaxial deposition of silver, gold and aluminium in (111) orientation is possible. The epitaxial temperatures range was from 250°C to 300°C. CdS films deposited on gold were found to be of hexagonal

structure, whereas films grown on aluminium, more precisely Al_2O_3, were found to proceed in the cubic initially, and then changed to a polycrystalline hexagonal structure as the thickness of the films was increased. Further improvement of deposition procedure by a two stage evaporation technique was shown to remove this polycrystalline region.

Thermo-e.m.f. measurement showed that CdS grown on gold was n-type, and that on aluminium p-type. The p-type reading obtained was attributed to the formation of an inversion layer at the Al_2O_3-CdS junction. Diode blocking action was observed in the resultant CdS on Al structure, but no photovoltaic effect was evident. Investigation of Al-MgO-CdS and Au-MgO-CdS diodes confirmed the MIS nature of the CdS on aluminium (i.e. Al-Al_2O_3-CdS) configuration. Experimentation with MgO thicknesses showed no instability problem and that significant photovoltaic effect was observed for MgO thickness of less than 40Å.

Future work

The results of this investigation have shown that device characteristics depend critically on the structural quality of CdS grown. X-ray Laue diffraction has shown that epitaxial films can be grown even on substrates with large lattice mismatchs. However, it is possible that the initial interface layer may be significantly different from the "bulk" of the CdS film, perhaps initial layer of several angstroms may be polycrystalline. It has been shown that even the best epitaxial CdS films deposited on spinel contained high concentration of cadmium vacancies. Reduction in lattice mismatch by suitable choice of substrates would also reduce the initial structural disorders. Further improvements in CdS growth may be possible by closer control of

of the constituent molecular beam fluxes to ensure that the optimum flux ratio is maintain throughout the evaporation. Mass spectrometer or quartz thickness monitor might be used to monitor the constituent fluxes separately during film deposition.

The Au-MgO-CdS structure has shown signs of photovoltaic effects when the insulator thickness is within a specific range. It is thought that further improvements in the solar conversion efficiencies of such MIS structures are possible if more precise control of the insulator thickness is applied, and if more suitable insulators are chosen as substrates for CdS growth. BaO ($a_o = 5.53$)[97] may be a possible alternative since the lattice mismatch between (111) BaO and CdS is only 5% compared with the present MgO/CdS combination of 28%.

REFERENCES

1. H. R. Blieden, International Solar Energy Society Meeting, Fort Collins (1974).

2. J. J. Loferski, J. Appl. Phys. 27, 777 (1956).

3. M. Wolf, Proc. IRE 48, 1246 (1960).

4. M. Wolf, J. Vac. Sci. Technol. 12, 984 (1975).

5. J. Lindmayer and J. F. Allison, COMSAT Tech. Rev. 3, 1 (1973).

6. A. K. Screeder, B. L. Sharama and R. K. Purakit, IEEE Trans. Electron. Devices ED-16, 309 (1969).

7. R. Sahai and A. G. Milnes, Solid-State Electron. 13, 1289 (1970).

8. H. J. Hovel, "Semiconductors and Semimetals", Vol. 11, Academic Press, New York (1975).

9. R. J. Stirn and Y. C. M. Yeh, Appl. Phys. Lett. 27, 95 (1975).

10. S. M. Veron and W. A. Anderson, Appl. Phys. Lett. 26, 707 (1975).

11. V. Dalal, H. Kressel and P. H. Robinson, J. Appl. Phys. 64, 1283 (1975).

12. R. V. D'aiello, P. H. Robinson and H. Kressel, Appl. Phys. Lett. 28, 231 (1976).

13. K. V. Ravi, J. Cryst. Growth 39, 1 (1977).

14. H. Fisher and W. Pschunder, 12th IEEE Photovoltaic Specialist Conference, Baton Rouge (1976).

15. J. Lindmayer, 12th IEEE Photovoltaic Spec. Conf.,Baton Rouge (1976).

16. J. M. Woodall and H. J. Hovel, J. Cryst. Growth 39, 108 (1977).

17. W. D. Johnston, J. Cryst. Growth 39, 117 (1977).

18. S. Wagner, J. L. Shay, K. J. Backmann, E. Beuhler and M. Bettini, J. Cryst. Growth 39, 128 (1977).

19. H. C. Hadley and W. F. Tseng, J. Cryst. Growth 39, 61 (1977).

20. A.L. Fahrenbruch, J Cryst. Growth 39, 73 (1977).

21. L. M. Fraas and Y. Ma, J. Cryst. Growth 39, 92 (1977).

22. W. Wagner and P. M. Bridenbaugh, J. Cryst. Growth 39, 151(1977).

23. M. Wolf, 9th IEEE Photovoltaic Spec. Conf., Silver Spring (1972).

24. M. Wolf, 10th IEEE Photovoltaic Spec. Conf., Palo Alto (1973).

25. M. Wolf, Energy Conversion 14, 9 (1974).

26. N. F. Foster, J. Appl. Phys. 38, 149 (1967).

27. J. Dresner and F. V. Shallcross, J. Appl. Phys. 34, 2390 (1963).

28. J. Berkwoitz and J. R. Marquart, J. Appl. Phys. 39, 275 (1963).

29. P. Goldfinger and M. Jeunehomme, Trans. Faraday Soc. 59, 2851 (1963).

30. L. S. Palatnik, M. N. Naboka and O. A. Obel'yaninova, Inorganic Mat. 6, 1689 (1970).

31. G. Ya,Pikus and G. N. Tal'nova, Sov. Phys.-Sol. State 12, 1065 (1970).

32. A. Y. Cho and J. R. Arthur, Prog. in Sol. State Chem. 10, 157 (1975).

33. A. Y. Cho, C. N. Dunn, R. L. Kuvas and W. E. Shroeder, Appl. Phys. Lett. 25, 224 (1974).

34. A. Y. Cho and H. C. Casey, Appl. Phys. Lett. 25, 288 (1974).

35. A. Y. Cho and F. K. Reinhart, Appl. Phys. Lett. 21, 355 (1972).

36. M. Knudsen, Ann. Physik 28, 999 (1909).

37. R. G. J. Frayser, "Molecular Rays", Cambridge University Press, Cambridge (1931).

38. C. T. Foxon, M. R. Boundary and B. A. Joyce, Surf. Sci. 44, 69 (1974).

40. C. A. Neugebauer, "Handbook of Thin Film Technology", Ch. 8, edited by L. I. Maissel and R. Glang, McGraw-Hill, New York (1970).

41. D. W. Pashley, "Recent Progress in Surface Science", Vol. 3, edited by J. F. Danielli, A. C. Riddiford and M. D. Rosenberg, Academic Press, New York (1970).

42. K. L. Chopra, "Thin Film Phenomena", McGraw-Hill, N.Y. (1969).

43. T. N. Rhodin and D. Walton, "Metal Surfaces", American Soc. for metals (1963).

44. J. P. Hirth and G. M. Pound, "Progress in Materials Science", Vol. 11 (1963).

45. K. G. Gunther, "Compound Semiconductor", Vol. 1, p.313, edited by R. K. Williardson and H. L. Goering, Reinhold Publishing Corp., New York (1961).

46. J. Frenkel, Z. Physik 26, 117 (1924).

47. K. G. Gunther, "The Use of Thin Films in Physical Investigations", edited by J. C. Anderson, Academic Press, New York, p.213 (1966).

48. H. Braune, S. Peter and V. Neveling, Z. Naturforsh 6a, 32 (1951).

49. L. Holland, "Vacuum Deposition of Thin Films", Chapman & Hall, London (1958).

50. R. L. Anderson, IBM J. Res. and Develop. 4, 283 (1960).

51. W. G. Oldham and A. G. Milnes, Solid-St. Electron. 7, 153 (1964).

52. J. M. Feldman, "The Physics and Circuit Properties of Transistors", Wiley & Son, New York (1972).

53. J. Bardeen, Phys. Rev. 71, 717 (1947).

54. C. A. Mead and W. G. Spitzer, Phys. Rev. 134, 713 (1964).

55. D. B. Holt, Thin Solid Films 24, 1 (1974).

56. B. E. Deal, J. Electrochem. Soc. 110, 527 (1963).

57. F. M. Livingston, Ph.D. Thesis, Dept. of Electronics and Electrical Eng., Glasgow University (1976).

58. F. A. Trumbore, Bell System Tech. J. 39, 205 (1960).

59. A. S. Grove, "Physics and Technology of Semiconductor Devices", Wiley & Son, New York (1967).

60. Union Carbide Corp., Technical leaflet on Boron Nitride.

61. A. R. Smellie, Ph.D. Thesis, Dept. of Electronics and Electrical Eng., University of Glasgow (1976).

62. R. E. Schlier and H. E. Farnsworth, J. Chem. Phys. 30, 917 (1959).

63. F. Jona, Appl. Phys. Lett. 6, 205 (1965).

64. D. Haneman, "Surface Physics of Phosphors and Semiconductors", edited by C. G. Scott and C. E. Reed, A.P., N.Y. (1975)

65. J. J. Lander and M. Morrison, J. Appl. Phys. 33, 2089 (1962).

66. G. J. Russel, H. K. Ip and D. Haneman, J. Appl. Phys. 37,3328 (1966).

67. B. A. Unvala and M. Censlive, Vacuum 23, 237 (1973).

68. E. G. McRae and P. J. Estrup, Surface Science 25, 1 (1971).

69. J. S. Hill and G. N. Simpson, J. Phys. E: Sci. Instr. 6, 299 (1973).

70. P. L. Jones, C. N. N. Litting, D. E. Mason and V. A. Williams, J. Phys. D: Appl. Phys. 1, 283 (1968).

71. V. K. Zwdykin et al., "Electron Optics and Electron Microscope", Wiley & Son, New York (1945)

72. D. B. Cullity, "Elements of X-ray Diffraction", Addison-Wesley, London (1959).

73. F. A. Shirland, Adv. Eng. Conversion 6, 201 (1966).

74. J. L. Shay, S. Wagner, K. J. Bachmann and E. Buehler, J. Appl. Phys. 47, 614 (1976).

75. Y. Y. Ma, A. L. Fahrenbruch and R. H. Bube, Appl. Phys. Lett. 30, 423 (1977).

76. C. K. Campbell and C. H. Morgan, Thin Solid Films 26, 213 (1975).

77. L. Bragg and G. F. Claringbull, "Crystal Structure of Minerals", Vol. IV, edited by L. Bragg, G. Bell & Son, London (1965).

78. J. Berkowitz and W. A. Chupka, J. Chem. Phys. 40, 287 (1964).

79. H. Holloway, "The Use of Thin Films in Physical Investigations", edited by J. C. Anderson, Academic Press, N.Y. (1966).

80. P. A. M. Stewart, Ph.D. Thesis, Faculty of Eng., University of Glasgow (1969).

81. R. E. Honig and D. A. Kramer, RCA Rev. 30 285 (1969).

82. C. H. Henry, K. Nassau and J. W. Shiever, Phys Rev. B 4, 2453 (1971).

83. D. W. Pashley, Advance Phys. 5, 173 (1956).

84. D. W. Pashley, Phil. Mag. 4, 316 (1959).

85. V.F.G. Tull, Proc. Roy. Soc. A 206, 219 (1951).

86. J. Fryer, Private Communication, Dept. of Chemistry, University of Glasgow.

87. O. Kubaschewski and B. E. Hopkins, "Oxidation of Metals and Alloys", Butterworth (1962).

88. B. Berlincourt, H. Jaffe and L. R. Shinozana, Phys. Rev. 129, 1009 (1963).

89. N. F. Foster, "Handbook of Thin Film Technology", Ch. 15, edited by L. I. Maissel and R. Glang, McGraw-Hill,N.Y. (1970).

90. R. Zare, N. R. Cook, Jr., and I. R. Shiozawa, Nature 189, 217 (1967).

91. G. A. Rozgonyi and N. F. Foster, J. Appl. Phys. 38, 5172 (1967).

92. R. A. Smith, "Semiconductors", Cambridge University Press, Cambridge (1959).

93. R. A. Smith, "Wave Mechanics of Crystalline Solids", Chapman & Hall, London (1961).

94. M. O. Aboelfotoh, 4th International Thin Film Congress, Loughborough University (1978).

95. M. D. Clark, S. Baidyaroy, F. Ryan and J. M. Ballantyne, I.E.D.M. abstracts, Washington (1974).

96. M. Cardona, W. Weistein and G. A. Wolff, Phys. Rev. 140, A633 (1965).

97. R. W. G. Wyckoff, "Crystal Structures", Vol. 1, Interscience, New York (1963).

98. S. M. Sze, "Physics of Semiconductor Devices", Interscience, New York (1969).

99. C. T. Sah, R. N. Noyce and W. Shockley, Proc. I.R.E. 45, 1228 (1957).

100. R. Kohler and L. Wauer, Solid-St. Electron. 14, 581 (1971).

101. J. Schewchun, M. A. Green and F. D. King, Solid-St. Electron. 17, 563 (1974).

102. A. H. M. Kipperman and M. H. Omar, Appl. Phys. Lett. 28, 620 (1976).

103. S. J. Fonash, Thin Solid Films 36, 387 (1976).

104. S. J. Fonash, J. Appl. Phys. 47, 3597 (1976).

105. M. A. Green, F. D. King and J. Schewchun, Solid-St. Electron. 17, 551 (1974).

106. M.A.Green and J.Schewchun, Solid-St. Electron. 17, 349 (1974).

107. J. A. St. Pierre, R. Singh, J. Schewchun and J. J. Loferski, 12th IEEE Photovoltaic Spec. Conf., Baton Rouge (1976).